Properties of Cellular Concrete Made with Combustion By-Products

by

Jonathan Stolz

A thesis submitted in partial fulfillment of the requirements for the degree of

Master of Science
in
Structural Engineering

Department of Civil and Environmental Engineering
University of Alberta

Abstract

With growing concern over global warming and greenhouse gas emissions, research must be undertaken to reduce the environmental footprint of buildings. Cellular concrete provides good strength to weight ratios and good thermal insulation because of its cellular structure. This makes it suitable for reducing the energy demands of buildings constructed with this material. However, the Portland cement currently used in cellular concrete releases large amounts of CO_2 during its production. Alternative materials to Portland cement can provide lower carbon footprints. Alkali activated materials can fully replace Portland cement with an alumino-silicate source which is reacted with an alkaline solution. Common alumino-silicate sources are often industrial by-products, so the use of alkali activated materials both reduces the need for Portland cement and diverts by-products from landfills. Renewably sourced ashes also have potential for replacing Portland cement. Ash from the burning of hog fuel in the pulp and paper industry can be used to partially replace the Portland cement in concrete mixes. Applying these more environmentally friendly materials to cellular concrete will produce a material with low carbon emissions for production and high environmental performance for buildings constructed using them.

In this thesis, cellular concretes are prepared with cast densities from 100 kg/m^3 to 1400 kg/m^3 out of alkali activated fly ash, and out of Portland cement blended with up to 20% wood ash. The mechanical, thermal, and acoustic properties of these cellular materials are characterised, and the effects of the differing cementitious materials on these properties are analysed. The cellular structure of the materials is characterised through the use of image analysis, and relationships between the structure and the thermal and acoustic properties of the materials are analyzed.

Preface

Chapter 3 of this thesis has been published as Stolz J., Boluk Y., Bindiganavile V. (2018) "Mechanical, Thermal and Acoustic Properties of Cellular Alkali Activated Fly Ash Concrete" *Cement and Concrete Composites.* 94 24-32. I was responsible for the preparation and testing of all specimens, the analysis of all data, and the preparation of the manuscript. Dr. Bindiganavile provided support in advising the research and editing the manuscript, while Dr. Boluk also assisted in editing the manuscript.

Chapter 4 of this thesis has been submitted for publication in *Journal of Construction and Building Materials* with the title "Wood Ash as a Supplementary Cementing Material in Thermal and Acoustic Insulating Foams" by myself, Dr. Yaman Boluk and Dr. Vivek Bindiganavile. I was responsible for the preparation and testing of all specimens, the analysis of all data, and the preparation of the manuscript. Dr. Bindiganavile provided support in advising the research and editing the manuscript, while Dr. Boluk also assisted in editing the manuscript.

Acknowledgements

I would like to thank Dr. Vivek Bindiganavile for supervising this research. This research would not have been possible without his advice and support throughout my studies. With his understanding and guidance, I have learned much about the world of academia, and much about myself.

I would like to thank Mr. Rizaldy Mariano for his assistance in the lab with acquiring equipment and supplies. I would like to thank Ms. Diane Caird for carrying out all of the the XRD testing, and Mr. Nathan Gerein for carrying out the scanning electron microscopy.

I would like to thank Ms. Binyu Xie for working as a lab assistant for me during the first summer of my studies. She provided a great deal of help in lab activities that formed chapter 3 of this thesis. I would like to thank Ms. Brianna Jackson for working as a lab assistant for me during the second summer of my studies. She assisted with analysis that contributed to chapter 5 of this thesis, and much more lab work not reported in this thesis.

I would like to thank Jillian Martin for her love and support during my studies.

Finally, I would like to thank my parents for providing me opportunities which have led to my undertaking of graduate studies, and for the support they have provided throughout my schooling.

Table of Contents

List of Figures

List of Tables

1.0 Introduction

1.1 Background

Growing concern over greenhouse gas emissions necessitate advancement over conventional building materials. Expectations for energy efficient buildings require materials which provide good thermal insulation. These materials themselves must also have a low environmental impact on production. Currently, autoclaved aerated cement is used as a lightweight material with moderate strength and good insulating properties; however, this material is energy intensive. It is made from Portland cement, which produces large volumes of carbon dioxide when produced, and it is autoclaved at high temperatures to release gas bubbles, requiring additional energy to produce. An alternative material which reduces the dependence on Portland cement and can be produced without heat treatment while maintaining good insulating properties would be a much more environmentally friendly choice.

Cellular concrete is produced primarily in two different ways. Chemically foamed concrete relies on a chemical reaction to produce gas bubbles in the concrete. A common example is the use of aluminum, which reacts in the alkaline environment of the cement to produce hydrogen gas. Another method of producing cellular concrete is to use a preformed foam method. This produces a material similar to autoclaved aerated cement, but does not require additional heat through autoclaving. Instead, bubbles are introduced to the cement in the form of a foam produced using a surfactant and special foam generating equipment. While this reduces the energy required for production, Portland cement is still used as the binder, resulting in the production of CO_2.

Fly ash has long been used as a cementitious material partially replacing Portland cement in concrete. Binders can also be prepared from fly ash with no Portland cement by a process called alkali activation. Fly ash is mixed with an alkaline solution which causes a reaction that produces synthetic stone which is similar to Portland cement based concrete. The benefit of alkali activated fly ash is that it is utilizing an industrial by-product, so no additional CO_2 is produced to make the material.

While fly ash is an attractive binder material for the near future, eventually coal fired power plants will be shut down, and stockpiles of fly ash will be depleted. Renewable sources of alumino-silicates provide a more long term solution to reducing dependence on Portland cement. Agriculturally sourced ashes have been used as supplementary cementing materials. Sugarcane bagasse ash is a by-product of sugar production and has been widely studied for its use in concrete. The pulp and paper industry produces a wood ash when unusable parts of trees such as the bark are burned to recover energy. This wood ash can be used to partially replace Portland cement in concrete.

By utilizing binders such as alkali activated fly ash or wood ash substituted Portland cement to make cellular concrete with a preformed foam method, a lightweight insulating building material could be produced with reduced CO_2 emissions and reduced energy requirements. For such a material to be used, its performance characteristics must be determined. The mechanical properties must be understood so that it can be used safely in structures. The thermal properties must be determined to show that material can provide good insulation for buildings. Acoustic properties are important for the comfort of occupants within the building.

1.2 Scope

An improved understanding of alkali activated materials shall allow for it to be used to make a variety of precast concrete products. At the same time, understanding how wood ash affects the performance of cellular cement-based composites will inform its usage as a supplementary cementing material. Further, an understanding of how the cellular network affects the thermal and acoustic properties of cellular cementitious materials could be applied to other rigid foams as well. With this outcome, the cellular network could be tailored to achieve performance characteristics specific to the application.

1.3 Outline of Thesis

Cellular concretes of varying densities were produced using an alkali activated fly ash binder and the mechanical, thermal, and sound absorption properties of the material were characterized. These same properties were then studied for cellular concretes made from a binder obtained through blending Portland cement with wood ash. In order to better understand the cellular structure of these materials, laser confocal microscopy and digital image analysis were used to characterize the porous structure of the cellular concretes. The results from the image analysis are then correlated to the thermal and acoustic performance.

2.0 Literature Review

2.1 Cellular Concrete

Cellular concrete is a cementitious system where the solid binder phase is filled with a number of small voids [Zhang et al. 2014]. ACI Committee 523 develops and reports on cellular concrete. Typically, the cellular system can range from 300 kg/m^3 to 1900 kg/m^3, with the optimal density range for thermal and sound insulation for adequate mechanical strength lying near that of water [Fouad 2006].

The air voids in cellular concrete can be formed through chemically induced formation of gas or through blending a preformed foam into the cement paste. In case of chemical foaming, introducing H_2O_2 or aluminum to the cement paste leads to chemical reactions that release gas bubbles within the hydrating system. In case of a preformed foam method, first a preformed foam is made by passing compressed air through a diluted surfactant in a foam generating machine and is then mixed with a slurry of cement and water [Zhang et al. 2014].

Cellular concretes have been extensively characterized for their thermal properties [Batool and Bindiganavile 2017a, Batool and Bindiganavile 2017b, Samson et al. 2017a, Samson et al. 2017b]. The cellular structure of the material results in low thermal conductivity, making it a good insulator. Foams prepared with gypsum or Portland cement have also been characterized as insulation for acoustic comfort [Laukaitis and Fiks 2006, Seddeq 2010, Wang and Zhao 2015, Skujans et al 2010]. The exposed cells leave a roughened surface which is suitable for absorbing sound.

Some work has been done to characterise the pore network of cellular concrete and relate that to its strength [Hilal et al. 2015, Kearsley and Wainwright 2001, Nambiar and Ramamurthy 2007,

Wee et al 2006]. It has been found that the strength of the cellular material is related to the relative density of the foamed cement raised to the 3/2 power [Gibson and Ashby 1997, Kearsley and Wainwright 2001]. Recent work relates the pore network to the thermal properties of the foams [Batool and Bindiganavile 2017, Batool and Bindiganavile 2018a, Batool and Bindiganavile 2018b].

Of interest for building occupant comfort are the acoustic properties of building materials. When sound waves strike an object, some sound energy is reflected back, some is transmitted through the object to the other side, and some is dissipated into other forms of energy. The sound reflected back is what makes a room echo, so it is important to minimize this component. It is quantified by the Sound Absorption Coefficient, which has a value from 0 to 1, where 0 indicates that all of the sound impacting a surface is reflected back and 1 indicates no sound is reflected back [Everest and Pohlmann 2009]. The sound energy transmitted through the material is quantified by the sound transmission loss, which measures in decibels, the difference in sound intensity between the side of the material with the sound source, and the opposite side of the material [Everest and Pohlmann 2009].

2.2 Alkali Activated Materials

Alkali activated materials are an environmentally friendly alternative to Portland cement. Alkali activated materials consist of an aluminosilicate precursor which is chemically activated with an alkaline agent. Common sources of the aluminosilicate precursor include ground granulated blast furnace slag, fly ash and metakaolin. Sodium or potassium hydroxide and sodium silicate solutions are commonly used as activators for the precursor [Provis et al. 2014]. Alkali activated

materials have been shown to have improved fire resistance [Singh et al. 2015] and frost resistance [Skvara et al. 2005] over Portland cement.

The use of alkali activation for generating cellular concrete is relatively recent [Abdollahnejad et al. 2015, Arellano et al. 2010, Ibrahim et al. 2017, Liu et al. 2016, Novais et al. 2016, Skvara et al. 2014, Zhang et al. 2014]. Strengths of cellular alkali activated materials range from 2 MPa to 30 MPa with densities from 550 kg/m^3 to 1350 kg/m^3. Heat curing of the alkali activated material at 80°C was found to double the compressive strength of the specimen, as compared to that cured under room temperature [Ibrahim et al. 2017].

2.3 Bio-Sourced Ash as a Supplementary Cementing Material

A number of recent studies have investigated the use of wood ash as supplementary cementing materials [Garcia and Sousa-Coutinho 2013, Hussain et al. 2017, Madrid et al. 2017, Setayeshgar et al. 2017, Othuman Mydin et al. 2014]. Wood ash is a renewable resource, unlike other common supplementary cementing materials. Along with other agro-sourced ash, this makes it particularly attractive to replace fly ash, upon termination of coal-fed power plants.

Wood ash has been used to replace up to 20% of the Portland cement in concrete without a significant loss of strength [Setayeshgar et al. 2017]. Wood ash has also been seen to reduce the thermal conductivity of cement, improving its insulation properties [Madrid et al. 2017]. This makes it an attractive supplementary cementing material.

With the existing body of research on cellular concrete, alkali activated materials, and bio-sourced supplementary cementing materials, study can be undertaken to apply foam concrete techniques to these more environmentally conscious concrete materials.

3.0 Mechanical, Thermal and Acoustic Properties of Cellular Alkali Activated Fly Ash Concrete[1]

3.1 Abstract

Efforts to reduce carbon emissions have led to interest in developing alternatives to Portland cement. Alkali activated fly ash is one such material that has potential to replace Portland cement. While the properties of alkali activated fly ash itself have been widely studied, its application for making cellular materials has not. Cellular concrete is a rigid, lightweight building material made by foaming cement paste. The resulting cellular solid has a good strength to weight ratio and good thermal insulating properties. The rough surface left by the air voids provides moderate sound absorption, which is beneficial for human comfort. In this study, a locally sourced fly ash is activated with sodium based alkaline agents and the resulting paste is foamed to produce a cellular alkali activated fly ash concrete. The mechanical, thermal, and acoustic properties are characterised for cellular alkali activated fly ash concrete with cast densities from 1000 kg/m^3 to 1400 kg/m^3.

---

[1] Jonathan Stolz, Yaman Boluk and Vivek Bindiganavile

Cement and Concrete Composites, *doi:* https://doi.org/10.1016/j.cemconcomp.2018.08.004

3.2 Introduction

The preceding decades have seen much needed standardization in the use of industrial by-products as supplementary cementing materials. With an increase in concerns over climate change and attendant goals to reduce carbon emissions, the construction industry continues to look for alternatives to Portland cement. This quest for materials with lower carbon footprint has of late, led to a renewed interest in alkali activated materials sourced from industrial and agricultural waste. Alkali activated systems are basically composed of two compounds: a binder and an activator. The binder is mainly amorphous, finely divided and rich in aluminosilicates and/or calcium silicates. A subset of such alkali-activated systems are known as geopolymers, wherein the binding phase is essentially an aluminosilicate gel [Provis et al. 2014]. Common sources of the aluminosilicate precursor include ground granulated blast furnace slag, fly ash and metakaolin. Sodium or potassium hydroxide and sodium silicate solutions are commonly used as activators for the precursor. Geopolymers have been shown to have improved fire resistance [Singh et al. 2015] and frost resistance [Skvara et al. 2005] over Portland cement.

Cellular composites made with Portland cement have been extensively studied and found useful, especially in non-structural applications, wherein thermal and acoustic insulation is desired. Due to their inherent cellular microstructure, these solid foams are much lighter than conventional concrete, possess lower thermal conductivity, higher acoustic absorption and, at the same time, offer adequate strength-to-weight ratio. Although the density of this cellular system can range from 300 kg/m^3 to 1900 kg/m^3, the optimal density range for thermal and sound insulation with adequate mechanical strength is near that of water [Fouad 2006]. Conventional cellular concrete is made by introducing air bubbles either through chemically induced formation of gas or through a foaming agent into cement paste [Zhang et al. 2014]. In case of the former, introducing

H_2O_2 or aluminum leads to chemical reactions that release gas bubbles within the hydrating system. In case of the latter, first a preformed foam is made by passing compressed air through a diluted surfactant in a foam generating machine [Zhang et al. 2014]. This preformed foam is then introduced into a freshly prepared slurry. In both cases, the air bubbles are entrapped within the hydrating cement paste and thus render the cellular air-void network.

The use of alkali activation for generating cellular concrete is relatively recent [Abdollahnejad et al. 2015, Arellano et al. 2010, Ibrahim et al. 2017, Liu et al. 2016, Novais et al. 2016, Skvara et al. 2014, Zhang et al. 2015]. The principal focus has been to optimize the mixture in order to achieve a satisfactory strength-to-density ratio, with thermal constants that are comparable to those seen for Portland cement based systems. Geopolymerization works best at high molarity of the alkali activator together with higher temperatures for curing. For a foamed geopolymer prepared with alkali activated fly ash, Ibrahim et al. [2017] found that the compressive strength doubles when the specimen was cured at 80°C, as compared to that under room temperature. Most prior studies report 12M concentration of NaOH or higher, in order to achieve sufficient strength [Abdollahnejad et al. 2015, Novais et al. 2016, Zhang et al. 2015]. As is well known about cellular solids, the strength of cellular concrete varies with the density to the 3/2 power [Gibson and Ashby 1997]. Skvara et. al. [2014] saw strengths from 2-8 MPa for densities ranging from 550 kg/m^3 to 900 kg/m^3, while Abdollahnejad et. al. [2015] obtained strengths from 2-7 MPa for densities from 730 kg/m^3 to 1350 kg/m^3. Besides fly ash, the use of slag [Liu et al. 2016], silica fume [Skvara et al. 2014] and metakaolin [Arellano et al. 2010, Novais et al. 2016] as the precursor has been examined, as per local availability. While the preceding reports indicate the use of aluminum or H_2O_2 create the bubbles, Zhang et. al. [2015] used a preformed foam to introduce the cellular microstructure to an alkali activated blend of slag and fly ash. The

latter obtained compressive strength as high as 30 MPa at 1200 kg/m^3. These lightweight systems offer excellent thermal resistance, which improves with a drop in the density. It is seen both with cellular polymers and cellular concrete that for a given composite density, the thermal conductivity is lower for larger mean pore size [Coquard and Baillis 2006, Batool and Bindiganavile 2017]. The typical range of density for lightweight cellular concrete is below 1000 kg/m^3, for which the thermal conductivity of cellular geopolymers lies between 0.15 W/mK to 0.6 W/mK [Abdollahnejad et al. 2015, Arellano et al. 2010, Novais et al. 2016, Skvara et al. 2014, Zhang et al. 2015].

Cellular solids are effective sound absorbing media and gypsum or Portland cement based foams have been extensively characterized as insulation for acoustic comfort [Laukaitis and Fiks 2006, Seddeq 2010, Wang and Zhao 2015, Skujans et al. 2010]. Often, the same physical characteristics benefit both thermal and acoustic insulation and so, morphologically fibrous and porous solids are seen to act as effective heat and sound barriers. The principal mode of dissipating sound is through friction for which, there should be sufficient porosity on the exposed surface of the proposed insulation. In addition, an increase in the tortuosity within the system is seen to impart more sound absorption for higher frequencies [Seddeq 2010]. For the same reason, the sound absorption coefficient is superior in open cell foams when compared to closed cell ones [Tiuc et al. 2014]. While the addition of fibres to cellular concrete augurs well from the mechanical standpoint, there is an optimal fibre dosage for maximum sound absorption. This appears to be related also to the compactibility of the mixture [Wang and Zhao 2015]. Whereas the mean cell size does not appear to affect the sound absorption for low frequencies, there appears to be a drop in the sound absorption coefficient with an increase in the cell size, for higher frequencies [Lu et al. 2000, Park et al. 2017].

In this study, a series of cellular concrete mixtures was prepared with an Alkali Activated Fly Ash (AAFA) and a preformed foam prepared with a foaming agent, and reinforced with glass microfibers. In what follows, the mechanical response – including the compressive strength and the modulus of elasticity, the thermal constants and, the sound absorption coefficient are described for a range of densities.

3.3 Experimental Procedure

3.3.1 Materials

The alkali activated material was prepared from a Class C1 fly ash sourced from the Genesee Power Generating Station in Warburg, Alberta, Canada. The chemical composition for this fly ash was determined in a previous study [Bindiganavile et al. 2016] by X-ray fluorescence and is shown in Table 3.1. The mineralogical composition of the ash was determined by X-ray diffraction, as shown in Figure 3.1. The composition was primarily quartz, mullite, and lime. The ash had a loss on ignition of 0.64% as determined by heating to 750°C as per ASTM D7348 [ASTM 2013].

Table 3.1: Composition of fly ash determined by X-ray fluorescence

MgO	Al_2O_3	SiO_2	SO_3	K_2O	CaO	TiO_2	MnO	Fe_2O_3	CuO	ZnO	As_2O_3	Br_2O	SrO	ZrO_2
0.9	15.57	50.16	1.63	1.82	17.6	1.93	0.13	9.61	0.04	0.04	0.02	0.07	0.35	0.11

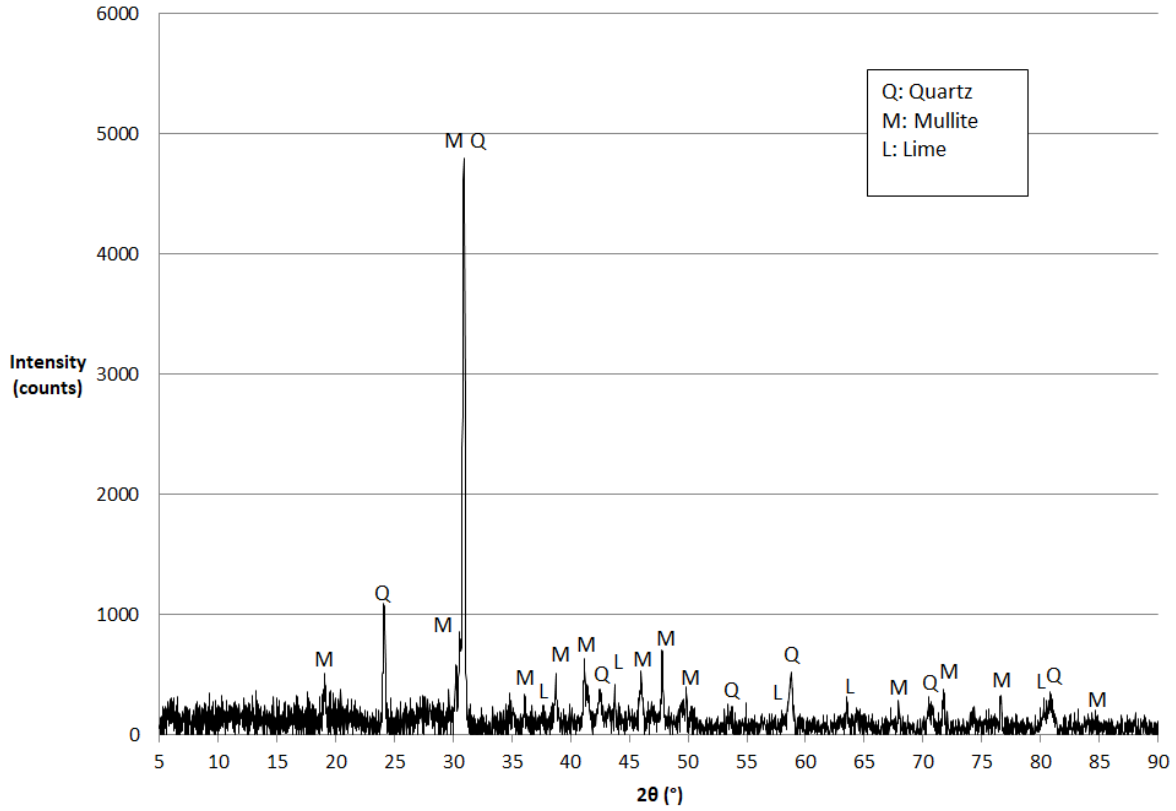

Figure 3.2: XRD Analysis of Class C1 Fly Ash

Of the two activators, sodium hydroxide solution was prepared to 8M concentration by dissolving solid sodium hydroxide pellets in distilled water. It should be mentioned here that the Civil Engineering Materials Laboratory at the University of Alberta has equipment that can only measure mass with the desired accuracy, but not the volume for this exercise. That is why, care had to be taken to accurately prepare this concentration without the use of a volumetric flask. Because the molarity is based on the volume of the final solution, the density of an 8M NaOH solution was used to calculate the mass for 1L of this solution. From that, the mass of 8 mol of NaOH was subtracted to find the amount of water required. This calculation led the author to prepare the target NaOH solution by dissolving 336 g of solid NaOH into 1000 g of water. The

other activator was a sodium silicate solution obtained commercially with its composition shown in Table 3.2. The silicon and sodium contents were determined by atomic absorption spectroscopy in a previous study performed by the author's laboratory [Bindiganavile et al. 2016]. Besides these, glass microfibers shown in Figure 3.2 were introduced into all the mixtures to improve the strength of the cellular material as shown by previous studies [Chen and Wang 2017, Jhatial et al. 2017, Mamun and Bindiganavile 2010]. These fibers were 45 Tex and 12mm long. This corresponds to a diameter of 37 μm with an aspect ratio of 328. A preformed foam was produced using a commercially sourced protein-based foaming agent conforming to ASTM C869 [ASTM 2016], diluted to a ratio of 1:33 with water. The resultant dilute was passed through a portable foam generator (see Figure 3.3) to produce a lightweight foam.

Table 3.2: Composition of Sodium Silicate

Water (%)	Sodium Silicate (%)	Molar Ratio	Density (g/cm^3)	Si (g/L)	Na (g/L)
60[(1)]	40[(1)]	3.2[(1)]	1.4[(1)]	58.65	2.38

[(1)]From supplier SDS

Figure 3.2: Glass Microfibres used in Foamed Composite

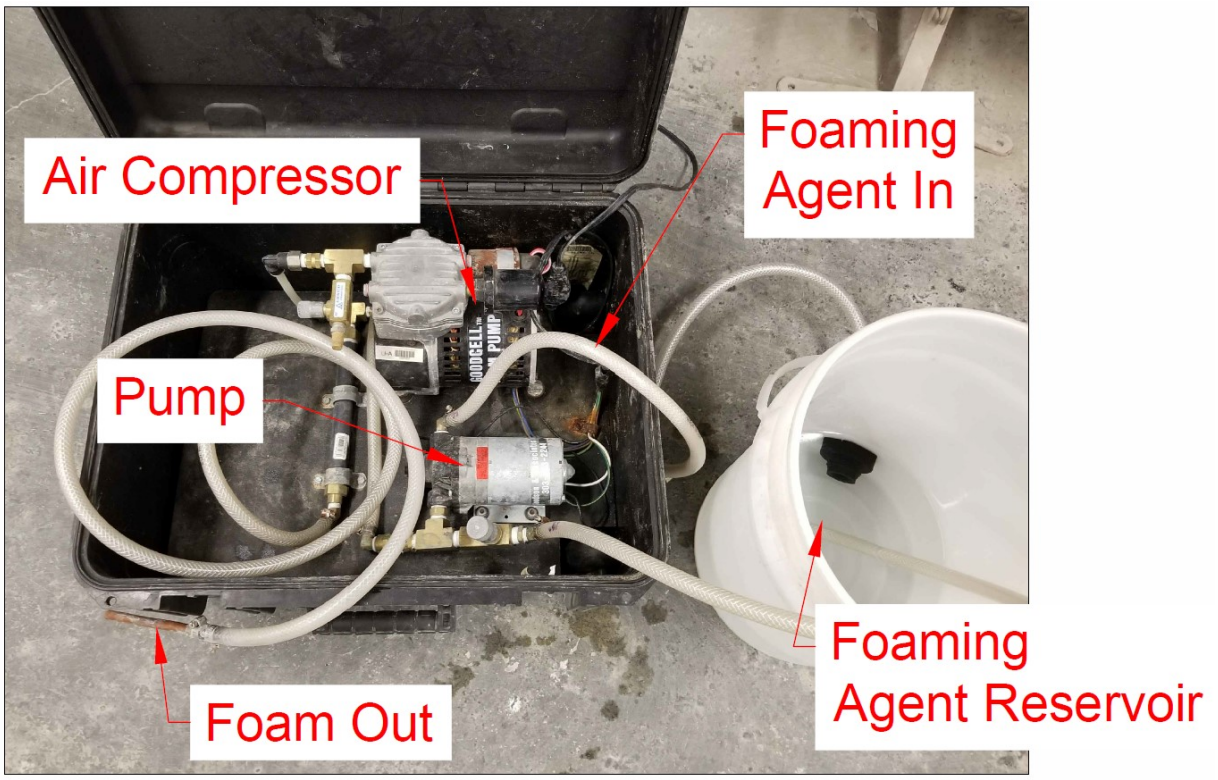

Figure 3.3: Portable Foam Generator

3.3.2 Specimen Preparation

Table 3.3 shows the mix proportions used to make the cellular alkali activated material. The fly ash and activators (in solution) were mixed in the ratio of 3:1 by mass. The activator itself consisted of one part 8M NaOH solution to two parts sodium silicate solution by mass.

The sodium silicate and sodium hydroxide solutions were mixed together and allowed to cool to room temperature. This solution was then introduced into a concrete mixer. Fly ash was added gradually to this mixer until a homogeneous paste was obtained. The glass microfibres were then introduced to the mixture at 1% by volume fraction. The pre-formed foam was now added to the

mixer. A small sample was extracted periodically from the mixer and weighed to determine the density, and more foam was added to the mixer until the sample reached the target cast density.

For each mixture, a batch of 6 litres was prepared. The mixtures were poured into plastic cylindrical moulds lined with waxed paper to facilitate their easy removal. Six Ø75mm x 150mm cylinders were cast to test mechanical properties and two Ø50mm x 100mm cylinders were cast to test the thermal properties. One cylinder, Ø100mm x 100mm in dimension and another, Ø50mm x 100mm in dimension, were cast to test the acoustic properties. All specimens were placed in a curing room at 22°C and 100% humidity. After 24 hours, the specimens were demoulded and returned to the curing room for a further 24 days. At 25 days after casting, the specimens were removed from the curing room and the ends were ground flat and parallel. All specimens were then left in the ambient indoor conditions of 22°C and 35% humidity for a further 3 days prior to testing.

Table 3.3: Mix proportions for 1 m^3 of cellular AAFA

Target Cast Density (kg/m^3)	Sodium Silicate Solution (kg)	8M NaOH (kg)	Fly Ash (kg)	Glass Fibre (kg)
1000	162	81	730	26.8
1200	195	98	880	26.8
1400	230	115	1030	26.8

3.3.3 Mechanical Testing Procedure

The compressive strength was determined as per ASTM C495/C495M-12 [ASTM 2012] in a universal testing machine. A displacement rate of 0.8 mm/min was used for all tests. Four

specimen replicates were tested for strength. Two of the specimens were fitted with a digital compressometer as shown in Figure 3.4 prior to test, which allowed for evaluating the modulus of elasticity and the Poisson's ratio.

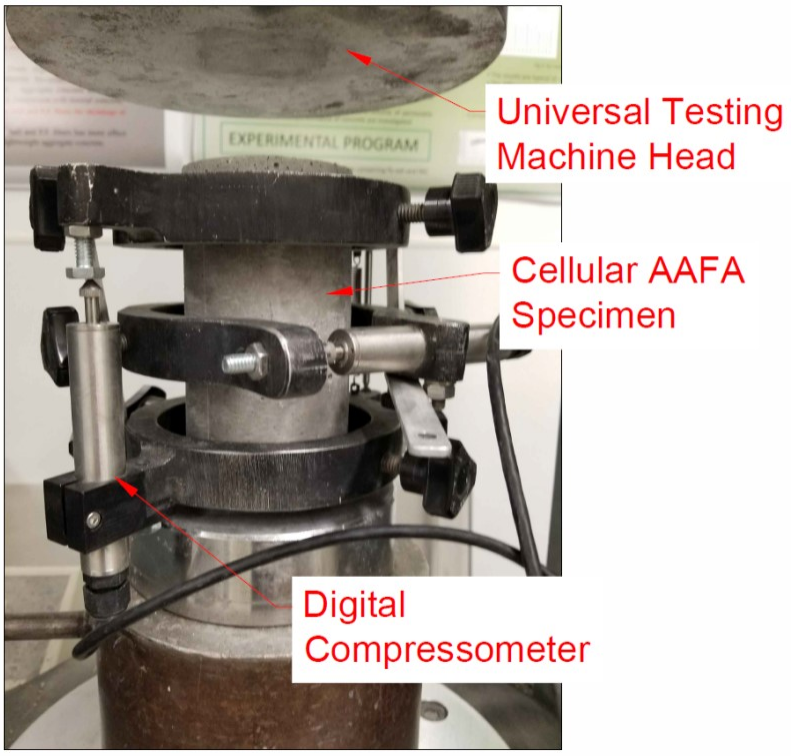

Figure 3.4: Cellular AAFA Specimen in a Digital Compressometer during a Compression Test

3.3.4 Thermal Testing Procedure

The thermal constants were determined using the transient plane source (TPS) method (ISO 22007-2 [ISO 2015]) using a Hot Disk TPS 1500 system. The sensor was a 3.189 mm diameter double spiral encased in Kapton. Two 50 mm x 100 mm cylinders were sawn into eight 25 mm thick disks. The Kapton sensor was inserted between a pair of disks as shown in Figure 3.5. An electric current is passed through the spiral, heating the specimen. As the temperature changes, the resistance of the spiral also changes, and the resulting voltage drop is measured. By

measuring the current and voltage drop through the sensor over a period of time, the thermal properties of the specimen can be calculated [Log and Gustafsson 1995]. Four pairs of disks were tested at each density and mixture.

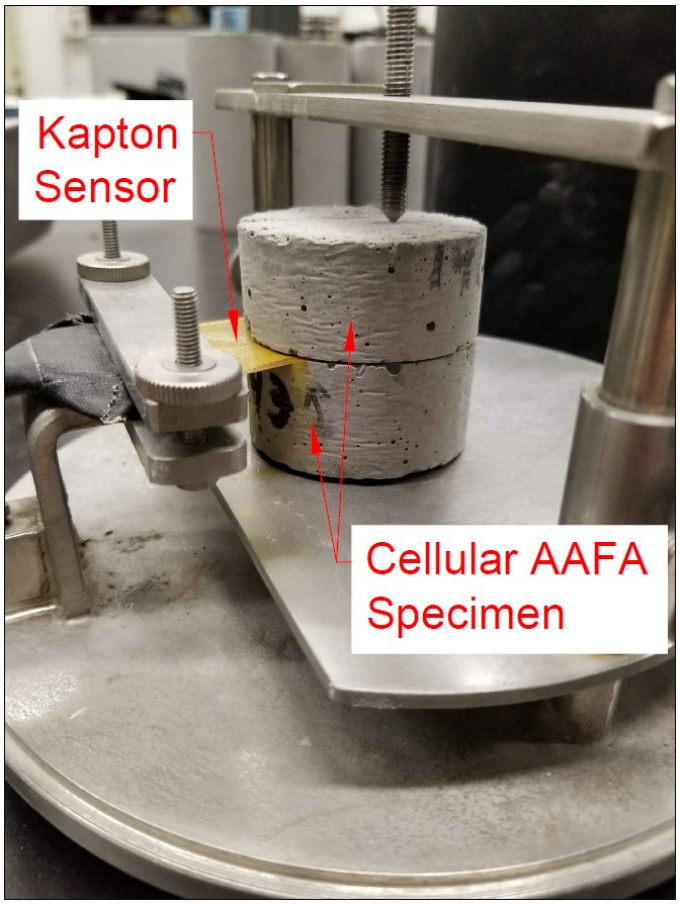

Figure 3.5: Transient Plane Source Sensor between Cellular AAFA Specimens

3.3.5 Acoustic Testing Procedure

The sound absorption of a material is described by the unitless sound absorption coefficient, α. It is a value that lies between 0 and 1, where 0 implies that all sound is reflected off the surface and 1 means that all sound is absorbed by the material [Everest and Pohlmann 2009]. When applied to sound insulation indoors, higher values of α are desirable to reduce the echo and related noise.

Acoustic testing was performed according to ASTM C384-04 [ASTM 2011]. The specimen is placed at the end of a tube and sound waves are sent down the tube to reflect off the specimen. The reflected sound forms a standing wave pattern in the tube. With a microphone probe, the locations and amplitudes of the maxima and minima of the standing wave are recorded. The Standing Wave Ratio, $SWR(x)$, at a location, x, from the face of the specimen, is the ratio of the maximum sound pressure to the minimum sound pressure at that location. The pressure reflection coefficient, Γ, and subsequently, the *normal incident* sound absorption coefficient, α_n, can be calculated as:

$$|\Gamma| = [SWR(0) - 1]/[SWR(0) - 1] \quad \ldots[1]$$

and

$$\alpha_{\mathrm{n}} = 1 - |\Gamma|^2. \quad \ldots[2]$$

This is repeated for each frequency of interest and the absorption coefficient may then be plotted.

As stated earlier, the specimens for acoustic testing were based on the diameter of the impedance tubes. The acoustic testing equipment is shown in Figure 3.6. The impedance tube was a Bruel & Kjaer Model 4002 equipment with a 100 mm diameter tube for low frequencies and a 30 mm diameter tube for high frequencies. Each cylinder at the respective diameter was cut to 50 mm thick disks and the faces were ground to expose the pore structure. The circumference was sanded down to allow it to fit snuggly inside the specimen holder for the respective impedance tube. The sound was sourced by a Bruel & Kjaer Type 1013 Beat Frequency Oscillator, while the acoustic response was measured with a Bruel & Kjaer Type 2113 Audio Frequency Spectrometer.

The standing wave pattern was measured at octave bands from 125 Hz to 6300 Hz and the normal incidence sound absorption coefficient was calculated on the basis of Equations [1] and [2]. One Ø100mm and one Ø30mm specimen were examined for each mixture. In each instance, five measurements of the absorption spectrum were taken per sample to report the average.

The Noise Reduction Coefficient (NRC) is a single value, defined in ASTM C423, as the average of sound absorption coefficients for 250 Hz, 500 Hz, 1000 Hz, and 2000 Hz [ASTM 2017]. This would typically be calculated based on random incident sound absorption coefficients; however, the authors applied the same calculation to normal incident sound absorption coefficients, α_n, determined with the standing wave method, to determine a single value that characterizes the sound absorption of the material.

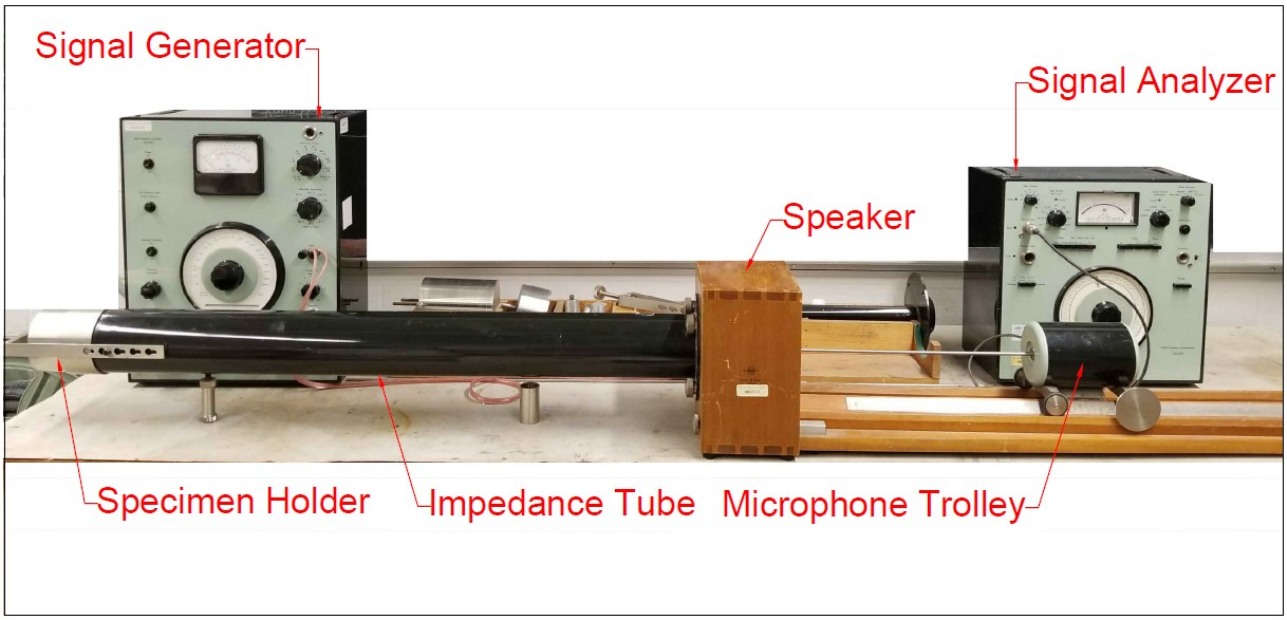

Figure 3.6: Impedance Tube Apparatus

3.4.0 Results and Discussion

3.4.1 Density of Cellular AAFA

In this study, the specimen density was measured at three stages namely, (i) at casting; (ii) at test and (iii) after oven drying. These densities are reported for each mixture in Table 3.4. The moisture content at test can be calculated from the oven dry density and density at test. The moisture content of the tested foams were 9.3%, 10.8% and 10.1% for foams with target densities of 1000 kg/m^3, 1200 kg/m^3 and 1400 kg/m^3 respectively.

Table 3.4: Densities of Cellular AAFA

Target Density	Cast Density	Density at Test	Oven Dry Density
1000 kg/m^3	1010 kg/m^3	940 ± 40 kg/m^3	860 ± 20 kg/m^3
1200 kg/m^3	1210 kg/m^3	1130 ± 40 kg/m^3	1020 ± 10 kg/m^3
1400 kg/m^3	1420 kg/m^3	1310 ± 25 kg/m^3	1190 ± 10 kg/m^3

3.4.2 Micrograph and XRD Analysis

Optical images of the cellular AAFA can be seen in Figure 3.7. At a density of 940 kg/m^3, a large number of small pores less than 1 mm in diameter can be seen. With an increase in the density, there appears to be an increase in the mean pore size. This may be attributed to the lower dosage of foam in the higher density mixtures, which makes them stiffer than the lighter mixtures. Consequently, a longer mixing time was necessitated to allow for the pre-formed foam to mix well with the paste. This in turn causes more bubbles to rupture and coalesce to form larger air voids.

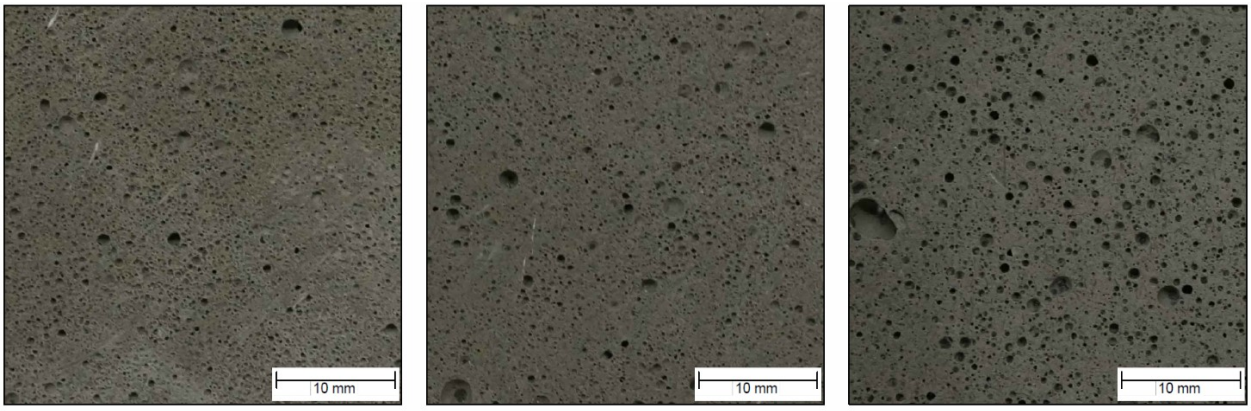

Figure 3.7: Surface of Cellular AAFA

In order to illustrate the microstructure of the solid phase in the cell walls, a Backscatter Scanning Electron Microscope (BSEM) image of the cellular AAFA at its heaviest namely, 1310 kg/m^3, is shown in Figure 3.8. The foams of other densities were prepared with the same paste, so at this magnification there is no difference in the appearance of the material. At 500X magnification, partially reacted and unreacted spherical fly ash particles are clearly visible embedded in the surrounding gel. Their presence suggests poor dissolution in the alkali medium. This could be due to the lower concentration of sodium hydroxide (at 8M) than seen in other studies. For instance, Rattanasak and Chindaprasirt [2009] found a significant increase in the dissolution of fly ash and consequently, in the strength of the resulting geopolymers, when the molarity of NaOH was raised from 5M to 10M.

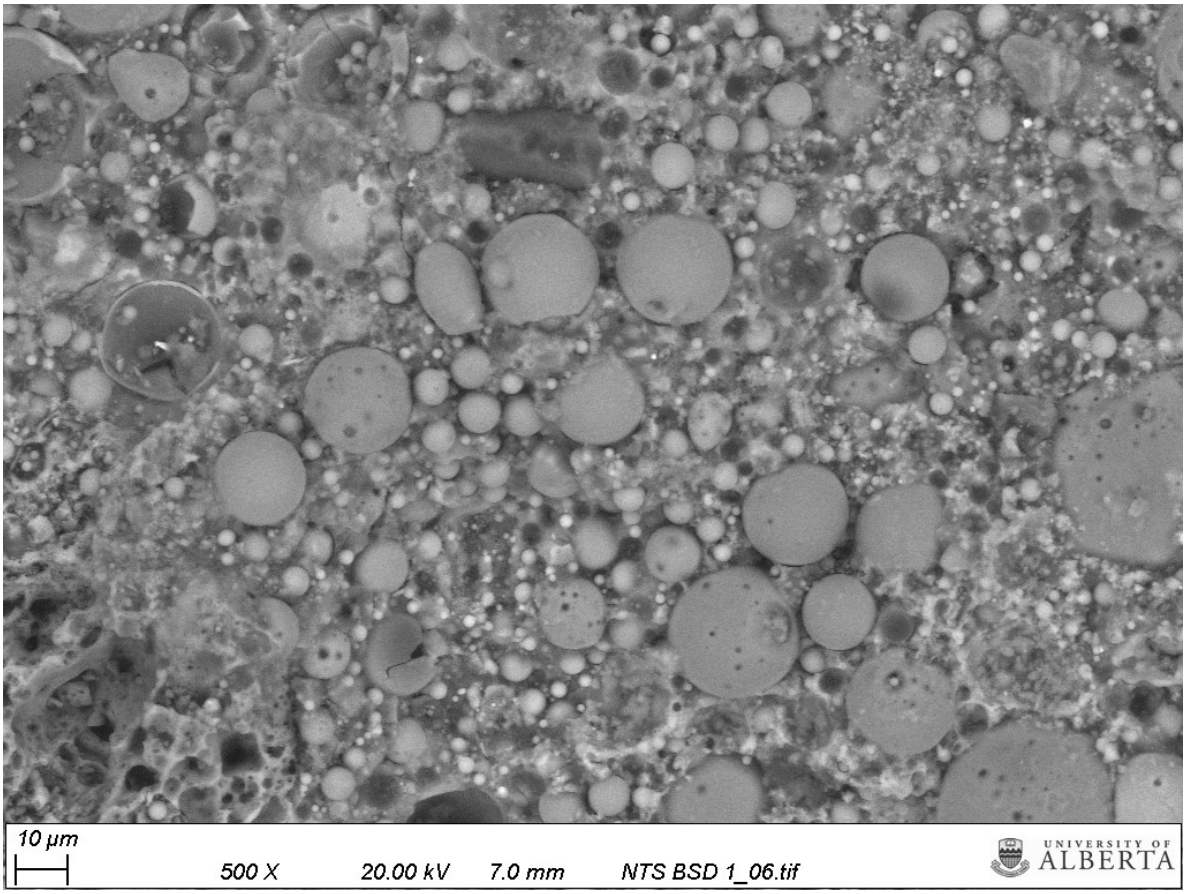

Figure 3.8: Backscatter Scanning Electron Microscope Image of Cellular AAFA of Density 1310 kg/m^3

X-ray diffraction of the AAFA is shown in Figure 3.9. This is representative of all densities of cellular AAFA produced in this study because the mix design for the paste was kept consistent. Notice that the crystalline phases are made up of quartz, calcite, mullite, and vaterite. The spectrum lacks the broad hump in the range of 2θ from 20° to 40° which is attributed to amorphous aluminosilicate gels [Criado et al. 2007]. Goncalves et al. [2017] activated the same fly ash used in this study with a solution of sodium silicate and 16M sodium hydroxide and found a significant rise on the XRD spectrum between 20° and 40°. This difference is likely due to the lower concentration of alkali activators used in this study resulting in a lower degree of reaction between the fly ash and the activator.

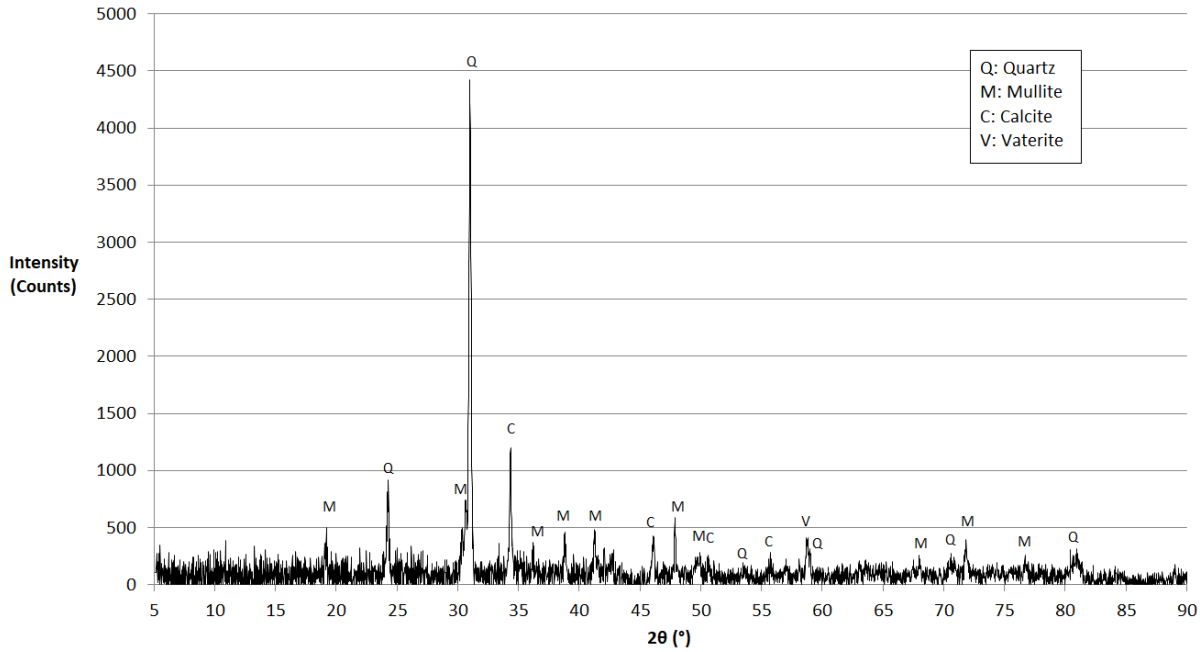

Figure 3.9: XRD Analysis of Cellular AAFA

3.4.3 Mechanical Properties

The compressive strength of the cellular AAFA is plotted against the density at test in Figure 3.10a. The strength ranged from 3.2 MPa at a density of 940 kg/m^3 to 9.3 MPa at 1310 kg/m^3. Increasing the density of the foam significantly improved the compressive strength. Based on prior results, the effect of density on strength was as expected for alkali activated foams [Zhang et al. 2015] and Portland cement based foamed concrete [Tiong-Huan and Saradhi 2006]. A power curve was fit to the compressive strength results from other studies on cellular alkali activated materials [Abdollahnejad et al. 2015, Arellano et al. 2010, Ibrahim et al. 2017, Liu et al. 2016, Novais et al. 2016, Skvara et al. 2014, Zhang et al. 2015] and is shown in grey on Figure 3.10a. The compressive strength of the AAFA in this study is similar to that seen for other foamed fly ash-based geopolymers of similar density [Abdollahnejad et al. 2015, Arellano et al. 2010, Novais et al. 2016] while using a lower concentration of NaOH and applying no heat

during curing. The compressive strength of the geopolymer foam was less than that produced by Zhang et. al. [2015], who blended slag with fly ash, used 12M NaOH in the activator and applied 24 hours of heat curing at 40°C, which ranged from 8 MPa to 30 MPa. The lower concentration of NaOH used and the lack of elevated curing temperature likely contributed to the lower strength found in this study. The cellular material produced in this study is unique in that it utilizes a Class C1 fly ash produced locally in Western Canada. The activator uses a lower concentration of NaOH than other studies, making the material safer to produce. The lack of heat curing applied to the cellular AAFA in this study reduces the cost and energy requirement of producing the material in comparison with other cellular materials which have been heat cured.

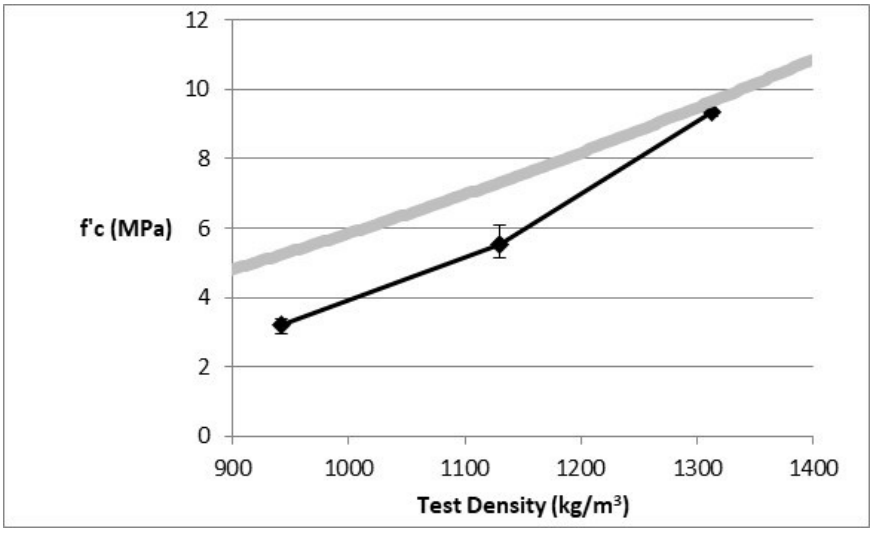

a)

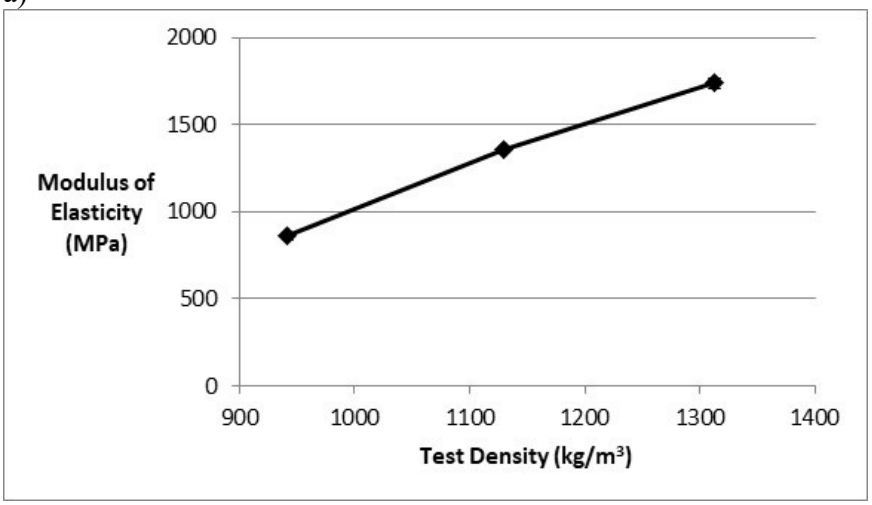

b)

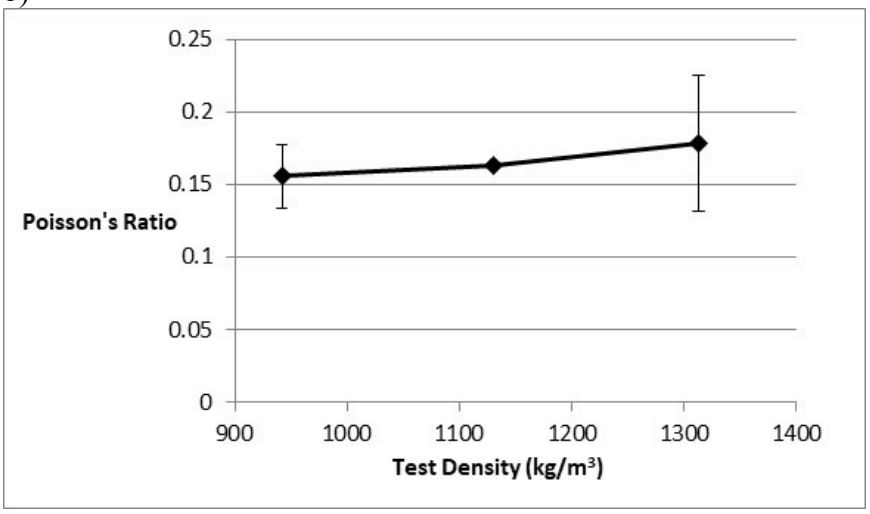

c)

Figure 3.10: a) Compressive Strength, b) Modulus of Elasticity and c) Poisson's Ratio, as a function of Density for Cellular AAFA

Figure 3.10b shows the modulus of elasticity of the cellular AAFA. The modulus doubled from 860 MPa to 1740 MPa in the range of density examined here. The value is significantly lower when compared with the modulus of elasticity for Portland cement foam concrete of similar density [Mamun and Bindiganavile 2010]. This is in keeping with the relatively lower strength for the cellular AAFA in this study. The Poisson's ratio of the cellular AAFA fell between 0.16 and 0.18 with little change with density, as shown in Figure 3.10c. This is similar to the trend seen in the Poisson's ratio for Portland cement foam as found by Mamun and Bindiganavile [2010], wherein little or no effect of density was observed.

3.4.4 Thermal Properties

The thermal conductivity of the cellular AAFA is plotted against its density in Figure 3.11a. At a dry density of 940 kg/m^3 the thermal conductivity was 0.23 W/mK which rose to 0.31 W/mK at a density of 1310 kg/m^3. This cellular AAFA has thermal conductivity in the range of other foamed geopolymers with similar densities [Novais et al. 2016, Skvara et al. 2014, Zhang et al. 2015]. While a 20% increase in the thermal conductivity resulted between the density from 940 kg/m^3 to 1130 kg/m^3, it was only marginally higher for a further increase in density to 1310 kg/m^3. The thermal diffusivity across the range of density examined here is plotted in Figure 3.11a. It was fairly constant, only ranging from 0.18 mm^2/s to 0.20 mm^2/s, which is somewhat lower than the diffusivity of 0.28 mm^2/s to 0.31 mm^2/s found by Zhang et. al. [2015] over the same range of density. Figure 3.11b shows the thermal conductivity and density of the cellular AAFA compared to other lightweight cementitious materials as reported in the NIST SRD81 database [Zarr et al. 2016]. Note that the cellular AAFA has thermal conductivities below the majority of other materials at a similar density.

The specific heat is plotted in Figure 3.11c. It increases from 1.18 MJ/m^{3}K at 940 kg/m^3 to 1.69 MJ/m^{3}K at 1310 kg/m^3. As would be expected, the specific heat increases near linearly with an increase in the density because there is a higher percentage of the paste material in the same bulk volume.

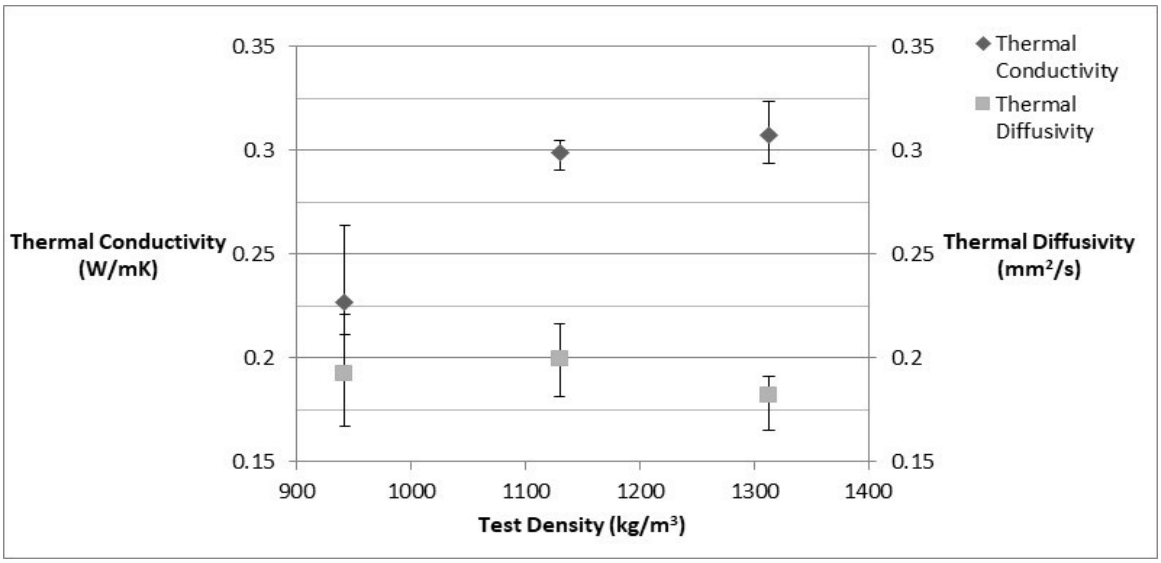

a)

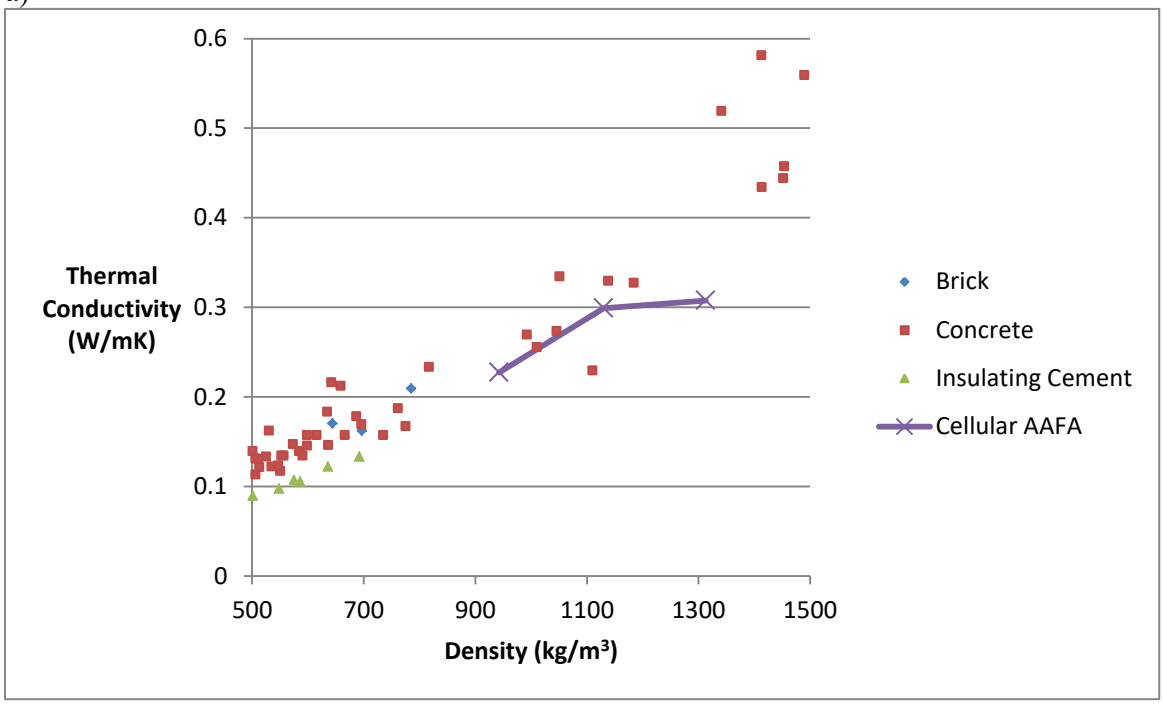

b)

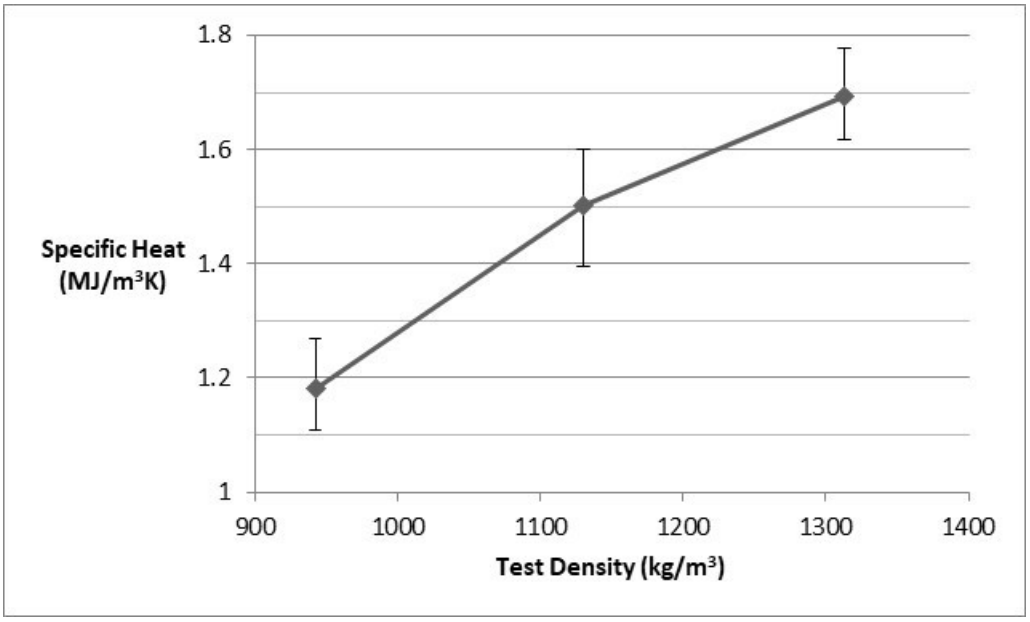

c)

Figure 3.11: a) Thermal Conductivity and Diffusivity of Cellular AAFA as a function of Density, b) Thermal Conductivity of Cellular AAFA Compared with Other Lightweight Materials From NIST SRD81, and c) Specific heat of Cellular AAFA as a function of Density.

One notes that the thermal conductivity of the present alkali activated fly ash paste was about 50% of that of Portland cement paste as determined in a previous study by the author's lab using the same methodology [Batool and Bindiganavile 2018]. For the same fly ash, when alkali activated with twice the concentration of NaOH (ie. 16 M), the thermal conductivity was about 15% higher than what was seen in this study [Goncalves et al. 2017].

3.4.5 Rule of Mixtures

A simple model was applied to the cellular AAFA to predict the thermal conductivity and specific heat capacity as the density was varied. The density, thermal conductivity, and specific

heat capacity of un-foamed AAFA were tested, and used to predict the properties of the cellular AAFA. A simple rule of mixtures similar to the work of Choktaweekarn et al. [2009] was used to relate the properties of the foam to the properties of the un-foamed paste as follows:

$$k_{foam} = k_{paste} * \rho_{foam}/\rho_{paste} + k_{air} * (1 - \rho_{foam}/\rho_{paste}) \quad \ldots[3]$$

and

$$c_{foam} = c_{paste} * \rho_{foam}/\rho_{paste} \quad \ldots[4]$$

The un-foamed paste has a density at test of 1590 kg/m^3, a thermal conductivity of 0.396 W/mK, and a specific heat capacity of 1.952 MJ/m^{3}K. These values were used to calculate predicted thermal properties for cellular AAFA at 940, 1130, and 1310 kg/m^3. The experimental values are plotted against the predicted values for thermal conductivity and specific heat capacity in Figure 3.12a and Figure 3.12b respectively. Note the proximity of the experimental values to the predicted values, for both thermal conductivity and specific heat capacity. This indicates a simple rule of mixtures can predict the thermal properties of a foamed AAFA to reasonable accuracy, provided that the properties of the un-foamed paste are known.

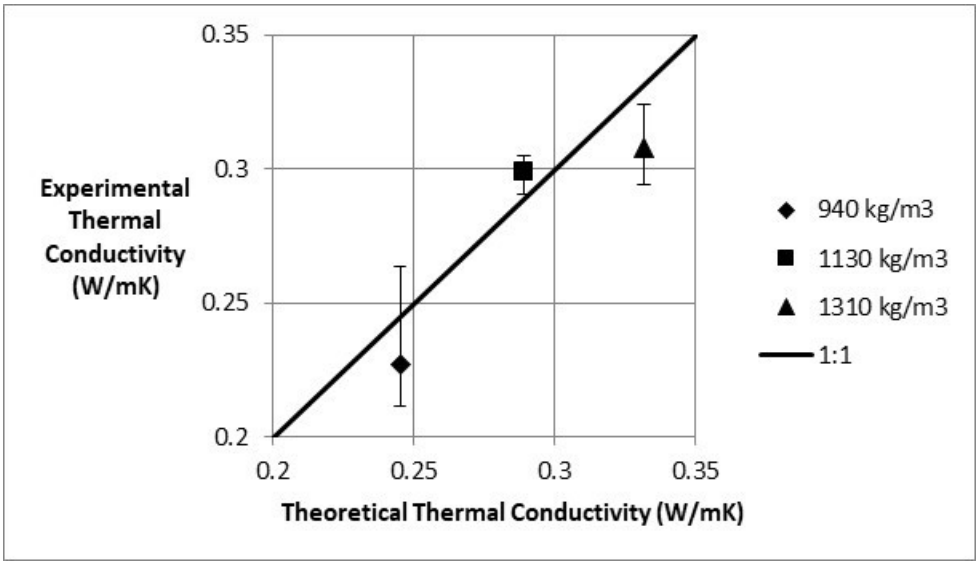

a)

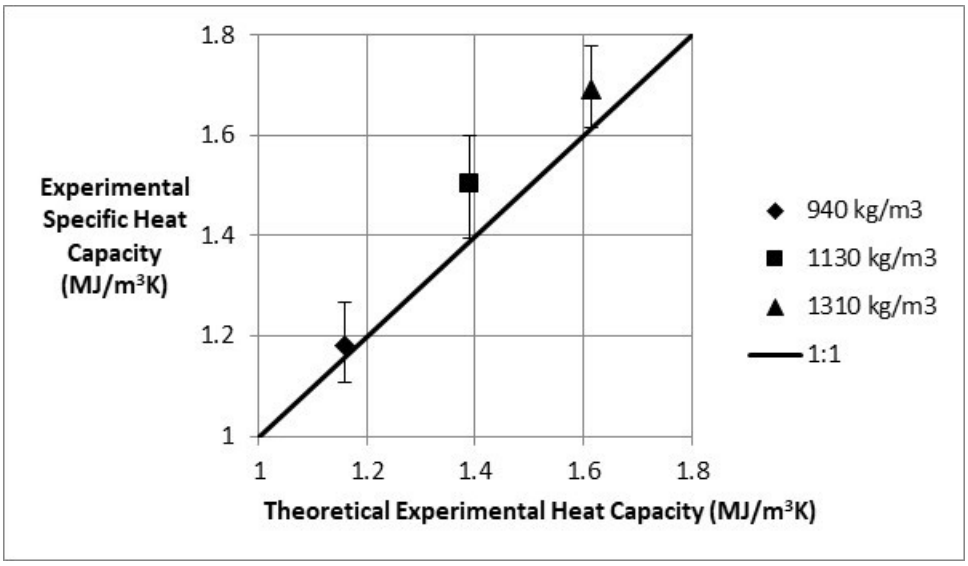

b)

Figure 3.12: Comparison between Experimental Data and Predicted Values for: a) Thermal Conductivity and b) Specific Heat Capacity, for Cellular AAFA

3.4.6 Acoustic Properties

The normal incidence sound absorption coefficient, α_n, for frequencies from 125 Hz to 6300 Hz are plotted in Figure 3.13a. A high absorption is seen at lower frequencies of 125 Hz and 250 Hz, which decreases rapidly and is very low in the range of 500 Hz to 2000 Hz. As the frequency increases further to 4000 Hz and 6300 Hz, the absorption coefficient was seen to increase again. These findings are similar to that reported by Zhang et. al. [2015]. The high absorption at low frequencies is beneficial to human comfort. Low frequency sounds from 10 Hz to 200 Hz can be very disruptive to people with a sensitivity to this kind of noise [Leventhall 2004].

The Noise Reduction Coefficients (NRC) were calculated from the absorption spectrum and are shown in Figure 3.13b. The NRC was highest for the 1130 kg/m^3 series, at 0.24. As expected, the higher density specimens had a significantly lower NRC at 0.11. The lowest density series had a slightly lower NRC than the intermediate density specimen, at 0.19. Laukaitis and Fiks [2006] studied the NRC of low density autoclaved aerated cements from 250 kg/m^3 to 500 kg/m^3 and found the NRC to decrease with an increase in the density. However, the NRC in that study at 500 kg/m^3 was significantly lower than that seen here for the 940 kg/m^3 cellular AAFA. Tiwari [Tiwari et al. 2004] tested the acoustic absorption of Portland cement paste reinforced with cenospheres. The NRC of the resulting paste increased with an increase in the cenosphere content up to 40% by volume. But thereafter, the NRC began to fall with higher cenosphere contents. This agrees with the results from the cellular AAFA which shows an optimum NRC at around 1130 kg/m^3, with higher or lower densities reducing the NRC. The NRC of this cellular AAFA is significantly higher than that of rough concrete, 0.03 [Vorländer 2008], and comparable (and sometimes superior to) gypsum acoustic tile, 0.20 [Anonymous 2017]. This higher NRC rating will reduce echoing in rooms built with cellular AAFA to an amount comparable to those built with traditional building materials.

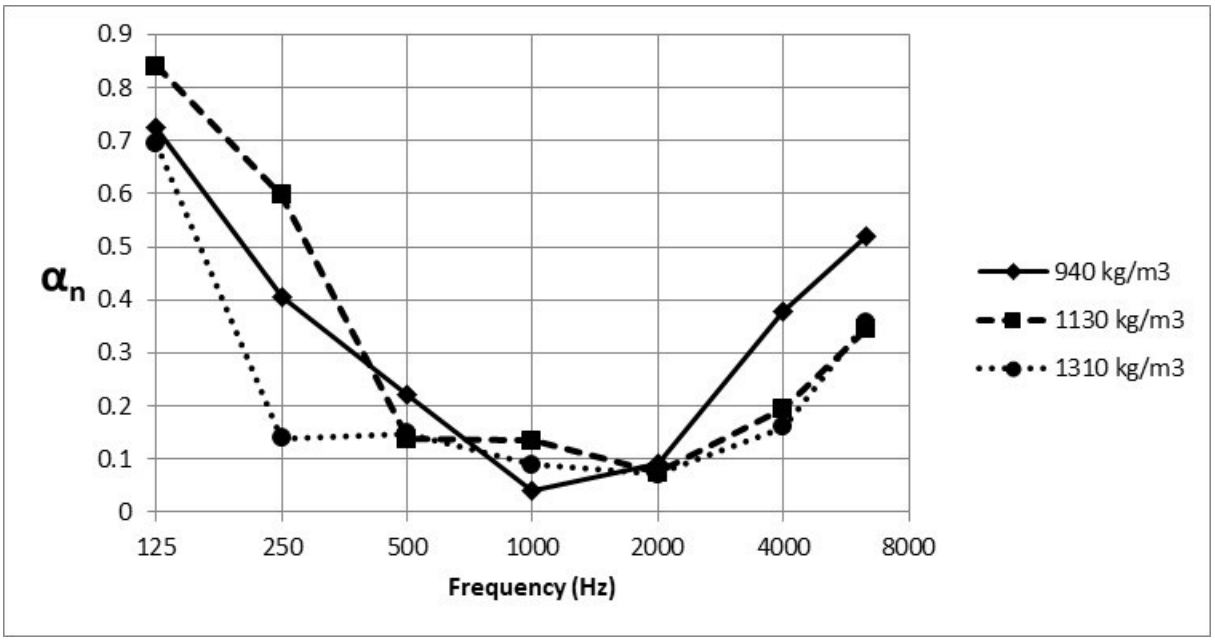

a)

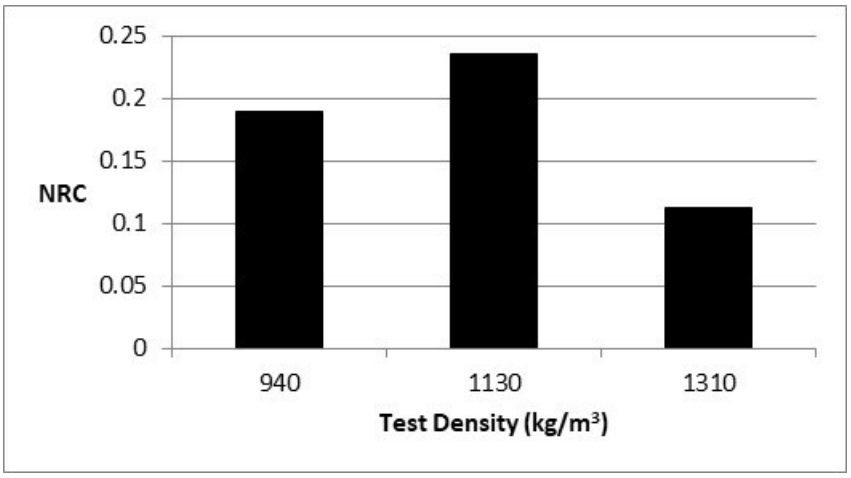

b)

Figure 3.13: a) Normal Incidence Sound Absorption Spectrum and b) Noise Reduction Coefficient (NRC), for various densities of cellular AAFA

3.5 Concluding Remarks

Cellular concrete was prepared by activating a class C fly ash with a sodium silicate and sodium hydroxide solution and blending the paste with preformed foam. The concentration of activators was deliberately lower than what is typically utilized and no heat was applied during the curing. The resulting system was cast to three densities, ranging from 1000 kg/m^3 to 1400 kg/m^3, and examined for its mechanical, thermal and acoustic properties. The results show that alkali activated fly ash may be designed as a cellular system to offer performance comparable to conventional Portland cement systems, and are therefore, a viable alternative in applications that require thermal and acoustic insulation. The specific findings are as follows:

- Compression tests yielded strength from 3.2 MPa to 9.3 MPa over the range of densities from 940 kg/m^3 to 1310 kg/m^3. The corresponding modulus of elasticity varied linearly from 860 MPa to 1740 MPa, while the associated Poisson's ratio remained nearly constant around 0.17.
- The thermal conductivity of this system rose from 0.23 W/mK at a density of 940 kg/m^3 to 0.31 W/mK at 1310 kg/m^3. The corresponding specific heat saw a linear increase from 1.18 MJ/m^{3}K to 1.69 MJ/m^{3}K. The thermal diffusivity remained around 0.19 mm^2/s across this range of density.
- The cellular AAFA shows high sound absorption at extreme frequencies, i.e. the low frequency range between 125 Hz - 250 Hz, and at high frequency range between 4000 Hz - 6300 Hz. However, from 500 Hz to 2000 Hz, the absorption coefficient was significantly lower at 0.1. The noise reduction coefficient was highest at 0.24 (i.e. 24% echo reduction) achieved for the density of 1130 kg/m^3.

3.6 References

Anonymous (2017). "Acoustic Ceiling Tiles and Panels." https://www.ceilume.com/shop/acoustic-ceiling-tiles/index.cfm#nrc25, (accessed 6 Dec 2017).

ASTM (2017). "C423 Standard Test Method for Sound Absorption and Sound Absorption Coefficients by the Reverberation Room Method." .

ASTM (2016). “C869/C869M-11 Standard Specification for Foaming Agents Used in Making Preformed Foam for Cellular Concrete.” .

ASTM (2013). "D7348 Standard Test Methods for Loss on Ignition (LOI) of Solid Combustion Residues." .

ASTM (2012). "C495/C495M Standard Test Method for Compressive Strength of Lightweight Insulating Concrete." .

ASTM (2011a). "C384 Standard Test Method for Impedance and Absorption of Acoustical Materials by Impedance Tube Method." .

Abdollahnejad, Z., Pacheco-Torgal, F., Flix, T., Tahri, W., and Barroso Aguiar, J. (2015). "Mix design, properties and cost analysis of fly ash-based geopolymer foam." *Construction & Building Materials,* 80 18-30.

Arellano Aguilar, R., Burciaga Díaz, O., and Escalante García, J. I. (2010). "Lightweight concretes of activated metakaolin-fly ash binders, with blast furnace slag aggregates." *Constr.Build.Mater.,* 24 1166-1175.

Batool, F., and Bindiganavile, V. (2018). "Thermal conductivity of hydrated paste in cement-based foam microstructure." *Adv.Civ.Eng.Mater.,* 7(1), 17-32.

Batool, F., and Bindiganavile, V. (2017). "Air-void size distribution of cement based foam and its effect on thermal conductivity." *Constr.Build.Mater.,* 149 17-28.

Bindiganavile, V., Goncalves, J. R. A., and Boluk, Y. (2016). "Crack growth resistance in fibre reinforced geopolymer concrete exposed to sustained extreme temperatures." *Key Eng Mat,* 711.

Chen, G., and Wang, K. (2017). "Mechanical and thermal properties of glass fibre-reinforced ceramsite-foamed concrete." *Indoor Built Environ.,* .

Choktaweekarn, P., Saengsoy, W., and Tangtermsirikul, S. (2009). "A model for predicting thermal conductivity of concrete." *Mag Concr Res,* 61(4), 271-280.

Coquard, R., and Baillis, D. (2006). "Modeling of heat transfer in low-density EPS foams." *J.Heat Transf.,* 128(6), 538-549.

Criado, M., Fernández-Jiménez, A., de, l. T., Aranda, M. A. G., and Palomo, A. (2007). "An XRD study of the effect of the SiO2/Na2O ratio on the alkali activation of fly ash." *Cem.Concr.Res.,* 37 671-679.

Everest, F. A., and Pohlmann, K. C. (2009). *Master handbook of acoustics.* McGraw-Hill, New York, NY ; London.

Fouad, F. H. (2006) "Chapter 47: Cellular Concrete." (169), 561.

Gibson, L. J., and Ashby, M. F. (1997). *Cellular solids : structure and properties.* Cambridge University Press, Cambridge.

Goncalves, J. R. A., Boluk, Y., and Bindiganavile, V. (2017). "Thermal properties of fibre reinforced alkali-activated concrete in extreme temperatures." *Magazine of Concrete Research,* 1-37.

Ibrahim, W. M. W., Hussin, K., Bakri Abdullah, M.,Mustafa Al, and Kadir, A. A. (2017). "Geopolymer Lightweight Bricks Manufactured From Fly Ash and Foaming Agent." *AIP Conference Proceedings,* 1835(1), 1-5.

ISO (2015). "Plastics - Determination of thermal conductivity and thermal diffusivity - Part 2: Transient plane heat source (hot disc) method (ISO 22007-2:2015)." .

Jhatial, A. A., Inn, G. W., Mohamad, N., Johnson Alengaram, U., Hung Mo, K., and Abdullah, R. (2017). "Influence of polypropylene fibres on the tensile strength and thermal properties of various densities of foamed concrete." *IOP Conference Series: Materials Science and Engineering,* .

Laukaitis, A., and Fiks, B. (2006). "Acoustical properties of aerated autoclaved concrete." *Applied Acoustics,* 67(3), 284-296.

Leventhall, H. (2004). "Low frequency noise and annoyance." *Noise Health,* (23), 59-72.

Liu, Z., Fan-long Kong, Ning-ning Shao, Ju-jia Zhang, Zhen-zhen Chen, and Dong-min Wang. (2016). "Strength and Microstructure of alkali-activated fly ash-slag foam geopolymer." *Journal of Solid Waste Technology & Management,* 42(1), 16-26.

Log, T., and Gustafsson, S. E. (1995). "Transient plane source (TPS) technique for measuring thermal transport properties of building materials." *Fire Mater.,* 19(1), 43-49.

Lu, T. J., Chen, F., and He, D. (2000). "Sound absorption of cellular metals with semiopen cells." *J.Acoust.Soc.Am.,* 108(4), 1697-1709.

Mamun, M., and Bindiganavile, V. (2010). "Drop-weight impact response of fibre reinforced cement based foams." *International Journal of Protective Structures,* 1(3), 409-424.

Novais, R. M., Ascensão, G., J.A. Labrincha, L.H. Buruberri, and M.P. Seabra. (2016). "Porous biomass fly ash-based geopolymers with tailored thermal conductivity." *J.Clean.Prod.,* 119 99-107.

Park, J. H., Yang, S. H., Lee, H. R., Yu, C. B., Pak, S. Y., Oh, C. S., Kang, Y. J., and Youn, J. R. (2017). "Optimization of low frequency sound absorption by cell size control and multiscale poroacoustics modeling." *J.Sound Vib.,* 397 17-30.

Provis, J. L., and Van Deventer, Jan Stephanus Jakob. (2014). *Alkali activated materials : state-of-the-art report, RILEM TC 224-AAM.* Springer, Dordrecht.

Rattanasak, U., and Chindaprasirt, P. (2009). "Influence of NaOH solution on the synthesis of fly ash geopolymer." *Minerals Engineering,* 22(12), 1073-1078.

Seddeq, H. S. (2010). "Sound absorption improvement for cementitious materials." *Can Acoust,* 38(4), 31-35.

Singh, B., Ishwarya, G., Gupta, M., and Bhattacharyya, S. K. (2015). "Geopolymer concrete: A review of some recent developments." *Construction and Building Materials,* 85 78-90.

Skujans, J., Iljins, U., Ziemelis, I., Gross, U., Ositis, N., Brencis, R., Veinbergs, A., and Kukuts, O. (2010). "Experimental research of foam gypsum acoustic absorption and heat flow." *Chem. Eng. Trans.,* 19.

Skvara, F., Jilek, T., and Kopecky, L. (2005). "Geopolymer materials based on fly ash." *Journal Ceramic-Silikaty,* 49(3), 195-204.

Skvara, F., Sulc, R., Zdenek, T., Petr, S., Vit, S., and Zlamalova, C. Z. (2014). "Preparation and Properties of Fly Ash-Based Geopolymer Foams." *Ceramics-Silikty, Vol 58, Iss 3, Pp 188-197 (2014),* (3), 188.

Tiong-Huan Wee, D.,Saradhi Babu. (2006). "Air-Void System of Foamed Concrete and its Effect on Mechanical Properties." *Materials Journal,* 103(1),.

Tiuc, A. E., Vasile, O., Usca, A. -., Gabor, T., and Vermesan, H. (2014). "The analysis of factors that influence the sound absorption coefficient of porous materials." *Rom.J.Acoustics Vib.,* 11(2), 105-108.

Tiwari, V., Shukla, A., and Bose, A. (2004). "Acoustic properties of cenosphere reinforced cement and asphalt concrete." *Appl.Acoust.,* 65 263-275.

Vorländer, M. (2008). *Auralization.* Springer, Berlin.

Wang, P., and Zhao, C. (2015). "Study on reducing railway noise by porous concrete sound-absorbing panel." *Mater.Res.Innov.,* 19 S51160.

Zarr, R., Chavez, J., Lee, A., Dalton, G., and Young, S (2016). *NIST Heat Transmission Properties of Insulating and Building Materials, NIST Standard Reference Database Number 81.* National Institute of Standards and Technology, Gaithersburg MD, 20899, .

Zhang, Z., Provis, J. L., Reid, A., and Wang, H. (2015). "Mechanical, thermal insulation, thermal resistance and acoustic absorption properties of geopolymer foam concrete." *Cement & Concrete Composites,* 62 97-105.

Zhang, Z., Zhang, Z., Wang, H., Provis, J. L., and Reid, A. (2014). "Geopolymer foam concrete: An emerging material for sustainable construction." *Constr.Build.Mater.,* 56 113-127.

4.0 Wood Ash as a Supplementary Cementing Material in Thermal and Acoustic Insulating Foams[2]

4.1 Abstract

While fly ash can be alkali activated to fully replace Portland cement in a concrete system, it is not a long term solution to reducing dependence on Portland cement. With governments committing to reducing the use of coal energy production, supplies of fly ash will dwindle. Renewably sourced materials offer a more long term alternative to Portland cement. One potential material is wood based ash. The pulp and paper industry burns unusable wood material such as bark to recover energy and in doing so produces a renewably sourced ash. This ash has been shown to act as a supplementary cementing material and is suitable for partially replacing Portland cement in concrete. This study investigates the applicability of wood ash as a supplementary cementing material in cellular concrete. Wood ash was used to replace up to 20% of the Portland cement in cellular concrete with cast densities ranging from 1000 kg/m^3 to 1400 kg/m^3. The mechanical, thermal, and acoustic properties of these materials were then studied.

[2] Jonathan Stolz, Yaman Boluk and Vivek Bindiganavile

A Version of this Chapter is Under Review, Journal of Construction and Building Materials, Manuscript No. CONBUILDMAT-D-18-03233

4.2 Introduction

Cement based foams have been widely studied for their use in non-structural applications. They can be prepared with densities ranging from 300 kg/m^3 to 1900 kg/m^3, but an optimal balance of thermal and mechanical properties is typically found with densities near that of water [Fouad 2006]. At lower densities, they may be used as fillers, soil stabilizers and for thermal insulation.

Cement based foams have been extensively characterized for their thermal properties [Batool and Bindiganavile 2017, Batool and Bindiganavile 2018, Samson et al. 2017a, Samson et al. 2017b]. An increase in the porosity significantly reduces its thermal conductivity, making the cement based foam an attractive material for use in energy efficient buildings. An additional impetus towards this energy consciousness was the utilization of industrial waste and by-products such as fly ash, slag, metakaolin and silica fume, all of which are known to further decrease the thermal conductivity of cement based foams [Batool and Bindiganavile 2017, Batool and Bindiganavile 2018].

Cellular solids are effective in absorbing sound to reduce echo and improve noise absorption [Lu et al. 2000, Tiuc et al. 2014, Wang and Lu 1999]. When sound strikes a porous surface, the waves enter the pore network and bounce off the many curved surfaces. Each time the sound wave is reflected, some sound energy is lost as heat, so when the sound escapes back out of the pore network it has significantly less energy than it did when it entered [Tiuc et al. 2014]. Gypsum or Portland cement based foams have been studied and found to be effective sound absorbers [Laukaitis and Fiks 2006, Seddeq 2010, Wang and Zhao 2015, Skujans 2010]. Between them, open cell structure is more favourable as it allows more sound to enter the pore network and dissipate its energy [Lu et al. 2000].

With increasing concern regarding greenhouse gas emissions, there is a great interest in finding alternative cementitious materials to Portland cement. For every 1000 kg of Portland cement produced, 900 kg to 1100 kg, or nearly an equal amount of CO_2 is produced from calcination of the raw materials to the burning of fossil fuels for energy to produce the clinker [NRMCA 2012]. Fly ash has been widely utilized in the concrete industry as a supplementary cementing material, but with pressure to reduce dependence on coal fired power plants, other replenishable sources for supplementing cement must be characterized. One such material is wood ash from the pulp and paper industry. Bark and other materials that are unusable for the production of paper products are burned as hog fuel producing ash as a by-product. At times, this wood waste has been co-fired with coal in a bid to reduce the dependence of thermal power plants on fossil fuel [Nicholls and Zerbe 2010]. A number of recent studies have investigated the use of wood ash as supplementary cementing materials [Garcia and Sousa-Coutinho 2013, Hussain et al. 2017, Madrid et al. 2017, Setayeshgar et al. 2017, Othuman Mydin et al. 2014]. Wood ash has been used to replace up to 20% of the Portland cement in concrete without a significant loss of strength. Wood ash has also been seen to reduce the thermal conductivity of cement, improving its insulation properties [Madrid et al. 2017].

To the author's knowledge, the present study marks a first in utilizing wood ash as a supplementary cementing material for insulating foams. In what follows, the mechanical, thermal, and acoustic properties of these cementitious foams are characterized for a range of cast densities. It is hoped that the data generated here will lead eventually to standards and guidelines for the widespread use of wood ash as a cement substitute.

4.3 Experimental Procedure

4.3.1 Materials

The Portland cement used throughout this study is classified as Type GU per CSA A3001 [CSA 2013], (corresponds to ASTM Type 1 [ASTM 2007]). The wood ash was supplied by an Alberta based pulp and paper mill from the combustion of hog fuel. The wood ash contained large particles of partially combusted fuel, which were removed by passing the ash through a 0.6 mm sieve. A backscattered electron microscope (BSEM) image of the sieved wood ash is shown in Figure 4.1. A wide variety of particle shapes and sizes can be observed. In particular, small crystalline particles are seen intermixed with larger, irregularly shaped particles that appear fibrous. The sieved wood ash was tested for loss on ignition by heating to 750°C as per ASTM D7348 [ASTM 2013] and was found to have 8.20% loss on ignition. The sieved wood ash was also analysed by X-ray fluorescence to determine its chemical composition, the results of which are shown in Table 4.4. Glass microfibers with a diameter of 37 μm and length of 12 mm were used to reinforce the cement foams. A protein-based foaming agent diluted in water to a ratio of 1:33 was used to produce the preformed foam used to create the cellular microstructure.

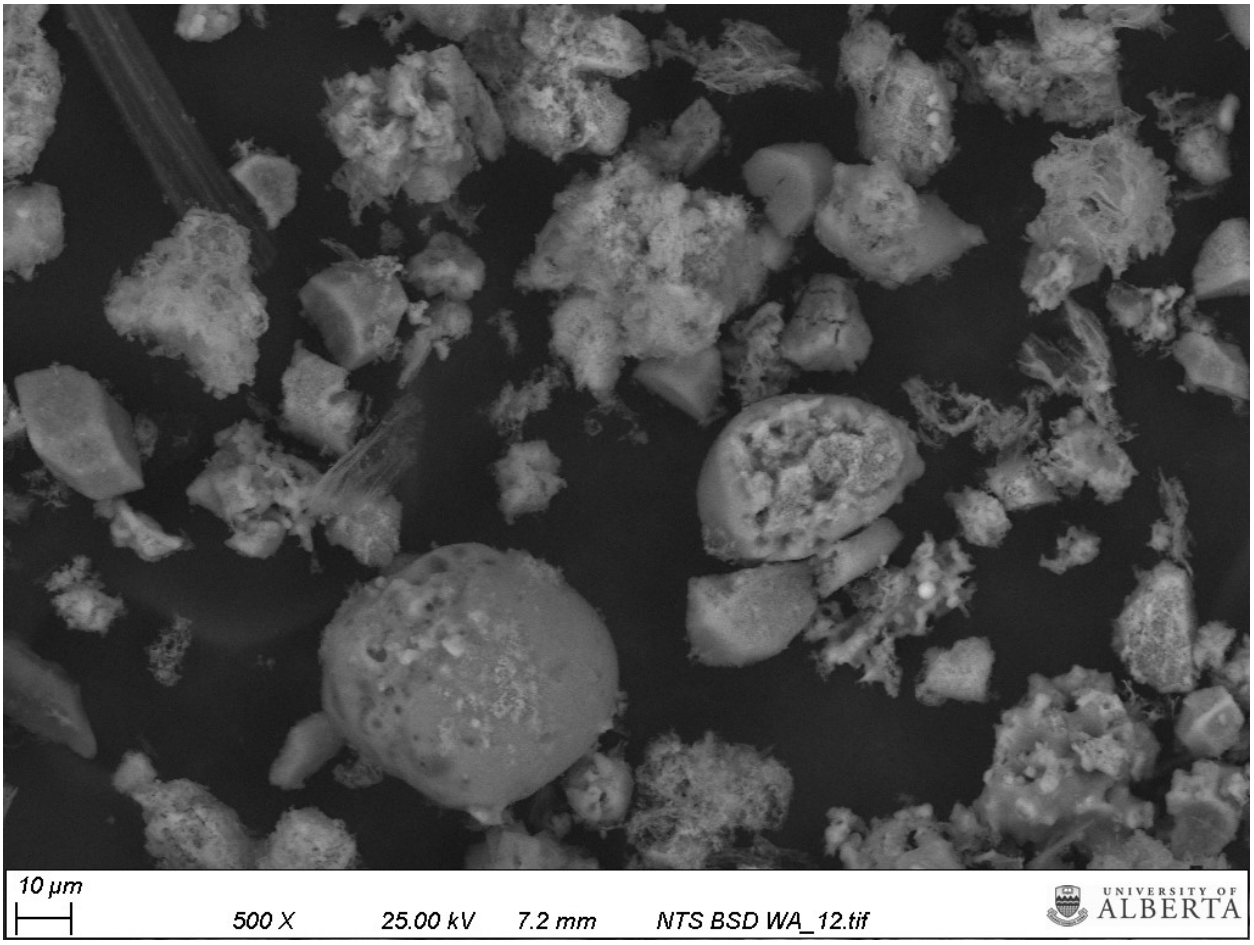

Figure 4.1: Backscattered Electron Microscope (BSEM) Image of the Wood Ash

Table 4.4: Composition of Wood Ash as found by X-Ray Fluorescence

1.22	2.21	1.62	5.29	4.69	82.7	0.28	0.38	1.05	0.23	0.34
Si	Y	P	S	K	Ca	Ti	Mn	Fe	Zn	Sr

4.3.2 Specimen Preparation

The mix designs for the cement foam specimens are presented in Table 4.5. The slurry was prepared based on a water to binder ratio of 0.69, with the Portland cement being replaced

variously by wood ash at 0%, 10%, or 20% by mass. Glass microfibers shown in Figure 4.2 were included at a volumetric ratio of 1% of the target volume of the foamed composite. This helps increase the strength by reinforcing the cellular microstructure. The fibres were 45 Tex and 12mm long. This corresponds to a diameter of 37 μm with an aspect ratio of 328. The cement-based foam was prepared with the help of a preformed foam. To begin with, a slurry was prepared by mixing water with the Portland cement (and wood ash, if any) in a drum mixer. Once the water was fully combined with the cement and wood ash, the glass microfibers were added and mixed until they were deemed evenly distributed in the slurry. At this point, using the foam generator shown in Figure 4.3, a pre-formed foam was produced using the diluted foaming agent described earlier. It was gradually introduced into the drum while the mixer continued to run. Periodically, a small sample of the resulting foamed cementitious slurry was taken out and weighed, thereby evaluating its density. Once the target cast density was achieved, the mixture was cast into cylindrical moulds. These moulds were lined with waxed paper to facilitate the easy removal of the samples later.

Figure 4.2: Glass Microfibres used in Foamed Composite

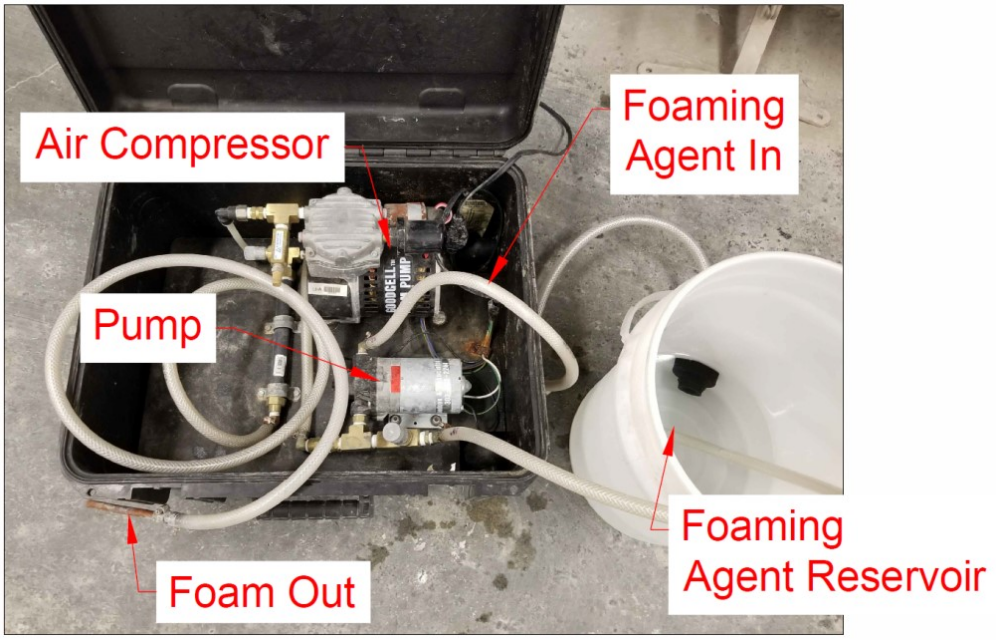

Figure 4.3: Generator for Preformed Foam

For each mixture, a total of 6 cylinders were cast having a diameter of 75 mm and 150 mm in height. Two additional cylinders were cast with a diameter of 50 mm and 100 mm in height. One cylinder, Ø100 mm x 100mm in dimension and another, with a diameter of 50 mm and 100 mm in height, were cast to fit the specimen holders for the acoustic test. The specimens were left covered and allowed to cure for 24 hours before being removed from their moulds. They were then kept in a chamber under controlled temperature (21 °C) and 100% humidity, for a further 24 days. At 25 days of curing, the specimens were moved to ambient conditions, so that they may be prepared for further tests. Four Ø75 mm X 150 mm specimens were end-ground and designated for compression testing. Two additional Ø75 mm x 150 mm specimens were dried overnight in an oven at 105 °C to obtain the oven-dried density of the mixture. The Ø50 mm x 100 mm cylinders were sawn to yield 3 pairs of disks, each 30 mm in thickness. These were assigned for thermal testing. Lastly, the Ø100 mm and Ø50 mm cylinders were cut to 50 mm

thickness and sanded to fit tightly within the Ø100 mm and Ø30 mm specimen holders within the impedance tube set-up. Thereafter, all the samples were allowed to dry for a further 3 days in ambient conditions prior to test.

Table 4.5: Cement Foam Mix Designs

	Cement (kg/m^3)	Wood Ash (kg/m^3)	Water (kg/m^3)	Glass Microfibers (kg/m^3)
1000 kg/m^3 0% Ash	575.9	0	397.3	26.8
1000 kg/m^3 10% Ash	518.3	57.6	397.3	26.8
1000 kg/m^3 20% Ash	460.7	115.2	397.3	26.8
1200 kg/m^3 0% Ash	694.2	0	479.0	26.8
1200 kg/m^3 10% Ash	624.8	69.4	479.0	26.8
1200 kg/m^3 20% Ash	555.4	138.8	479.0	26.8
1400 kg/m^3 0% Ash	812.5	0	560.7	26.8
1400 kg/m^3 10% Ash	731.3	81.2	560.7	26.8
1400 kg/m^3 20% Ash	650.0	162.5	560.7	26.8

4.3.3 Compression Test

Compressive strength tests were performed according to ASTM C495/C495M-12 [ASTM 2012]. A displacement rate of 0.8 mm/s was used as per this standard. As stated earlier, four cylinders were designated for compression out of each batch. Two specimens were tested initially to determine the peak compressive load. The remaining two were fitted with a digital compressometer as shown in Figure 4.4, in order to measure the axial and transverse strains in the sample, with the load increasing up to 50% of the peak compressive load found earlier. The stress and strain measurements were logged by a data acquisition system at 1 Hz.

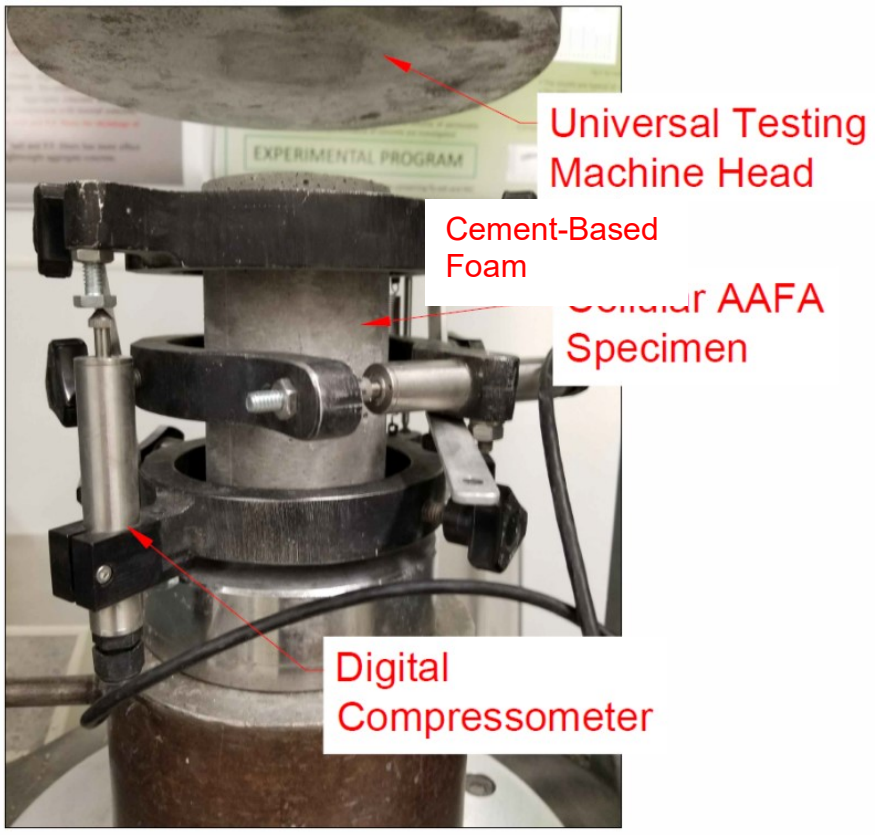

Figure 4.4: Cement-Based Foam Specimen in a Digital Compressometer during a Compression Test

4.3.4 Thermal Test

The thermal constants were measured using the Transient Plane Source (TPS) method, as described in ISO 22007-2 [ISO 2015], with a Hot Disk TPS 1500 system. These tests were performed in ambient conditions (room temperature 21° C). Each test ran for 180 s and employed heat generated by a power of 51.33 mW. After each test, the same pair of specimens were oven dried at 105° C for 24 hours, and thereafter, allowed to cool to room temperature in a sealed, desiccated environment. Each such pair was retested to obtain the thermal constants of the mixture under oven dried conditions. The sensor was a 3.189 mm radius double spiral encased in Kapton. This Kapton sensor was sandwiched between a pair of disks, as shown in Figure 4.5. A change in the temperature is accompanied by a change in the resistance of the spiral, and the resulting voltage drop is measured. By measuring the current and voltage drop through the sensor over a period of time, the thermal properties of the specimen can be calculated [Log and Gustafsson 1995].

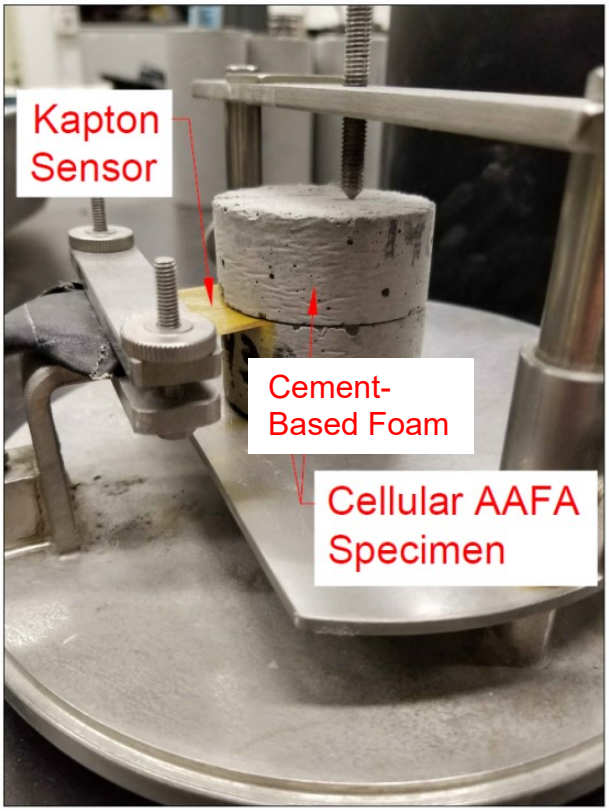

Figure 4.5: Cement Foam Specimen Mounted for Thermal Testing

4.3.5 Acoustic Test

The cement-based foams were tested for acoustic performance using an impedance tube, as described in ASTM C384-04 [ASTM 2011]. The apparatus is shown in Figure 4.6. The impedance tube was a Bruel & Kjaer Model 4002 equipment with a 100 mm diameter tube for low frequencies and a 30 mm diameter tube for high frequencies. Each cylinder at the respective diameter was cut to 50 mm thick disks and the faces were ground to expose the pore structure. The circumference was sanded down to allow it to fit snuggly inside the specimen holder for the respective impedance tube. The sound was sourced by a Bruel & Kjaer Type 1013 Beat Frequency Oscillator, while the acoustic response was measured with a Bruel & Kjaer Type

2113 Audio Frequency Spectrometer. The standing wave pattern was measured using the microphone trolley connected to an analogue audio frequency spectrometer. The Standing Wave Ratio, $SWR(x)$, at a location, x, from the face of the specimen, is the ratio of the maximum sound pressure to the minimum sound pressure at that location. The pressure reflection coefficient, Γ, and subsequently, the *normal incident* sound absorption coefficient, α_n, can be calculated as:

$$|\Gamma| = [SWR(0) - 1]/[SWR(0) - 1] \quad \ldots[1]$$

and

$$\alpha_{\mathrm{n}} = 1 - |\Gamma|^2. \quad \ldots[2]$$

This is repeated for each frequency of interest and the absorption coefficient may then be plotted. By measuring the locations and amplitudes of the maxima and minima of the standing wave, the normal incident sound absorption coefficient, α_n, can be calculated for that specific frequency. This coefficient ranges from 0 to 1, where 0 implies that all sound is reflected off the surface and 1 means that all sound is absorbed by the material [Everest and Pohlmann 2009]. When applied to sound insulation indoors, higher values of α_n are desirable to reduce the echo and related noise.

The Noise Reduction Coefficient, NRC, is the average of the sound absorption coefficients specifically measured at 250 Hz, 500 Hz, 1000 Hz, and 2000 Hz, as defined in ASTM C423. Typically, this would be calculated using the *random* incident sound absorption coefficients, but the same can be done with the *normal* incident sound absorption coefficients, which yields a convenient measure of the sound insulating performance of the material.

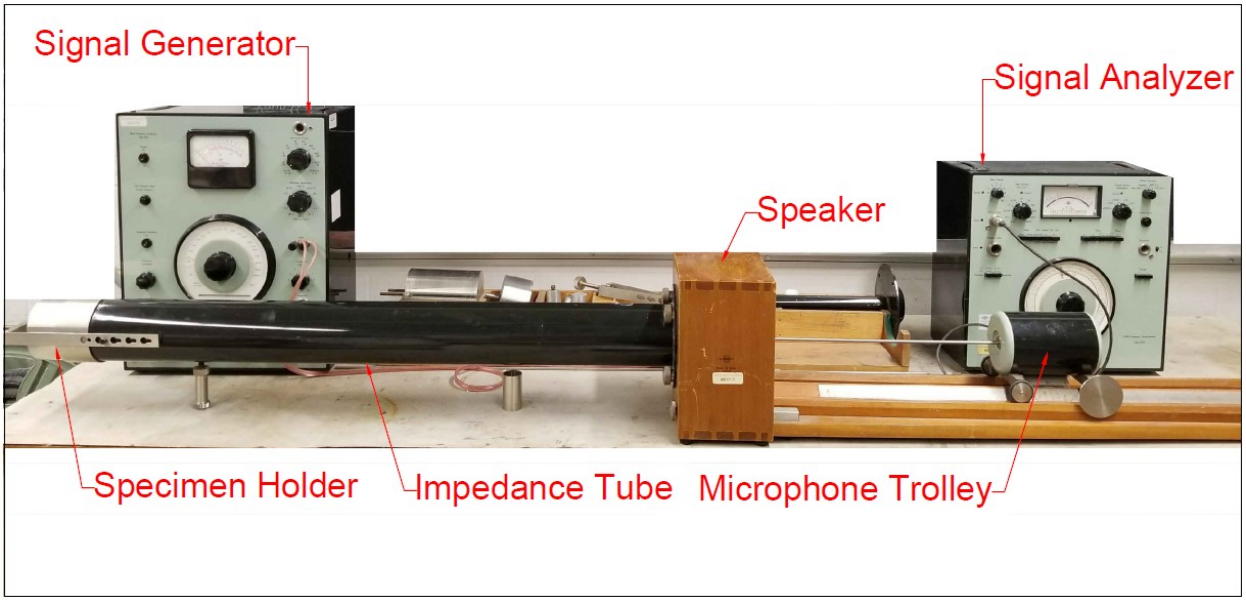

Figure 4.6: Impedance Tube Apparatus for Determining Normal Incident Sound Absorption Coefficient

4.4 Results and Discussion

4.4.1 Densities

The density of the cement-based foams was measured at casting, after 3 days drying in ambient conditions, and after oven drying. These are reported in Table 4.6. Note that adding increasing amounts of wood ash to the Portland cement binder causes a larger difference between the oven dry, and cast densities. This shows that there is a higher percentage of free water left in mixtures with higher wood ash contents.

Table 4.6: Densities for Cement Foam with Wood Ash

Target Cast Density (kg/m^3)	Percentage of Wood Ash	Actual Cast Density (kg/m^3)	Ambient Dried Density (kg/m^3)	Oven Dried Density (kg/m^3)
1000	0%	1026	930	736
	10%	1022	892	710
	20%	1004	855	679
1200	0%	1230	1128	865
	10%	1155	1028	830
	20%	1170	1017	841
1400	0%	1400	1317	1074
	10%	1308	1183	971
	20%	1357	1219	981

4.4.2 Microstructural Properties

Figure 4.7 displays backscattered electron microscope (BSEM) images of the cement-based foam samples containing 0%, 10%, or 20% wood ash, respectively. An increase in the wood ash appears to leave fewer crystalline phases visible in the micrograph. The fibrous particles seen in the unreacted wood ash were not observed in the hydrated products of blended binder, suggesting that much of the wood ash went into reaction in the hydrated paste. Figure 4.8 displays laser confocal micrographs of the cement-based foams showing the cellular structure of the material. The porosity of the foams clearly increases with decreasing density.

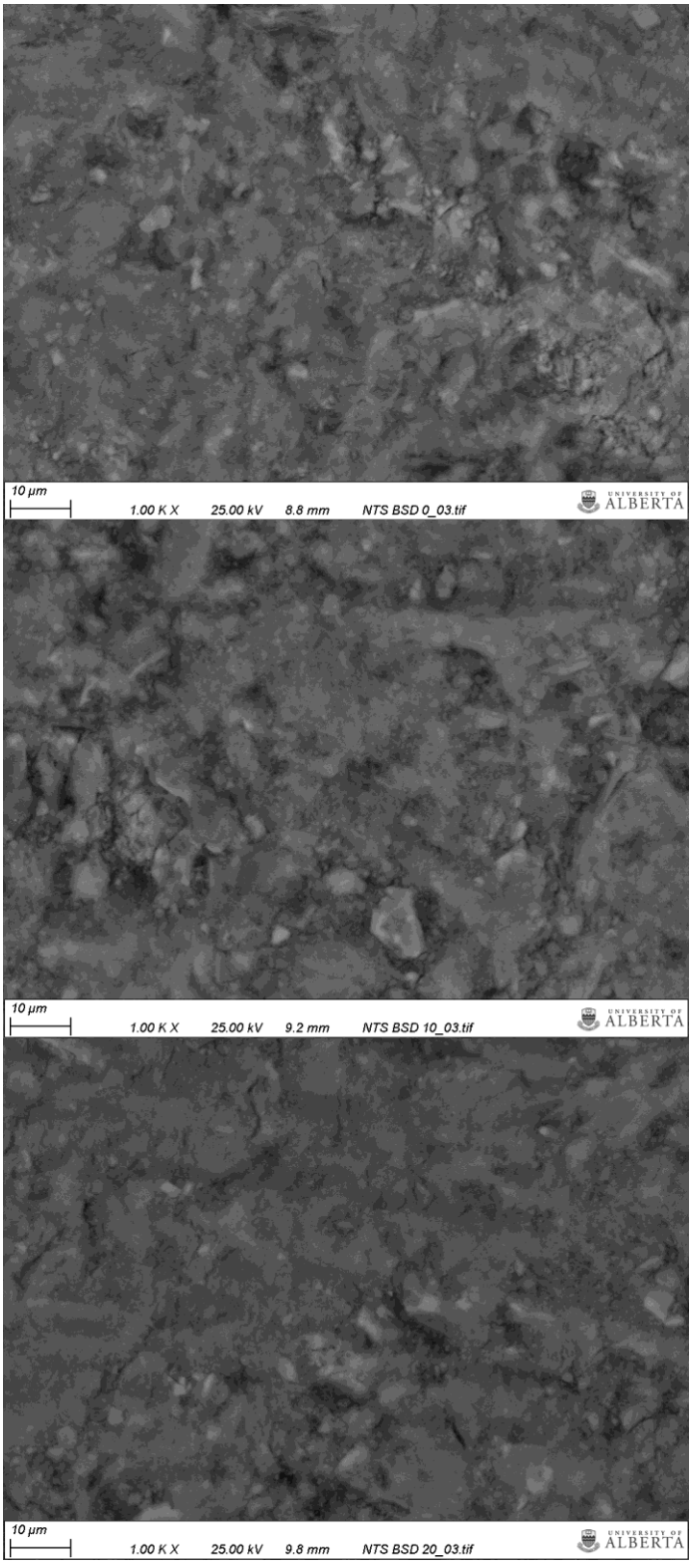

Figure 4.7: Backscattered Electron Microscope Images of Cement with 0%, 10%, and 20% (Top to Bottom) Wood Ash

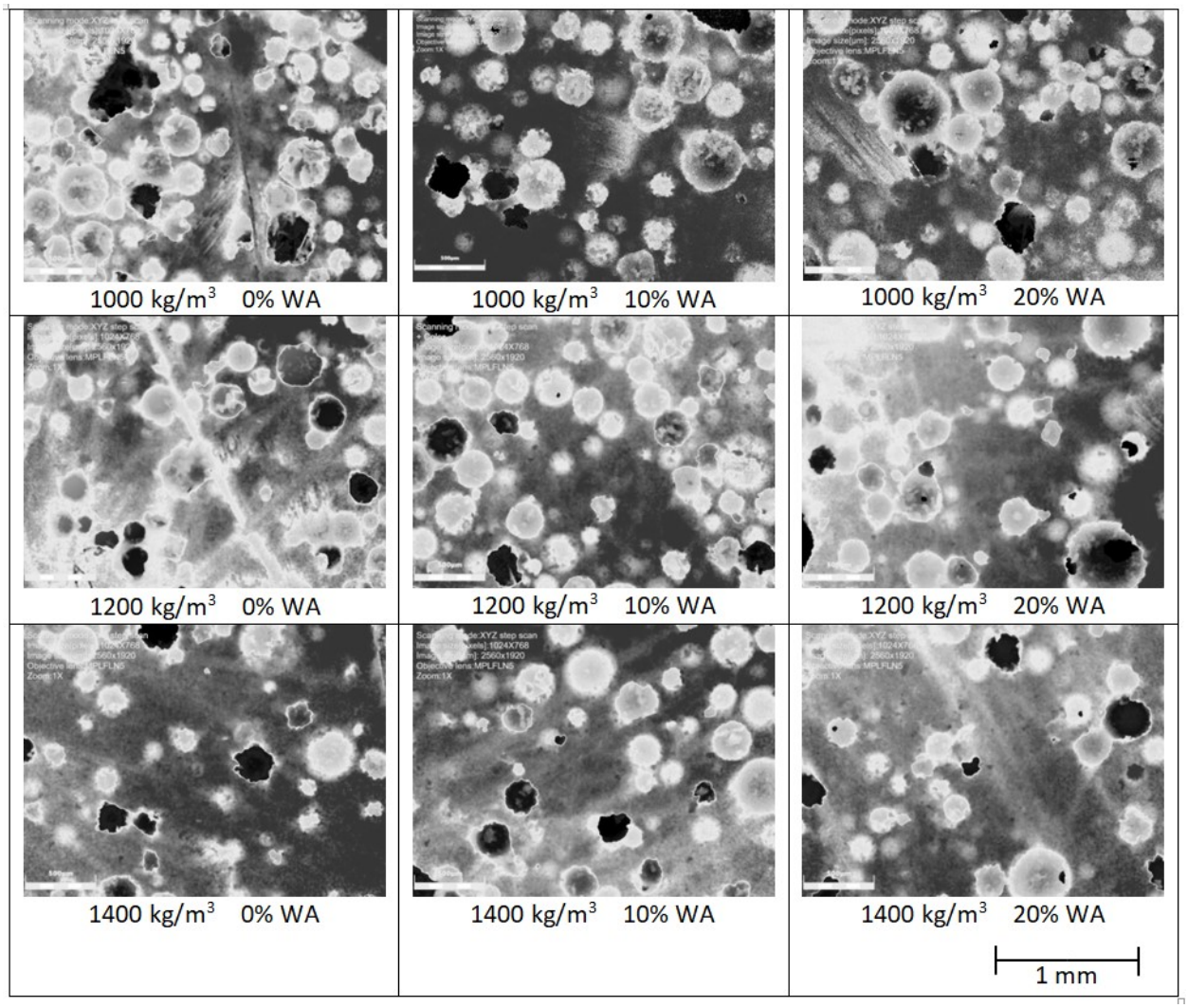

Figure 4.8: Micrographs of Cement Composite Foams

Figure 4.9 displays the X-ray diffractograms taken for the powder samples representing the solid cell walls in the cementitious foam. Notice the significant presence of Portlandite and Ettringite in all mixtures, while Calcite and Apophyllite also appear, albeit to a lesser extent. Recall from Table 4.4 that the wood ash is rich in calcium oxide. From the rising intensity of Portlandite peaks in the X-ray spectra, it appears that blending wood ash into the binder results in an increase in the Portlandite phase in the hydrated paste.

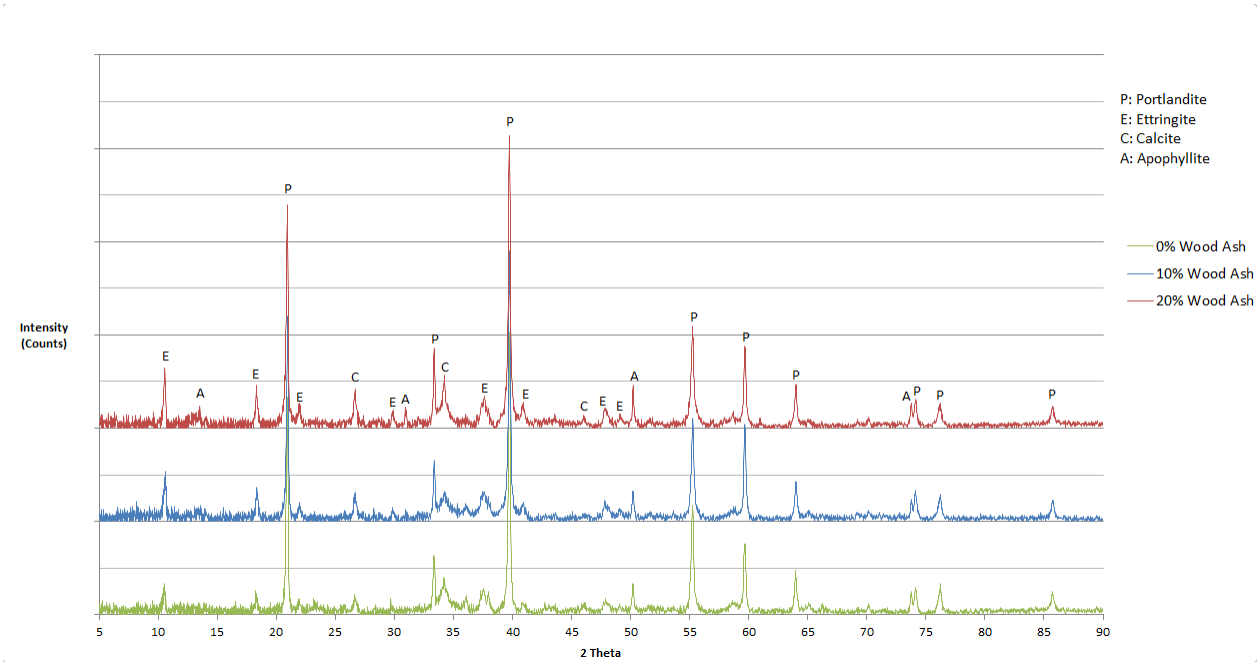

Figure 4.9: XRD Analysis of Cement With 0%, 10%, and 20% Wood Ash

4.4.3 Mechanical Properties

Figure 4.10a-c shows the stress-strain response in compression as found for the various mixtures. The ultimate compressive strength of the cement foams is plotted against their ambient dried densities in Figure 4.11. Note the pronounced leftward shift of data points for the blended binders compared to data points for the reference series with Portland cement alone. This is caused by the loss of greater amounts of free water, as more wood ash is used. The reference Portland cement based foam has strengths from 7 MPa to 14.5 MPa across the density range. Whereas adding wood ash at 10% cement replacement to the binder did not significantly affect the compressive strength, at 20% cement replacement, there was a 20% drop in strength but also a reduction in density. Setayeshgar 2017 also found that increasing amounts of wood ash in cement reduced the compressive strength.

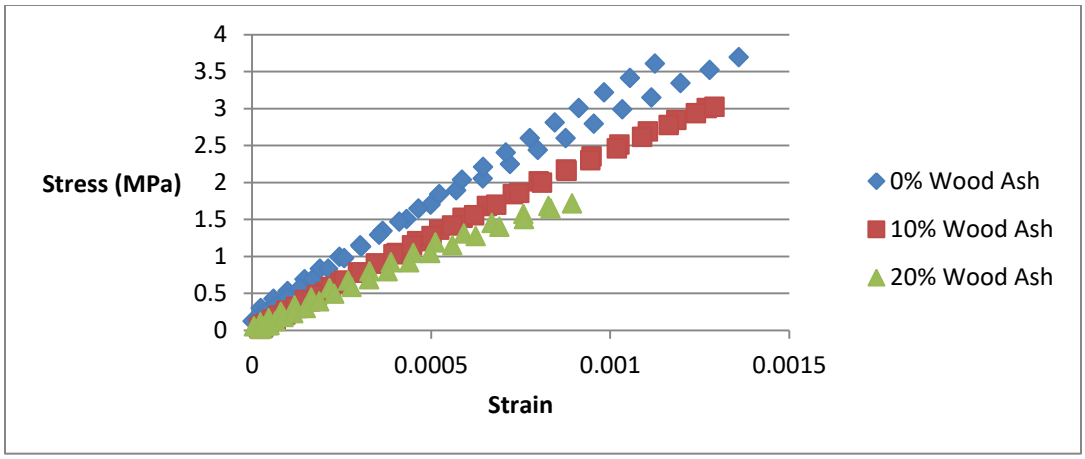

Figure 4.10a: Stress Strain Curves for Composite Foams with 1000 kg/m^3 Cast Density

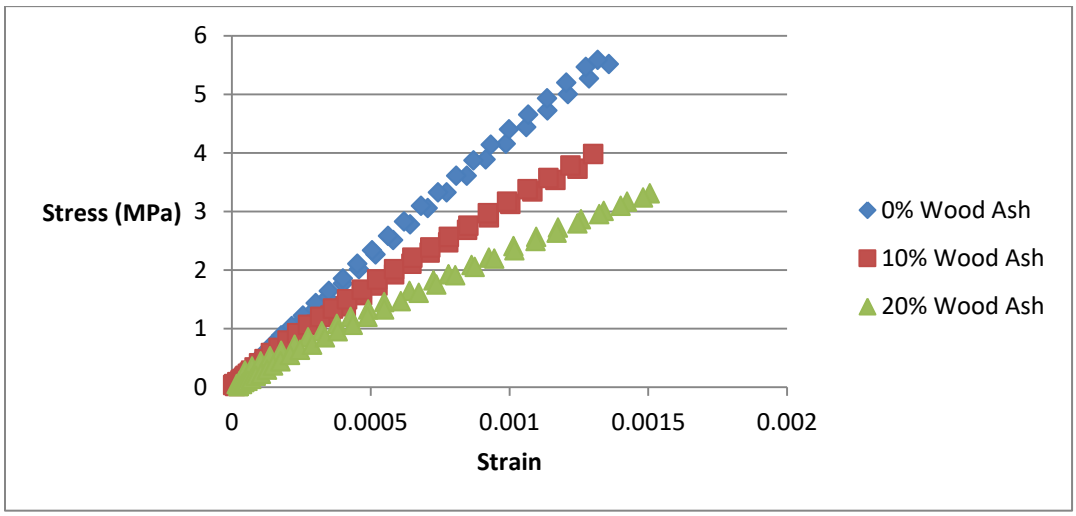

Figure 4.10b: Stress Strain Curves for Composite Foams with 1200 kg/m^3 Cast Density

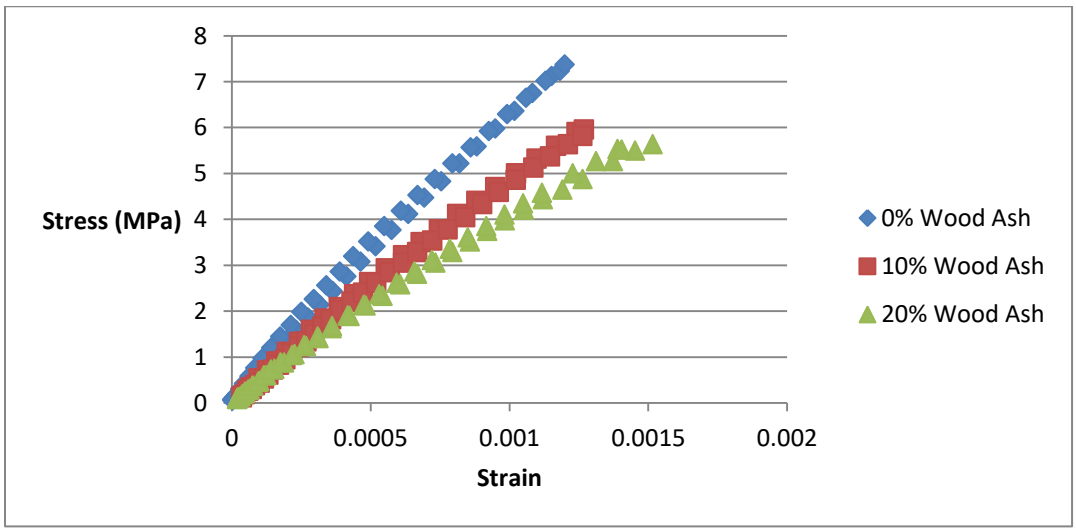

Figure 4.10c: Stress Strain Curves for Composite Foams with 1400 kg/m^3 Cast Density

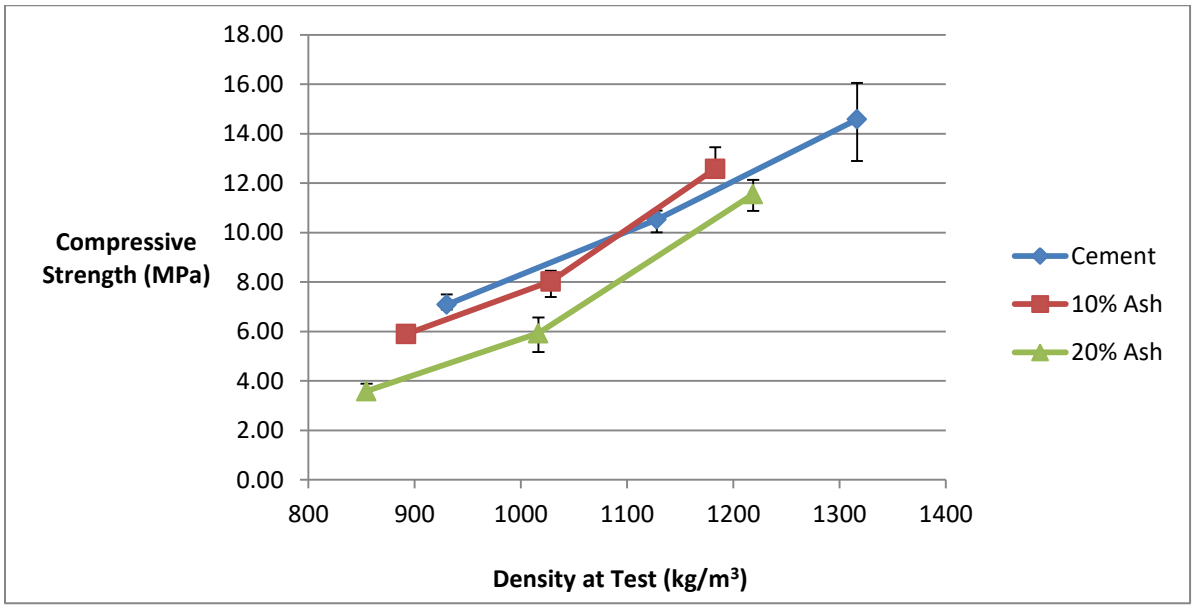

Figure 4.11: Compressive Strength for Cement Foam with Wood Ash

The modulus of elasticity and Poisson's ratio for the cement-based foams are presented in Figure 4.12a and Figure 4.12b respectively. The modulus of elasticity ranged from 2860 MPa to 6160 MPa for the reference foam mixture containing Portland cement alone. When incorporating wood ash in the binder, there was no significant change upon 10% cement substitution, but a 35% drop upon 20% cement substitution. This correlates with the trends seen in the compressive strength of the foams. In general, the Poisson's ratio rose with the density at test with a 20-25% increase corresponding to the 40% rise in density. This was true across the three mixture compositions. In lighter foams, the buckling of the cell wall leads to a collapse mechanism under compression, which in turn leads to lower transverse strains. A lower Poisson's ratio is therefore as expected.

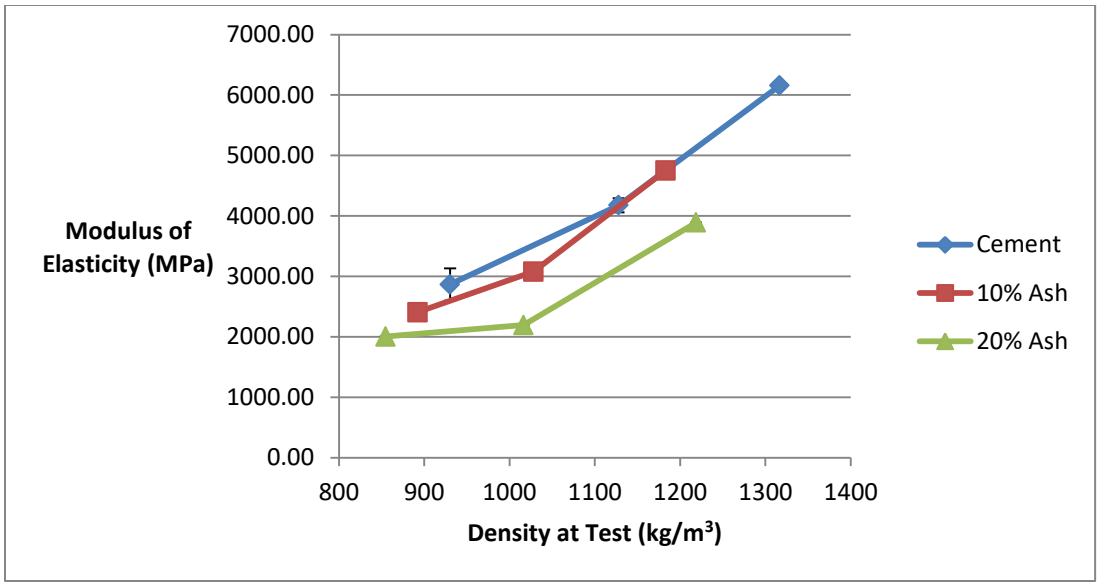

Figure 4.12a: Modulus of Elasticity for Cement Foam with Wood Ash

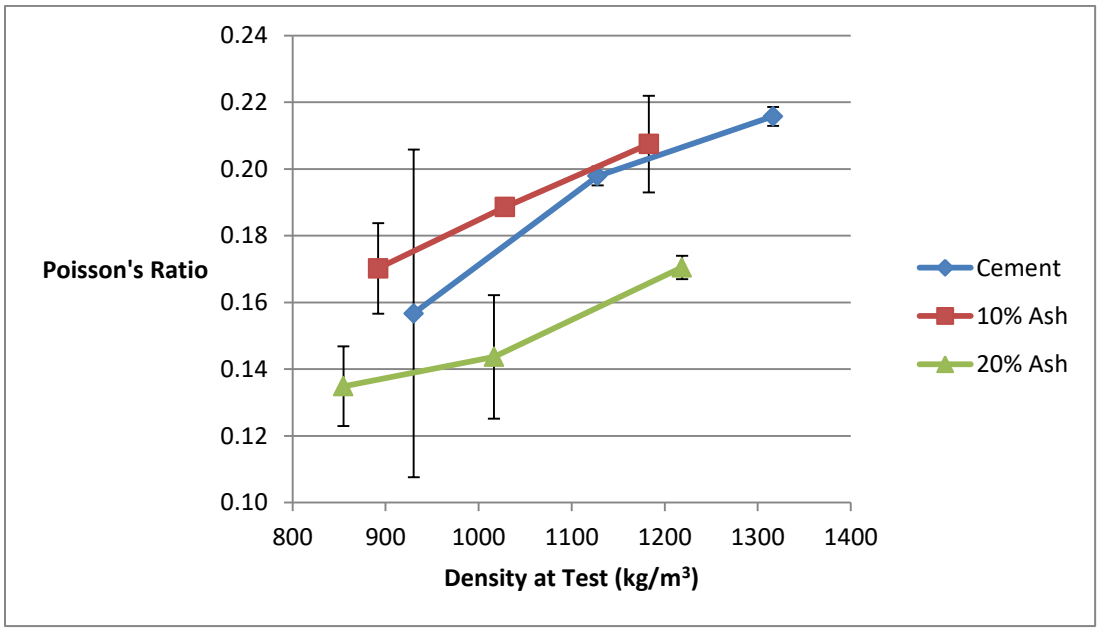

Figure 4.12b: Poisson's Ratio for Cement Foam with Wood Ash

4.4.4 Thermal Properties

The thermal conductivity and heat capacity of ambient dried cement foams are plotted against their ambient dried densities in Figure 4.13a and Figure 4.13b, respectively. Note that the thermal conductivity of the reference mixture containing Portland cement alone was between 0.44 W/mK to 0.56 W/mK, while that for the blended binder was between 0.32 W/mK to 0.53 W/mK. The addition of wood ash noticeably reduces the thermal conductivity of the cement-based foams, but there is little to differentiate between cement substitution with 10% wood ash with 20% wood ash. In case of the heat capacity, there was an inconsistency in the variation with density, that was deemed due to the moisture contained within. As was mentioned earlier, in order to eliminate the effect of free water on the measured thermal properties, the same specimens were oven dried, and thereafter, tested again.

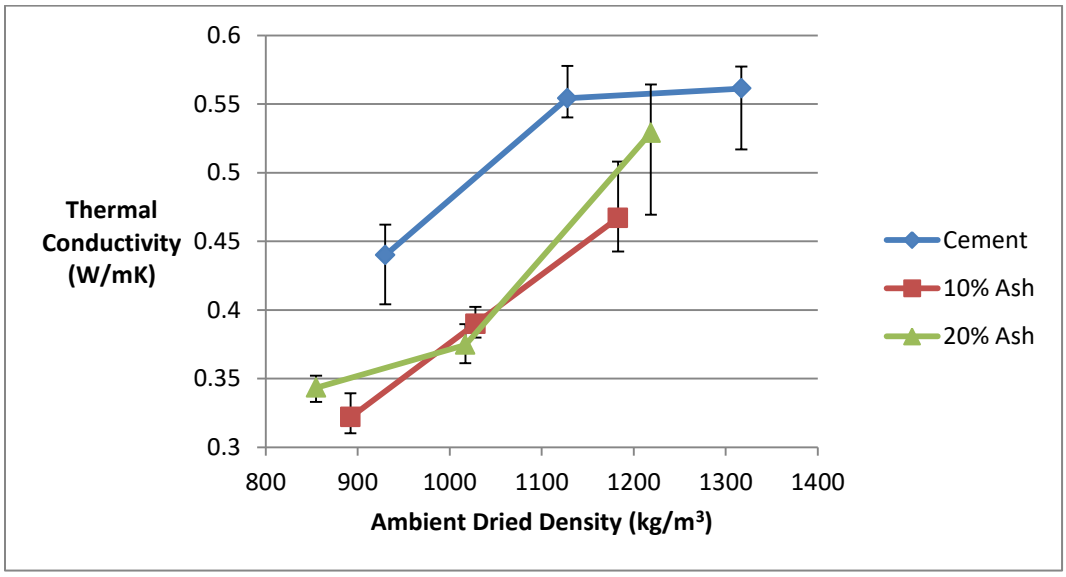

Figure 4.13a: Thermal Conductivity of Ambient Dried Cement Foam with Wood Ash

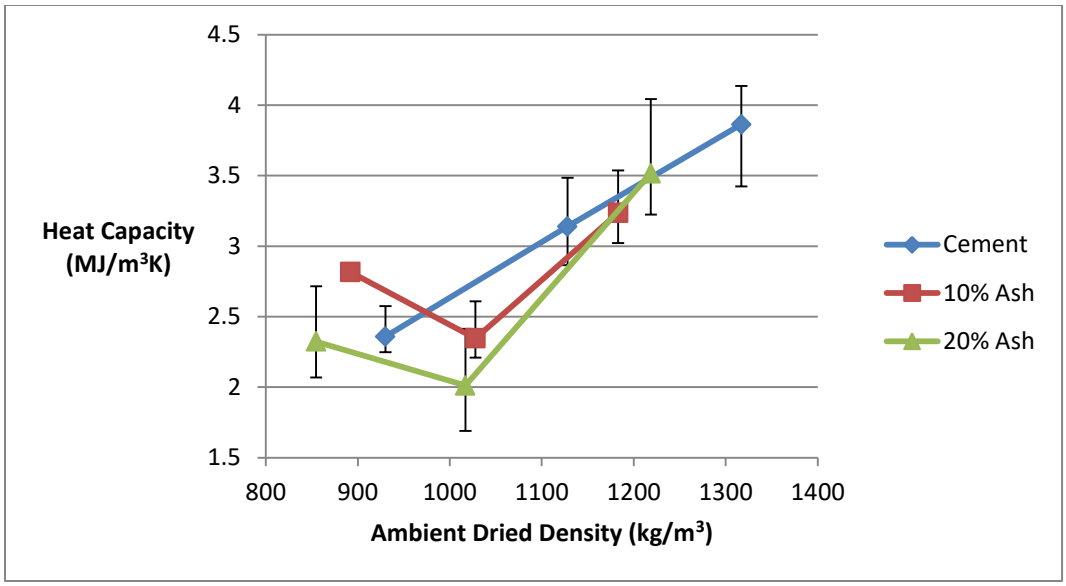

Figure 4.13b: Heat Capacity of Ambient Dried Cement Foam with Wood Ash

The thermal conductivity and heat capacity of the oven dried cement-based foams are shown in Figure 4.14a and Figure 4.14b, respectively. The thermal conductivity is plotted over a background of thermal conductivities of other materials from the NIST SRD81 database [Zarr et al. 2016]. As expected upon oven drying, the specimens depict a significantly reduced thermal conductivity and heat capacity. Adding wood ash to the binder caused a 15% drop in thermal conductivity, although once again, there was little difference between the binders containing 10% and 20% wood ash. Oven drying led to a 30% drop in the thermal conductivity across all samples. The heat capacity of the oven-dried cement-based foams increased with density as is expected. This suggests that the inconsistency seen previously was due to the irregularity in the moisture contained in the specimen as it dried under ambient conditions. The heat capacity of the oven dried foams shows very little change with the use of wood ash.

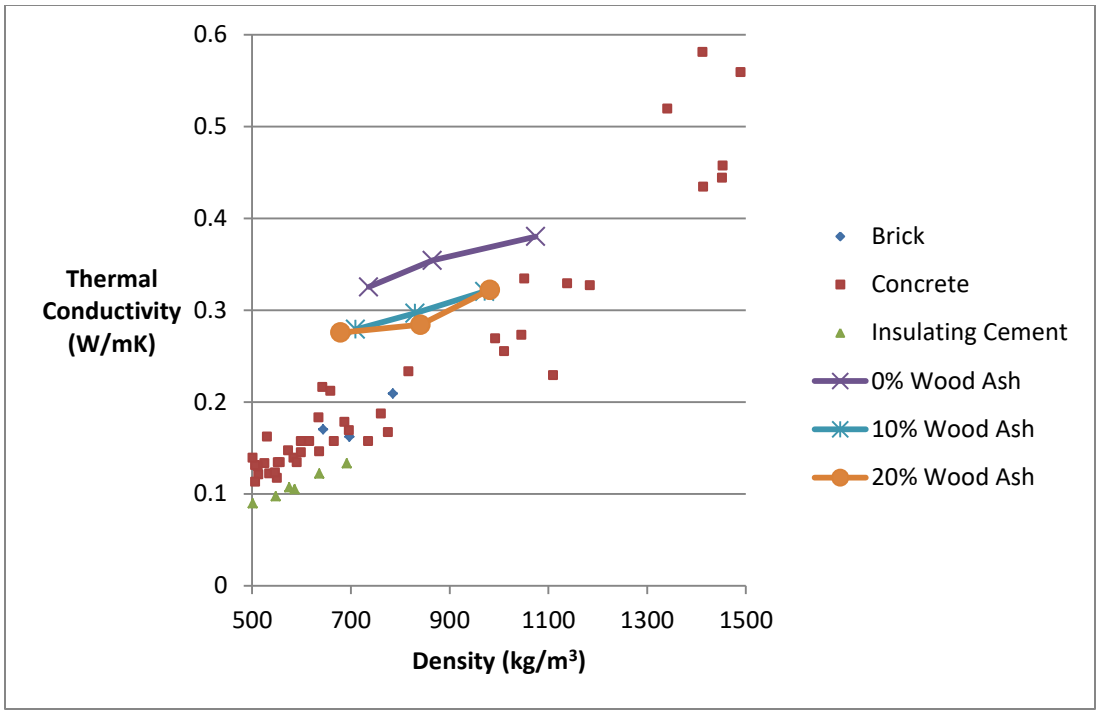

Figure 4.14a: Thermal Conductivity of Oven Dried Cement Foam with Wood Ash

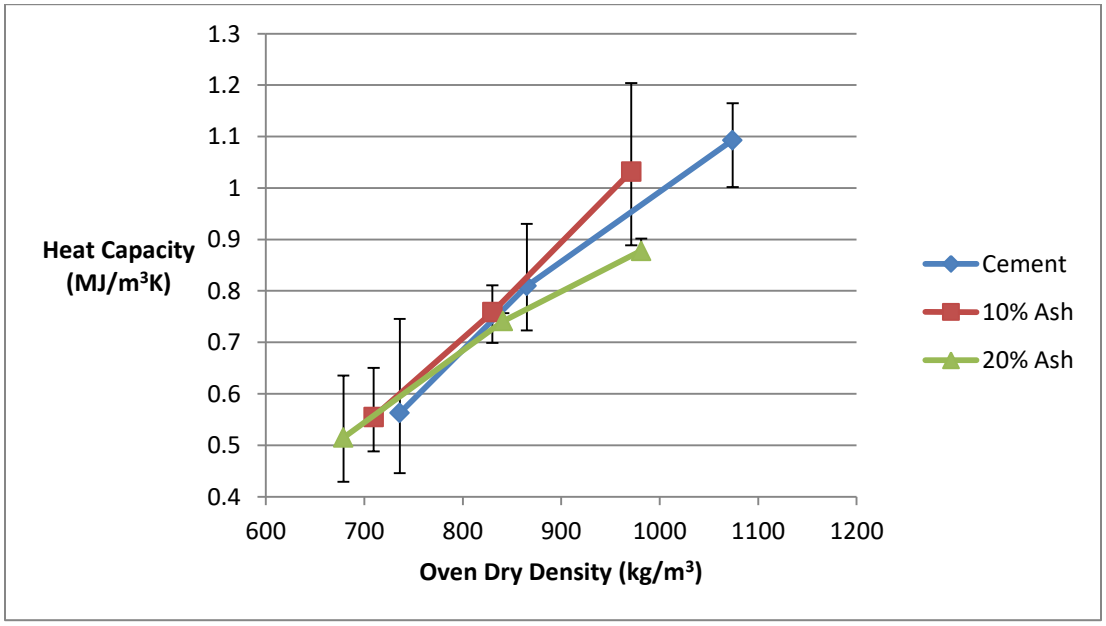

Figure 4.14b: Heat Capacity of Oven Dried Cement Foam with Wood Ash

4.4.5 Acoustic Properties

The normal incident sound absorption coefficients for frequencies from 125 Hz to 6300 Hz are presented in Figure 4.15a-c, grouped according to their cast density. One notes that in general, the cement-based foams have high sound absorption at very low frequencies and very high frequencies, but relatively low absorption in the range of 250 Hz to 2000 Hz. Kim et al. produced sound absorbing concrete by the addition of cellulose fibres and foaming agents and similarly found the material to have distinct peaks and valleys [Kim et al. 2018]. The location of these peaks was largely affected by the void ratio in the concrete. Similar tends can be seen in the foam geopolymer produced by Zhang et al. [2015] and the foamed geopolymer produced by the author, and reported in chapter 3.

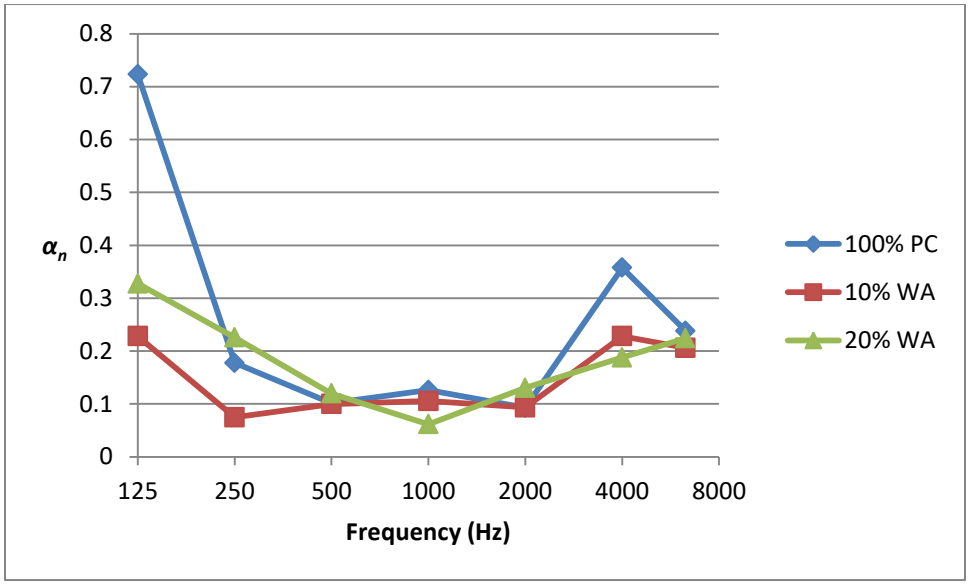

Figure 4.15a: Sound Absorption Coefficient for Cement Foams cast near 1000 kg/m^3

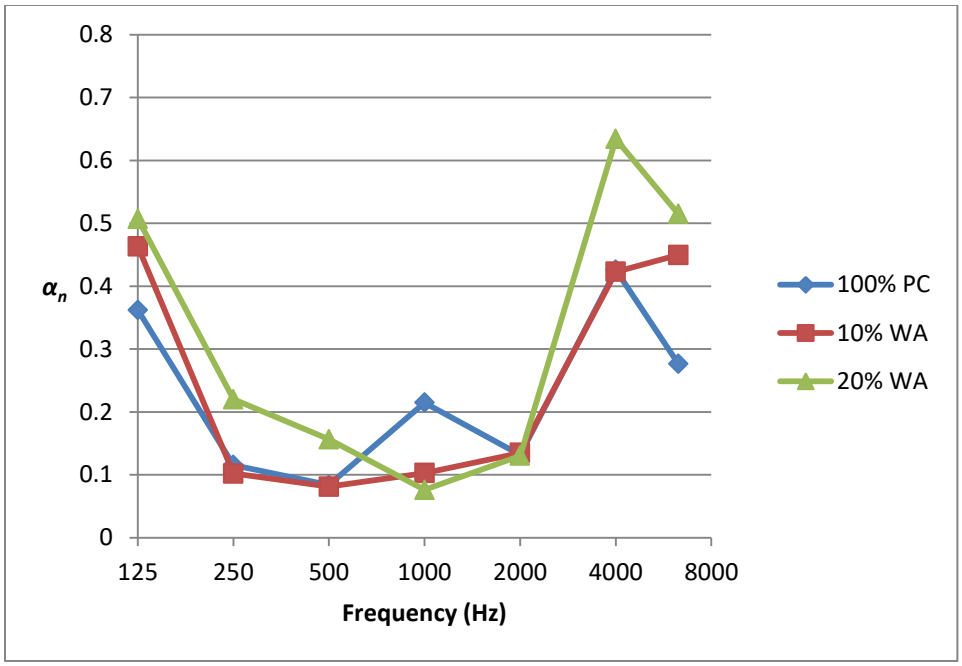

Figure 4.15b: Sound Absorption Coefficient for Cement Foams cast near 1200 kg/m^3

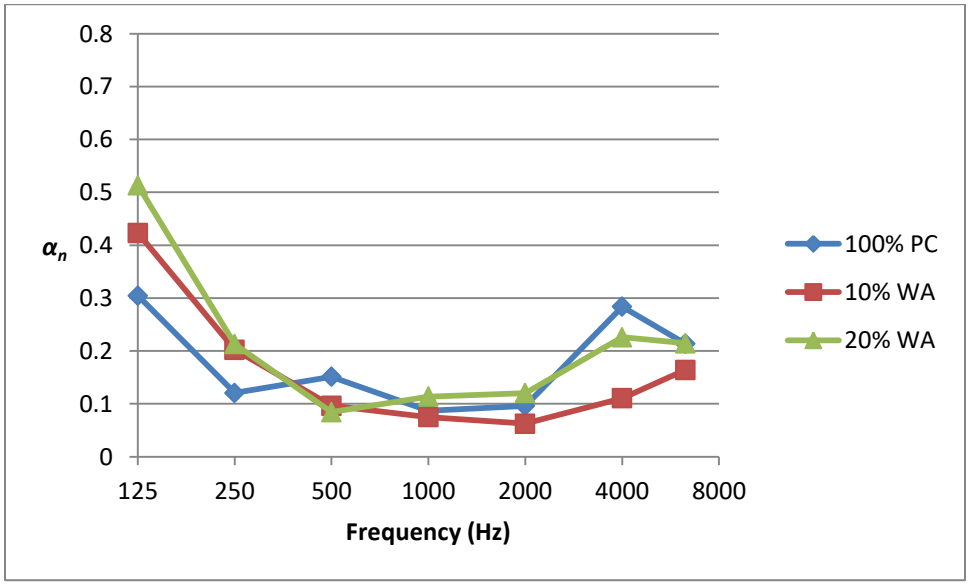

Figure 4.15c: Sound Absorption Coefficient for Cement Foams cast near 1400 kg/m^3

The noise reduction coefficients for the cement-based foams are shown in Figure 4.16. As seen therein, the NRC ranged from 0.08 to 0.14. The NRC for a selection of other common materials is shown for reference [Vorländer 2008]. The cement-based foams perform as well, or better than many common materials. In terms of binder composition, the NRC was highest for the reference mixture containing Portland cement alone. However, it appears that the intermediate density, cast at around 1200 kg/m^3, produced the highest noise reduction coefficient across the mixtures. A similar trend was seen in geopolymer foams cast in the same range of densities. Although a lower density foam is typically a better sound insulator, sound absorption depends not only on the total porosity but also on the surface roughness. A closer look is warranted in order to understand why the foams that contained wood ash, although leading to lower densities at test, still showed up at lower NRC than the reference series containing Portland cement alone, in spite of the latter being heavier. Studies are ongoing to quantify the internal air-void network and tortuosity.

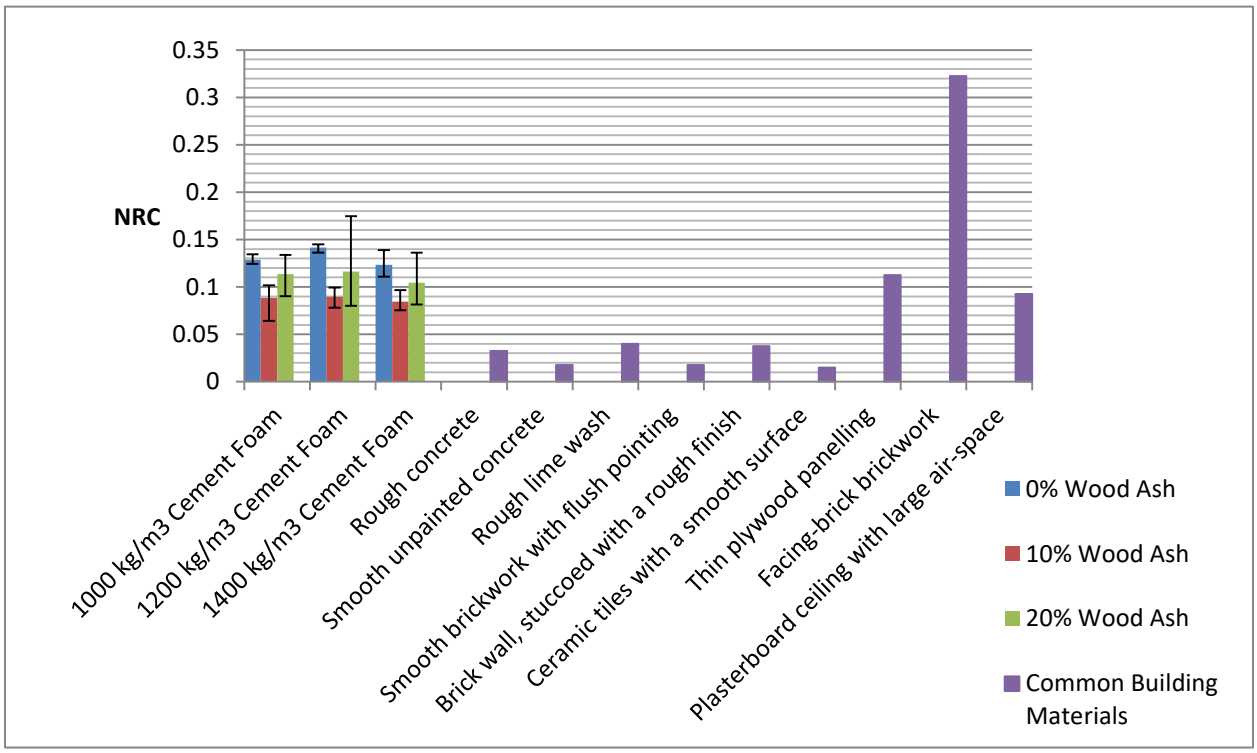

Figure 4.16: Noise Reduction Coefficients of Cement Foams with Wood Ash

4.6 Concluding Remarks

Wood ash from the combustion of hog fuel was used as a supplementary cementing material in the production of cement-based foams. The cellular composites were cast at densities from 1000 kg/m^3 to 1400 kg/m^3 by blending in up to 20% wood ash as cement replacement. They were tested to evaluate their mechanical, thermal, and acoustic properties. The addition of wood ash resulted in a measurable drop in density, accompanied by a reduction in thermal conductivity and acceptable mechanical performance at 10% cement replacement. Substituting up to 10% Portland cement with wood ash in cementitious foams is thus a viable alternative towards sustainable

thermal insulation. The experimental results presented here lead to the following specific findings:

The wood ash obtained from Alberta's pulp and paper mills was seen to be rich in calcium oxides, marking it as a source of basic oxides for cement substitution. This was borne out from the X-ray diffractograms conducted on the solid phase constituting the foam cell wall, where a greater intensity was noted for Portlandite.

Cement based foams were consistently lighter when wood ash was introduced as cement substitute. Wood ash also appeared to increase the water demand during the production of the foamed composite.

There was no significant change in strength at 10% cement substitution but, a 25% drop in strength and elastic modulus was registered in case of binder containing 20% wood ash.

The thermal conductivity of cementitious foams was 15% lower when blending in wood ash. In oven dried systems, there was no perceptible difference in the heat capacity.

Cement-based foams containing wood ash displayed lower NRC than the reference mixture. The optimal density was near that of water, resulting in the highest NRC across all compositions.

4.7 References

Anonymous (2017). "Acoustic Ceiling Tiles and Panels." https://www.ceilume.com/shop/acoustic-ceiling-tiles/index.cfm#nrc25, (accessed 6 Dec 2017).

ASTM (2013). "D7348 Standard Test Methods for Loss on Ignition (LOI) of Solid Combustion Residues." .

ASTM (2012). "C495/C495M Standard Test Method for Compressive Strength of Lightweight Insulating Concrete." .

ASTM (2011a). "C384 Standard Test Method for Impedance and Absorption of Acoustical Materials by Impedance Tube Method." .

ASTM (2007). "C150 Standard Specification for Portland Cement." .

Batool, F., and Bindiganavile, V. (2018). "Thermal conductivity of hydrated paste in cement-based foam microstructure." *Adv.Civ.Eng.Mater.,* 7(1), 17-32.

Batool, F., and Bindiganavile, V. (2017). "Air-void size distribution of cement based foam and its effect on thermal conductivity." *Constr.Build.Mater.,* 149 17-28.

CSA (2013). "CSA A3001-13 Cementitious Materials Used in Concrete." .

Everest, F. A., and Pohlmann, K. C. (2009). *Master handbook of acoustics.* McGraw-Hill, New York, NY ; London.

Fouad, F. H. (2006) "Chapter 47: Cellular Concrete." (169), 561.

Garcia, M. D. L., and Sousa-Coutinho, J. (2013). "Strength and durability of cement with forest waste bottom ash." *Constr.Build.Mater.,* 41 897-910.

Hussain, Z., Maqsood, R., Din, M. I., Khan, S. M., Shahnaz, A., Rashid, M., and Ameen, S. (2017). "Enhanced mechanical properties of wood ash and fly ash as supplementary cementitious materials." *Adv.Appl.Ceram.,* 116(7), 355-361.

ISO (2015). "Plastics - Determination of thermal conductivity and thermal diffusivity - Part 2: Transient plane heat source (hot disc) method (ISO 22007-2:2015)." .

Kim, H., Hong, J., and Pyo, S. (2018). "Acoustic characteristics of sound absorbable high performance concrete." *Appl.Acoust.,* 138 171-178.

Laukaitis, A., and Fiks, B. (2006). "Acoustical properties of aerated autoclaved concrete." *Applied Acoustics,* 67(3), 284-296.

Log, T., and Gustafsson, S. E. (1995). "Transient plane source (TPS) technique for measuring thermal transport properties of building materials." *Fire Mater.,* 19(1), 43-49.

Lu, T. J., Chen, F., and He, D. (2000). "Sound absorption of cellular metals with semiopen cells." *J.Acoust.Soc.Am.,* 108(4), 1697-1709.

Madrid, M., Orbe, A., Rojí, E., and Cuadrado, J. (2017). "The effects of by-products incorporated in low-strength concrete for concrete masonry units." *Constr.Build.Mater.,* 153 117-128.

Nicholls, D., and Zerbe, J. (2012). "Cofiring biomass and coal for fossil fuel reduction and other benefits-status of North American facilities in 2010." *USDA for.Serv.Gen.Tech.Rep.PNW GTR,* (867), 1-22.

NRMCA (National Ready Mixed Concrete Association Concrete). (2012). "CO2 Fact Sheet." *NRMCA Publication Number 2PCO2,* .

Othuman Mydin, M. A., Mohamed Shajahan, M. F., Ganesan, S., and Sani, N. M. (2014). "Laboratory investigation on compressive strength and micro-structural features of foamed concrete with addition of wood ash and silica fume as a cement replacement." *MATEC Web of Conferences,* .

Samson, G., Phelipot-Mardelé, A., and Lanos, C. (2017a). "Thermal and mechanical properties of gypsum-cement foam concrete: effects of surfactant." *Eur.J.Environ.Civ.Eng.,* 21(12), 1502-1521.

Samson, G., Phelipot-Mardelé, A., and Lanos, C. (2017b). "A review of thermomechanical properties of lightweight concrete." *Mag Concr Res,* 69(4), 201-216.

Seddeq, H. S. (2010). "Sound absorption improvement for cementitious materials." *Can Acoust,* 38(4), 31-35.

Setayeshgar, P., Boluk, Y., and Bindiganavile, V. (2017). "Efficacy of forest based ash as a supplementary cementing material for concrete." *Can.J.Civ.Eng.,* 44(8), 652-660.

Skujans, J., Iljins, U., Ziemelis, I., Gross, U., Ositis, N., Brencis, R., Veinbergs, A., and Kukuts, O. (2010). "Experimental research of foam gypsum acoustic absorption and heat flow." *Chem. Eng. Trans.,* 19.

Tiuc, A. E., Vasile, O., Usca, A. -., Gabor, T., and Vermesan, H. (2014). "The analysis of factors that influence the sound absorption coefficient of porous materials." *Rom.J.Acoustics Vib.,* 11(2), 105-108.

Vorländer, M. (2008). *Auralization.* Springer, Berlin.

Wang, P., and Zhao, C. (2015). "Study on reducing railway noise by porous concrete sound-absorbing panel." *Mater.Res.Innov.,* 19 S51160.

Wang, X., and Lu, T. J. (1999). "Optimized acoustic properties of cellular solids." *J.Acoust.Soc.Am.,* 106(2), 756-765.

Zarr, R., Chavez, J., Lee, A., Dalton, G., and Young, S (2016). *NIST Heat Transmission Properties of Insulating and Building Materials, NIST Standard Reference Database Number 81.* National Institute of Standards and Technology, Gaithersburg MD, 20899, .

Zhang, Z., Provis, J. L., Reid, A., and Wang, H. (2015). "Mechanical, thermal insulation, thermal resistance and acoustic absorption properties of geopolymer foam concrete." *Cement & Concrete Composites,* 62 97-105.

5.0 Correlating the Air-Void Network of Cellular Cementitious Materials Utilizing Combustion Byproducts with Physical Properties

5.1 Abstract

Cellular cementitious materials are attractive for construction because of the high strength to weight ratio they offer while providing good thermal insulation and acoustic absorption. These properties are dictated by the cellular structure of the material, and the properties of the solid phase of the material. The solid phase of cementitious materials has been deeply investigated in the past, but relatively little has been done to understand the cellular structure of cellular cementitious materials and how it affects the thermal and acoustic properties of the material. This study investigates the cellular structure of cellular materials made from alkali activated fly ash and from Portland cement blended with wood ash and quantifies the porosity, fractal dimension, and tortuosity of the cellular network. These parameters are then compared with the thermal and acoustic properties of the materials to identify any relationship.

5.2 Introduction

Foam concretes have been well characterized for their physical properties. These lightweight materials can be prepared with densities ranging from 300 kg/m^3 to 1900 kg/m^3, but an optimal balance between the mechanical strength and requirements of thermal insulation is typically found with densities around 1000 kg/m^3[Fouad 2006]. Foam concretes are typically prepared by introducing gas bubbles to a cement paste, either by mixing in a preformed foam or by adding chemicals which react to produce gas in the paste [Zhang et al. 2014].

It is well recognized that the production of Portland cement results in the emission of large amounts of CO_2. For every 1000 kg of Portland cement produced, 900 kg to 1100 kg of CO_2 is produced from the calcination of the raw materials and the burning of fossil fuels for energy to produce the clinker [NRMCA 2012]. For this reason, it has become necessary to investigate materials that can function as alternatives to Portland cement. Ashes resulting as industrial waste have been identified as one such class of materials that can partially replace the Portland cement in a concrete mix. For long, fly ash from coal combustion in thermal power plants has been widely used, but nowadays bio-sourced ash from the combustion of wood or agricultural by-products have been identified as another possible supplementary cementitious material [Garcia and Sousa-Coutinho 2013, Hussain et al. 2017, Madrid et al. 2017, Othuman Mydin et al. 2014, Setayeshgar et al. 2017]. Wood sourced ash has been used to replace up to 20% of the Portland cement in concrete without a significant loss of strength, and has been seen to reduce the thermal conductivity of the concrete as well [Madrid et al. 2017].

Another way to reduce the use of Portland cement is to substitute totally with a class of alkali-activated materials. These materials completely eliminate the Portland cement and instead are made with a precursor rich in alumino-silicate, which is chemically activated with a strong

alkaline agent. Fly ash, metakaolin, and blast furnace slag are commonly used as the source of alumino-silicates, while the alkali activator is typically a blend of sodium or potassium silicate with sodium or potassium hydroxide [Provis et al. 2014].

There has been much research characterizing the mechanical and thermal properties of foam cementitious systems, but the actual structure of the air-void network has not received as much attention. Some work has been done to characterise the cellular network and relate it to the strength of the foams [Hilal et al. 2015, Kearsley and Wainwright 2001, Nambiar and Ramamurthy 2007, Wee et al. 2006] and some to relate the cellular network to the thermal properties of the foams [Batool and Bindiganavile 2017, Batool and Bindiganavile 2018], but these studies have focussed on Portland cement based foams. No work has been done to quantify the cellular structure of foamed alkali-activated fly ash systems nor on foamed cement systems utilizing wood sourced ash.

Therefore, the present study was undertaken to investigate the structure of the cellular network in foam concrete prepared with alkali-activated fly ash (AAFA) and with Portland cement blended with a wood sourced ash. Laser confocal microscopy is used to generate height maps of the cut surface of the foams and digital image analysis techniques are used to quantify the cellular network.

5.3 Experimental Procedure

5.3.1 Materials and Sample Preparation

Three different densities of foam concrete were prepared with different binder materials. One binder was an alkali activated fly ash prepared by blending class C1 fly ash from a local coal power plant with an activator of 8M sodium hydroxide solution and sodium silicate solution. The mix design for the cellular alkali activated fly ash is presented in Table 5.1. Portland cement blended with wood ash from a local pulp and paper mill was also used as a binder for preparing cellular materials. The Portland cement used was type GU per CSA A3001[CSA 2013] (corresponds to ASTM Type 1[ASTM 2007]). The wood ash content was varied from 0% to 20% by mass. The mix design for the cellular cement is presented in Table 5.2. All of the foam concretes were reinforced with glass microfibers at a dosage of 1% by volume. The microfibers had a diameter of 37 μm and length of 12mm.

Table 5.1: Mix Design of Cellular Alkali Activated Fly Ash

Target Cast Density (kg/m^3)	Sodium Silicate Solution (kg)	8M NaOH (kg)	Fly Ash (kg)	Glass Microfibers (kg)
1000	162	81	730	26.8
1200	195	98	880	26.8
1400	230	115	1030	26.8

Table 5.2: Mix Design of Cellular Cement

Target Density and Ash Content	Cement (kg)	Wood Ash (kg)	Water (kg)	Glass Microfibers (kg)
1000 kg/m^3 0% Ash	575.9	0	397.3	26.8
1000 kg/m^3 10% Ash	518.3	57.6	397.3	26.8
1000 kg/m^3 20% Ash	460.7	115.2	397.3	26.8
1200 kg/m^3 0% Ash	694.2	0	479.0	26.8
1200 kg/m^3 10% Ash	624.8	69.4	479.0	26.8
1200 kg/m^3 20% Ash	555.4	138.8	479.0	26.8
1400 kg/m^3 0% Ash	812.5	0	560.7	26.8
1400 kg/m^3 10% Ash	731.3	81.2	560.7	26.8
1400 kg/m^3 20% Ash	650.0	162.5	560.7	26.8

In order to prepare the foam concrete, the liquid components of the binder were put into the drum of a concrete mixer and the ash or cement was gradually introduced while the mixer was running. Once the mixture had fully combined to form a slurry, the glass fibers were sprinkled into the rotating drum of the mixture, and mixing continued until the fibers were well dispersed. At this point, a preformed foam was produced by running a diluted protein based foaming agent through a portable foam generator. The preformed foam was gradually added to the drum of the

mixer while it was still running, and was allowed to blend into the slurry. Periodically, a small sample was taken from the mixer and weighed to determine the approximate cast density. When enough foam was added that the target cast density was reached, the foamed material was cast in to cylindrical plastic moulds. The specimens were removed from their moulds after 24 hours were and placed in a curing room at 21°C and 100% humidity for a further 24 days. At 25 days after casting, the specimens were removed from the curing room and the ends were cut and polished to expose the cellular structure of the material. The specimens were then left in ambient conditions to dry prior to further testing.

Further details on the materials and sample preparation can be found in chapters 3 and 4.

5.3.2 Confocal Microscopy

3D images of the top surface of each specimen were taken using an Olympus 3000 laser confocal microscope. The images were taken with a 1x objective lens, resulting in a resolution of 0.4 pixels/μm. Each image covered an area 2560 μm x 1920 μm. This level of magnification allowed sufficient resolution to clearly identify the macropores created in the foaming process while also capturing large connected regions in a single image. The 3D images were saved as colour coded 2D height maps for further processing. Nine images were taken for each mix design and each density.

5.3.3 Image Processing

Image analysis was performed using the image analysis software, FIJI [Schindelin et al. 2012]. First, colour thresholding was used to convert the coloured 2D height maps into binary images of

the pores. An example of one such height map and the corresponding binary image can be seen in Figure 5.1. Each image was thresholded individually to ensure that the resulting binary image accurately captured the pores. These binary images could then be used for various software based image analyses.

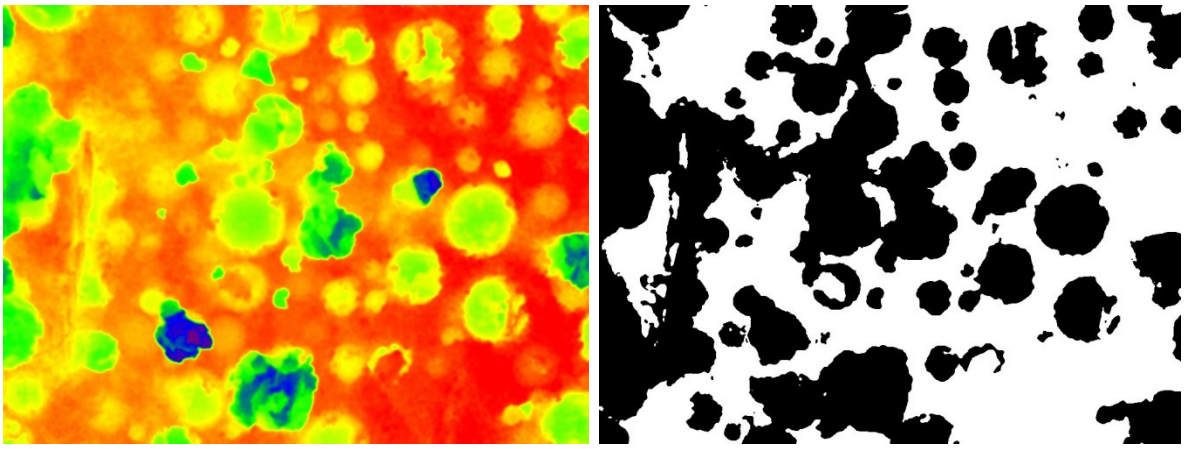

Figure 5.1: 2D Height Map and Corresponding Binary Image of Cellular Concrete

The fractal dimension, D_f, of the pores was determined using the box-counting method on the binary image of the pores. The fractal dimension of the solid phase was also determined by inverting the binary image of the pores, and again performing the box-counting procedure.

The tortuosity of the pore space was determined by measuring the geodesic diameter of each pore space and dividing this by the Euclidean distance between the endpoints of this diameter. This value was calculated for each region of interconnected pore space in an image, and the average tortuosity of all the pores was taken to be the tortuosity of that image. The MorphoLibJ [Legland et al. 2016] plugin for FIJI was used to determine the geodesic diameters and the coordinates of the endpoints of this diameter.

5.3.4 Determination of Sound Absorption Parameters

The sound absorption of the foam concrete was determined using an impedance tube, as described in ASTM C384-04 [ASTM 2011]. More details on the determination of the sound absorption can be found in chapters 3 and 4. The normal incident sound absorption coefficient, α_n, was measured for frequencies from 125 Hz to 6300 Hz. This absorption coefficient is a value from 0 to 1 where 0 implies that all sound is reflected off of the material and 1 implies that all sound is absorbed by the material [Everest and Pohlmann 2009]. The other acoustical parameter is the Noise Reduction Coefficient (NRC). ASTM C423 defines the noise reduction coefficient, as the average of random incident sound absorption coefficients taken at 250 Hz, 500 Hz, 1000 Hz, and 2000 Hz [ASTM 2017]. In this study, the same calculation was applied to the normal incident sound absorption coefficients to serve as a single value to characterise the sound absorption of the materials. This value is referred to as NRC, despite using normal incident absorption coefficients instead of random incident sound absorption coefficients.

5.3.5 Determination of Thermal Conductivity

The thermal conductivity of the cellular cementitious materials was determined by the transient plane source method (ISO 22007-2). Specimens were cut into pairs of disks which sandwiched a sensor. The sensor was a 3.189mm radius double spiral encased in Kapton. Electricity is applied through the spiral, and the change in resistance is measured over time. From this, the thermal properties of the specimen can be calculated. Tests were performed at an ambient temperature of 21°C. Each test was run for 180s and was heated with 51.33 mW of power.

5.4 Results and Discussion

The porosity of the foam concretes as determined by image analysis is presented in Figure 5.2. As expected, the porosity decreases with increasing density of the material. This is because the change in density with a given binder is caused by increasing the number of pores also. It can be seen that the foam concrete prepared with AAFA has a slightly lower porosity than that for foams of the same density prepared with Portland cement. This is because the AAFA binder has a slightly lower density that Portland cement binder, so fewer air voids are sufficient to reach the same lower density.

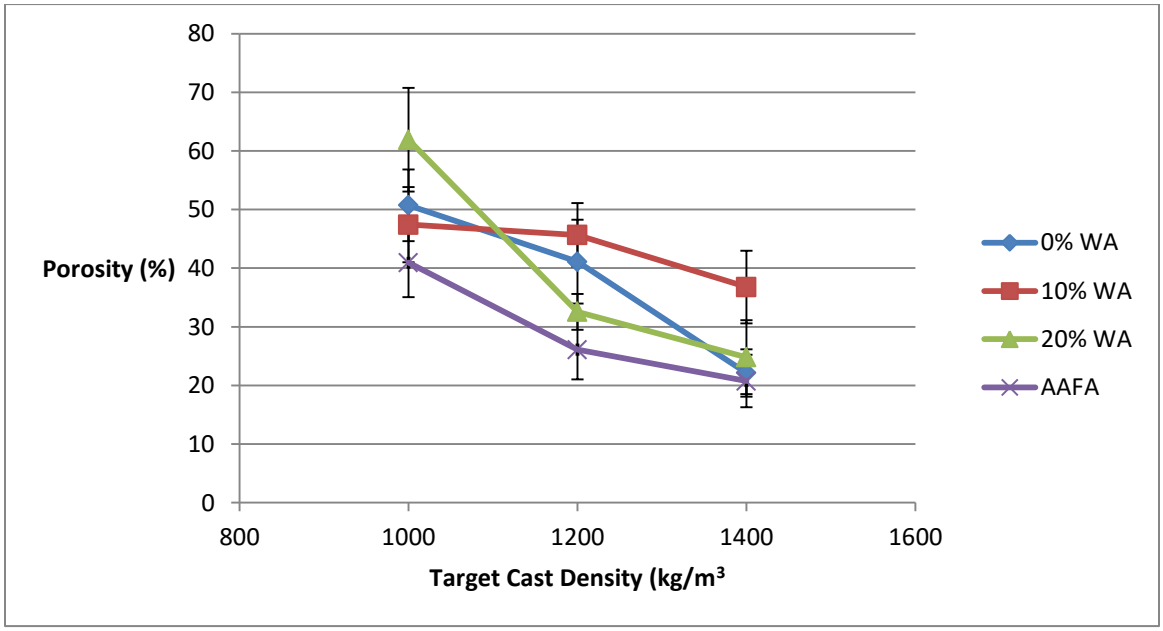

Figure 5.2: Porosity of the Cellular Materials

It is worthwhile to see how the fractal nature of the cellular structure varies in the microstructure of the present cellular systems. The fractal dimensions of the pore space and the solid phase are presented in Figure 5.3 a) and b) respectively. The values shown are the average of 9

measurements, and the error bars show the standard deviation of those 9 measurements. Across all binders and densities, D_f of the pores is rather high, ranging from 1.67 to 1.87. A trend of decreasing fractality of the pores with increasing density is apparent. This same trend was seen when Tian et. al. looked at the fractal nature of pores in cement foams [Tian et al. 2011]. When looking at the solid phase of the material, the opposite trend can be seen, with D_f increasing with density. This trend has been seen before for the solid phase of foam cements by Karam and Tonyan [1993]. The type of binder used to produce the cellular material had little effect on the fractal dimension of the pores or the solid phase.

Figure 5.4 displays D_f of the pores as a function of the porosity of the cellular material. It can be seen that D_f increases approximately linearly with the porosity.

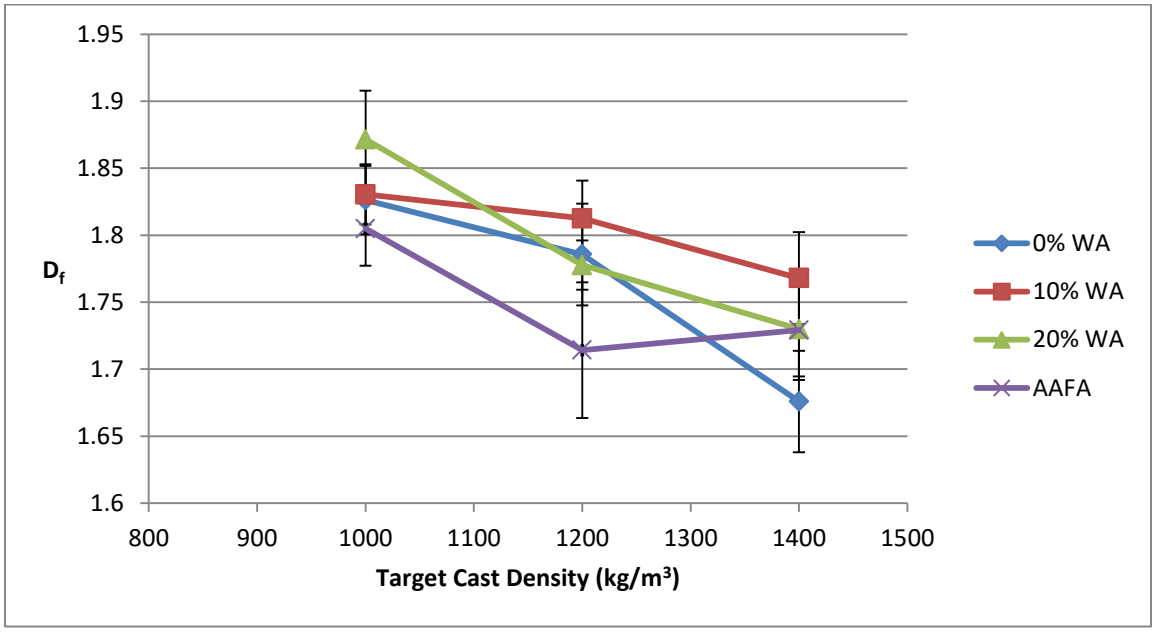

(a)

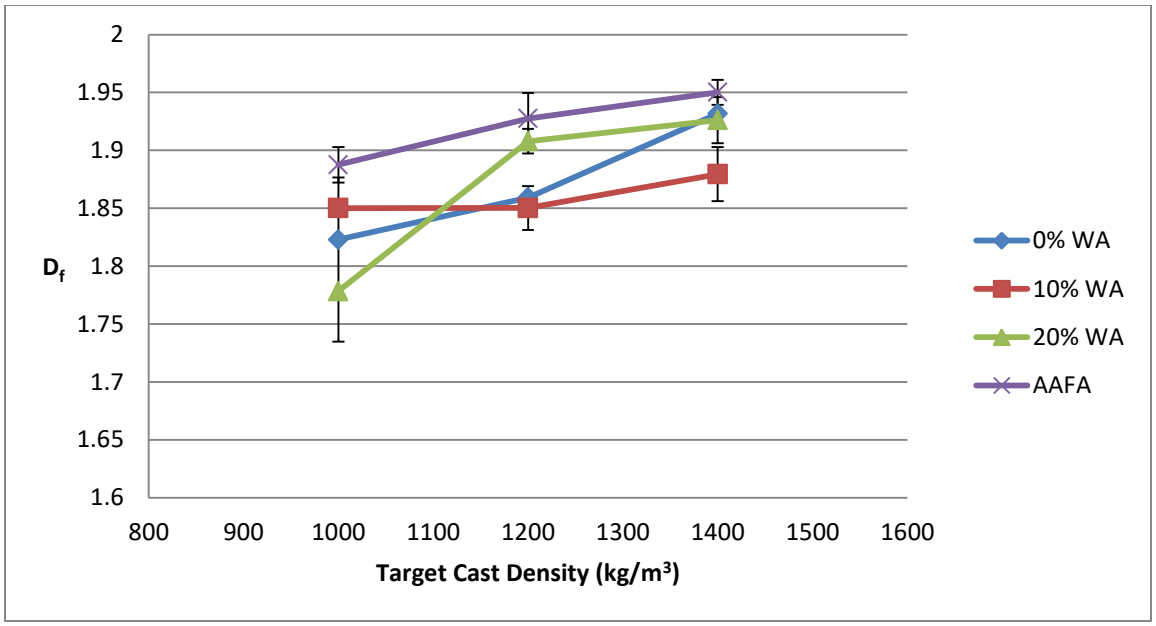

(b)

Figure 5.3: Fractal Dimension of the (a) Pores and (b) Solid Phase of Cellular Materials

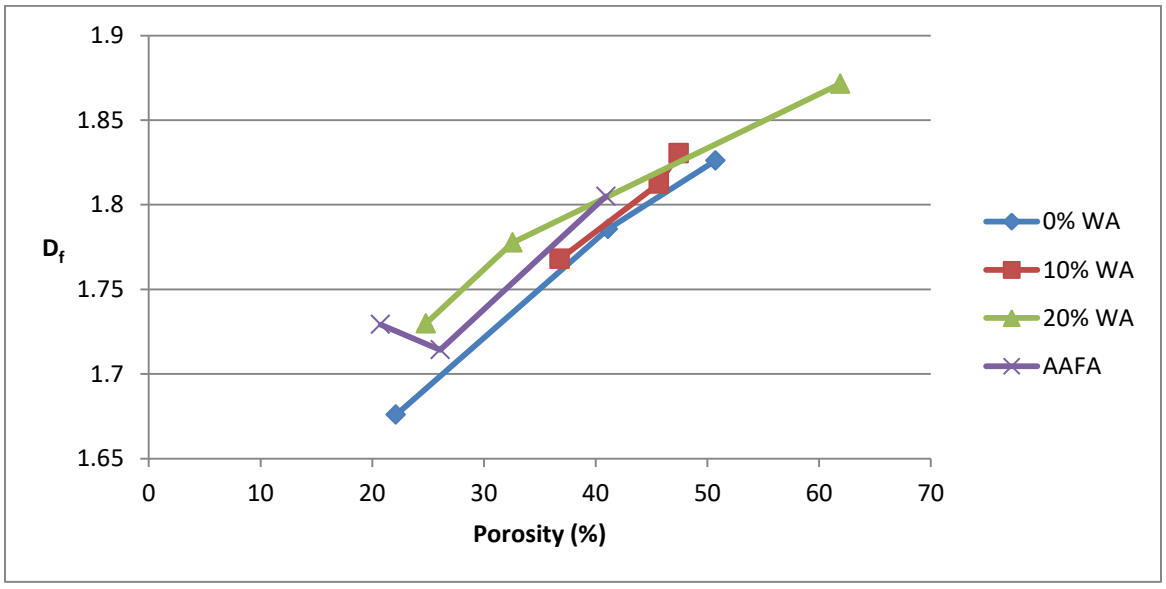

Figure 5.4: Fractal Dimension of Pores as a Function of Porosity

Another parameter that defines the air-void network is the tortuosity of the network. The tortuosity of the pore network is presented in Figure 5.5. It is quite low, and there is little variation in tortuosity across densities and mix designs. The low tortuosity is likely due to the large number of pores which are not interconnected. These pores individually have tortuosities very close to 1 because a straight path can be drawn across the near circular pores. As a result, the average tortuosity of all the pores is very low. Again, there is not much variation in tortuosity for mixtures with varying addition of wood ash and for the alkali activated fly ash mixtures.

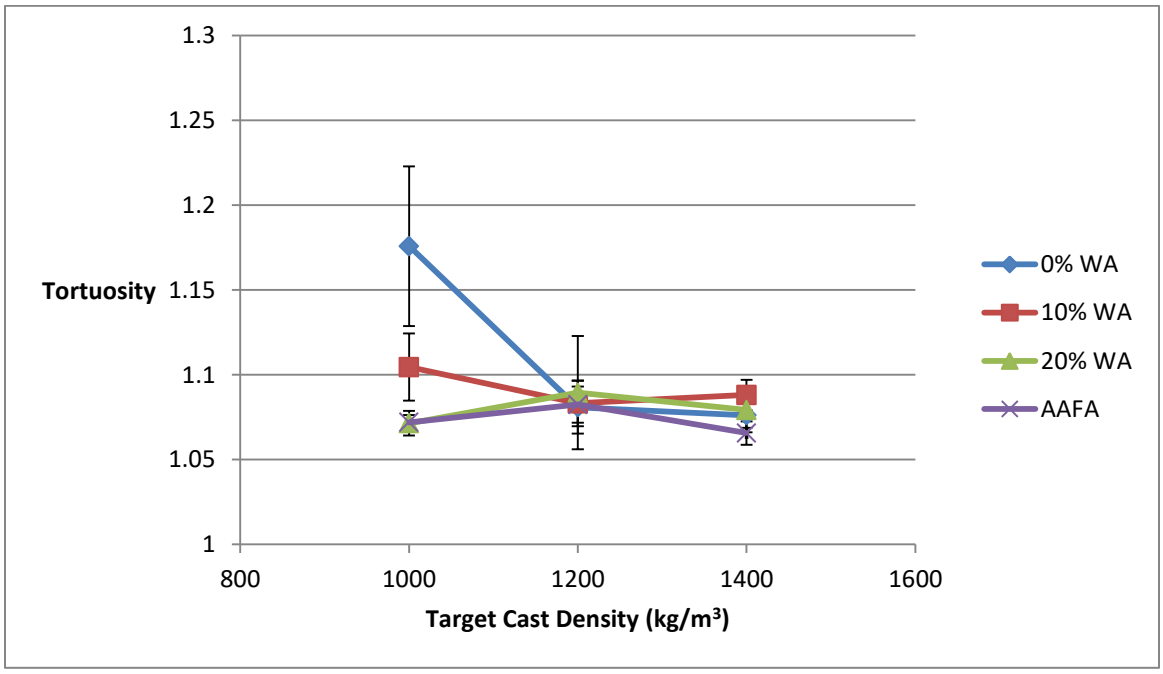

Figure 5.5: Tortuosity of the Pores of Cellular Materials

In Figure 5.6, the thermal conductivity is plotted against D_f of the cells in the cellular cementitious materials. A trend of decreasing thermal conductivity with increasing D_f is seen across each mix design. This same trend has been found before for Portland cement based foams [Tian et al. 2011]. This relationship could be more a result of the changing porosity. Increasing

D_f of the cells coincides with increasing porosity, so the changes in thermal conductivity could instead be attributed to the porosity.

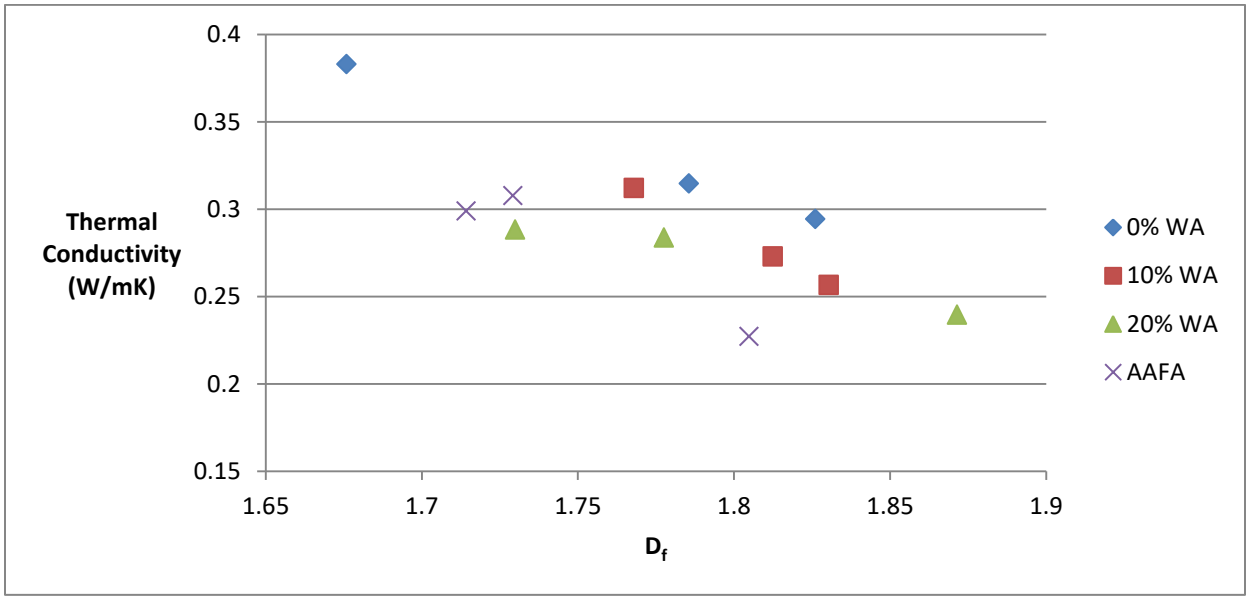

Figure 5.6: Thermal Conductivity as a Function of Fractal Dimension of Cells in Cellular Cementitious Materials

Attempts were made to find a correlation between the noise reduction coefficient of the cellular materials and the structural parameters discussed above. In Figure 5.7a, the NRC is plotted against the porosity of the cellular materials. No clear trend is apparent from the data. The NRC values have very little variation with the porosity. Figure 5.7b plots the NRC against the fractal dimension of the pores. Again, most data points show little variation of the NRC with D_f, and no clear trend is visible. For the 0% wood ash material, there is an increase in tortuosity at 1000 kg/m^3, but it is still a low value of tortuosity and this change is not seen for the other mix designs. Figure 5.7c shows the NRC plotted against the tortuosity of the pores. The AAFA appears to have increasing NRC with increasing tortuosity, but this pattern is not seen with any of the other binder materials. Therefore, across the range of materials and densities studied here,

no definite conclusions could be made about the effect of structural parameters of the pore network on the noise reduction coefficient of the cellular material.

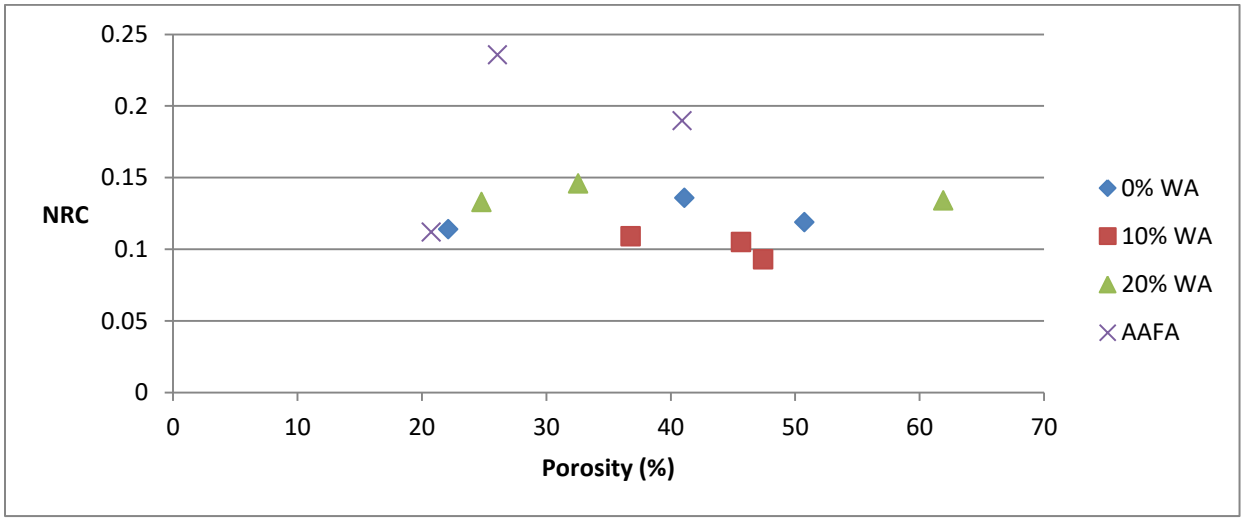

(a)

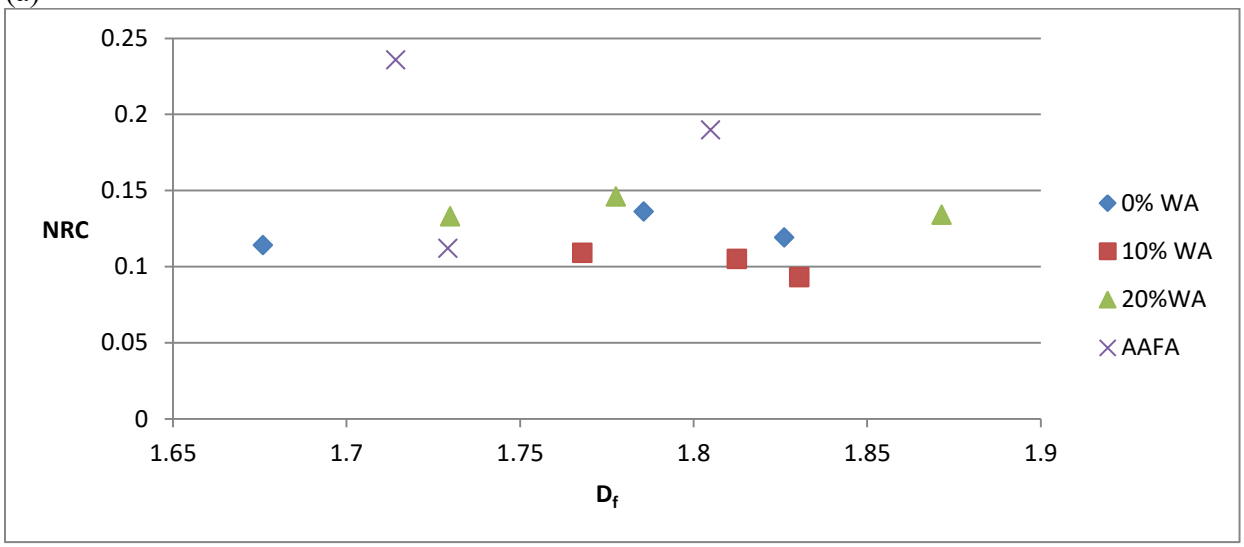

(b)

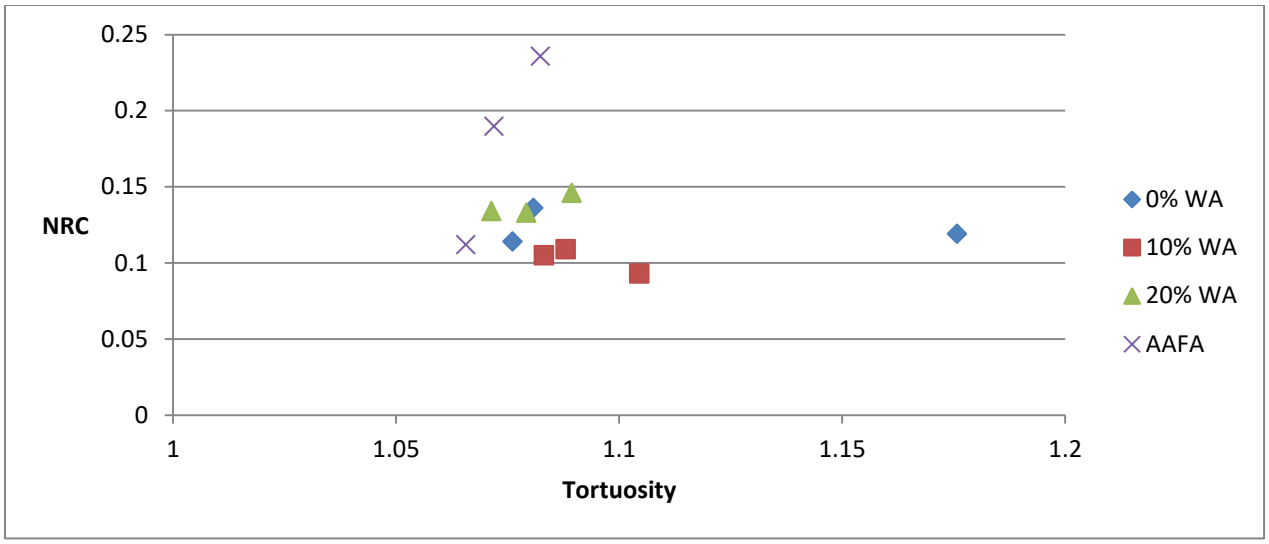

(c)

Figure 5.7: NRC as a Function of (a) Porosity, (b) Fractal Dimension and (c) Tortuosity

5.5 Conclusions

Foam concretes of cast densities from 1000 kg/m^3 to 1400 kg/m^3 were prepared by mixing preformed foam with alkali activated fly ash binder or a binder of Portland cement blended with wood ash. These foams were subsequently images using laser confocal microscopy and the images were analysed to characterize the pore structure of the foams. Analysis was performed to relate the thermal and acoustic properties of the foams to their pore structures. The findings were as follows:

- With increasing density of the foam concrete, the porosity decreased and the fractal dimension of the pores decreased. D_f of the solid phase increased with increasing density. The tortuosity of the pore network was low due to the larger number of unconnected pores in the foam concrete.
- When thermal conductivity was plotted against D_f of the cells, the thermal conductivity was found to decrease with increasing D_f.

- No definite pattern could be found relating NRC to porosity, fractal dimension, or tortuosity.

5.6 References

ASTM (2017). "C423 Standard Test Method for Sound Absorption and Sound Absorption Coefficients by the Reverberation Room Method." .

ASTM (2011a). "C384 Standard Test Method for Impedance and Absorption of Acoustical Materials by Impedance Tube Method." .

ASTM (2007). "C150 Standard Specification for Portland Cement." .

Batool, F., and Bindiganavile, V. (2018). "Quantification of factors influencing the thermal conductivity of cement-based foam." *Cem.Concr.Compos.,* 91 76-86.

Batool, F., and Bindiganavile, V. (2017). "Air-void size distribution of cement based foam and its effect on thermal conductivity." *Constr.Build.Mater.,* 149 17-28.

CSA (2013). "CSA A3001-13 Cementitious Materials Used in Concrete." .

Everest, F. A., and Pohlmann, K. C. (2009). *Master handbook of acoustics.* McGraw-Hill, New York, NY ; London.

Fouad, F. H. (2006) "Chapter 47: Cellular Concrete." (169), 561.

Garcia, M. D. L., and Sousa-Coutinho, J. (2013). "Strength and durability of cement with forest waste bottom ash." *Constr.Build.Mater.,* 41 897-910.

Hilal, A. A., Thom, N. H., and Dawson, A. R. (2015). "On void structure and strength of foamed concrete made without/with additives." *Constr.Build.Mater.,* 85 157-164.

Hussain, Z., Maqsood, R., Din, M. I., Khan, S. M., Shahnaz, A., Rashid, M., and Ameen, S. (2017). "Enhanced mechanical properties of wood ash and fly ash as supplementary cementitious materials." *Adv.Appl.Ceram.,* 116(7), 355-361.

Schindelin, J., Arganda-Carreras, I., Frise, E., Kaynig, V., Longair, M., Pietzsch, T., Preibisch, S., Rueden, C., Saalfeld, S., Schmid, B., Tinevez, J.Y., White, D. J., Hartenstein, V., Eliceiri, K., Tomancak, P., and Cardona, A. (2012). "Fiji: an open-source platform for biological-image analysis", *Nature Methods,* 9(7**)**, 676-682

Karam, G. N., and Tonyan, T. D. (1993). "Fractal morphology of cement foams." *Mater Lett,* 16(5), 278-280.

Kearsley, E. P., and Wainwright, P. J. (2001). "The effect of high fly ash content on the compressive strength of foamed concrete." *Cem.Concr.Res.,* 31(1), 105-112.

Legland, D., Arganda-Carreras, I., and Andrey, P. (2016), "MorphoLibJ: integrated library and plugins for mathematical morphology with ImageJ", *Bioinformatics (Oxford Univ Press,)* 32(22), 3532-3534

Madrid, M., Orbe, A., Rojí, E., and Cuadrado, J. (2017). "The effects of by-products incorporated in low-strength concrete for concrete masonry units." *Constr.Build.Mater.,* 153 117-128.

Nambiar, E. K. K., and Ramamurthy, K. (2007). "Air-void characterisation of foam concrete." *Cem.Concr.Res.,* 37(2), 221-230.

NRMCA (National Ready Mixed Concrete Association Concrete). (2012). "CO2 Fact Sheet." *NRMCA Publication Number 2PCO2,* .

Othuman Mydin, M. A., Mohamed Shajahan, M. F., Ganesan, S., and Sani, N. M. (2014). "Laboratory investigation on compressive strength and micro-structural features of foamed concrete with addition of wood ash and silica fume as a cement replacement." *MATEC Web of Conferences,* .

Provis, J. L., and Van Deventer, Jan Stephanus Jakob. (2014). *Alkali activated materials : state-of-the-art report, RILEM TC 224-AAM.* Springer, Dordrecht.

Setayeshgar, P., Boluk, Y., and Bindiganavile, V. (2017). "Efficacy of forest based ash as a supplementary cementing material for concrete." *Can.J.Civ.Eng.,* 44(8), 652-660.

Tian, W. L., Yang, J. B., and Zhao, X. Y. (2011). "Study on properties of foam concrete based on fractal theory." *Adv. Mater. Res.,* 194-196.

Wee, T. -., Babu, D. S., Tamilselvan, T., and Lim, H. -. (2006). "Air-void system of foamed concrete and its effect on mechanical properties." *ACI Mater.J.,* 103(1), 45-52.

Zhang, Z., Zhang, Z., Wang, H., Provis, J. L., and Reid, A. (2014). "Geopolymer foam concrete: An emerging material for sustainable construction." *Constr.Build.Mater.,* 56 113-127.

6.0 Conclusions and Recommendations

6.1 Conclusions

Cellular concrete was produced from alkali activated fly ash and from Portland cement blended with wood ash by utilizing a preformed foam method. These materials offer a more environmentally friendly alternative to lightweight concretes such as autoclaved aerated cement.

The compressive strength of cellular AAFA ranged from 3 MPa to 9 MPa at cast densities from 1000 kg/m^3 to 1400 kg/m^3 and the strength of cellular cement with wood ash ranged from 4 MPa to 12 MPa across the same range of densities. With this strength, the materials would be suitable for non-load bearing applications.

The thermal conductivity of cellular AAFA ranged from 0.23 W/mK to 0.31 W/mK and the thermal conductivity of cellular cement with wood ash ranged from 0.32 W/mK to 0.52 W/mK. The cellular AAFA provides slightly better insulation than the wood ash cement, though the wood ash cement still has comparable thermal conductivity to other building materials of similar density.

The noise reduction coefficients of the cellular materials ranged from 0.1 to 0.25. While this level of sound absorption is not as high as dedicated acoustic materials, it does outperform solid concrete and other relatively non-porous building materials.

Parameters characterizing the cell structure followed expected trends. As the density of the cellular concretes was increased, porosity decreased and the fractal dimension of the pores decreased. The large number of unconnected pores meant that the tortuosity of the pores was low

and fairly constant. When looking at the effect of these pore parameters on the noise reduction coefficient, no clear relationships could be determined.

6.2 Recommendations

These studies only investigated the thermal properties of the cellular cementitious materials at ambient temperatures. These properties vary with temperature, so future work to study these materials at extreme temperatures would be prudent.

The effect of acid attack on the AAFA should be investigated because the cellular AAFA could be exposed to acids in soil if it were used as a void filling material in geotechnical applications.

Further study should be carried out to improve the mix design of the alkali activated material. The local fly ash is relatively low in alumina, so work could be done to correct this by blending with an alternative alumina source. Optimizing this mix design could greatly improve the mechanical strength of the material.

Investigation into alternative foaming agents to use in alkali activated materials should be undertaken. The protein based agent used in this study performed well in cement based systems, but in the alkali activated system, large quantities of the bubbles ruptured, necessitating a large volume of foam to be added to achieve target densities. A foaming agent with better stability in a highly alkaline environment would be much more efficient.

Research should be done to look at utilizing wood ash in an alkali activated material. The mineral composition of wood ash is not well suited to alkali activation on its own, but it may be suitable for blending with other precursor materials.

Bibliography

Anonymous (2017). "Acoustic Ceiling Tiles and Panels." https://www.ceilume.com/shop/acoustic-ceiling-tiles/index.cfm#nrc25, (accessed 6 Dec 2017).

ASTM (2017). "C423 Standard Test Method for Sound Absorption and Sound Absorption Coefficients by the Reverberation Room Method." .

ASTM (2016). “C869/C869M-11 Standard Specification for Foaming Agents Used in Making Preformed Foam for Cellular Concrete.” .

ASTM (2013). "D7348 Standard Test Methods for Loss on Ignition (LOI) of Solid Combustion Residues." .

ASTM (2012). "C495/C495M Standard Test Method for Compressive Strength of Lightweight Insulating Concrete." .

ASTM (2011a). "C384 Standard Test Method for Impedance and Absorption of Acoustical Materials by Impedance Tube Method." .

ASTM (2007). "C150 Standard Specification for Portland Cement." .

Abdollahnejad, Z., Pacheco-Torgal, F., Flix, T., Tahri, W., and Barroso Aguiar, J. (2015). "Mix design, properties and cost analysis of fly ash-based geopolymer foam." *Construction & Building Materials,* 80 18-30.

Arellano Aguilar, R., Burciaga Díaz, O., and Escalante García, J. I. (2010). "Lightweight concretes of activated metakaolin-fly ash binders, with blast furnace slag aggregates." *Constr.Build.Mater.,* 24 1166-1175.

Batool, F., and Bindiganavile, V. (2018a). "Quantification of factors influencing the thermal conductivity of cement-based foam." *Cem.Concr.Compos.,* 91 76-86.

Batool, F., and Bindiganavile, V. (2018b). "Thermal conductivity of hydrated paste in cement-based foam microstructure." *Adv.Civ.Eng.Mater.,* 7(1), 17-32.

Batool, F., Prasad, N. G. N., and Bindiganavile, V. (2018). "Statistical modeling of thermal conductivity for cement-based foam." *J.Build.Eng.,* 19 449-458.

Batool, F., and Bindiganavile, V. (2017). "Air-void size distribution of cement based foam and its effect on thermal conductivity." *Constr.Build.Mater.,* 149 17-28.

Bindiganavile, V., Goncalves, J. R. A., and Boluk, Y. (2016). "Crack growth resistance in fibre reinforced geopolymer concrete exposed to sustained extreme temperatures." *Key Eng Mat,* 711.

Bonakdar, A., Babbitt, F., and Mobasher, B. (2013). "Physical and mechanical characterization of Fiber-Reinforced Aerated Concrete (FRAC)." *Cement and Concrete Composites,* 38 82-91.

Charles, P., Dominique, J., Delisée Christine, and Malvestio Jérôme. (2011). "3D Morphological Characterization of Phonic Insulation Fibrous Media." *Adv.Eng.Mater.,* 13(3), 156-164.

Cheah, C. B., Samsudin, M. H., Ramli, M., Part, W. K., and Tan, L. E. (2017). "The use of high calcium wood ash in the preparation of Ground Granulated Blast Furnace Slag and Pulverized

Fly Ash geopolymers: A complete microstructural and mechanical characterization." *J.Clean.Prod.,* 156 114-123.

Chen, G., and Wang, K. (2017). "Mechanical and thermal properties of glass fibre-reinforced ceramsite-foamed concrete." *Indoor Built Environ.,* .

Chevillotte, F., and Perrot, C. (2017). "Effect of the three-dimensional microstructure on the sound absorption of foams: A parametric study." *J.Acoust.Soc.Am.,* 142(2), 1130-1140.

Choktaweekarn, P., Saengsoy, W., and Tangtermsirikul, S. (2009). "A model for predicting thermal conductivity of concrete." *Mag Concr Res,* 61(4), 271-280.

Coquard, R., and Baillis, D. (2006). "Modeling of heat transfer in low-density EPS foams." *J.Heat Transf.,* 128(6), 538-549.

Criado, M., Fernández-Jiménez, A., de, l. T., Aranda, M. A. G., and Palomo, A. (2007). "An XRD study of the effect of the SiO2/Na2O ratio on the alkali activation of fly ash." *Cem.Concr.Res.,* 37 671-679.

CSA (2013). "CSA A3001-13 Cementitious Materials Used in Concrete." .

Everest, F. A., and Pohlmann, K. C. (2009). *Master handbook of acoustics.* McGraw-Hill, New York, NY ; London.

Fouad, F. H. (2006) "Chapter 47: Cellular Concrete." (169), 561.

Garcia, M. D. L., and Sousa-Coutinho, J. (2013). "Strength and durability of cement with forest waste bottom ash." *Constr.Build.Mater.,* 41 897-910.

Gibson, L. J., and Ashby, M. F. (1997). *Cellular solids : structure and properties.* Cambridge University Press, Cambridge.

Goncalves, J. R. A., Boluk, Y., and Bindiganavile, V. (2017). "Thermal properties of fibre reinforced alkali-activated concrete in extreme temperatures." *Magazine of Concrete Research,* 1-37.

Henon, J., Pennec, F., Alzina, A., Absi, J., Smith, D. S., and Rossignol, S. (2014). "Analytical and numerical identification of the skeleton thermal conductivity of a geopolymer foam using a multi-scale analysis." *Comput Mater Sci,* 82 264-273.

Hilal, A. A., Thom, N. H., and Dawson, A. R. (2015). "On void structure and strength of foamed concrete made without/with additives." *Constr.Build.Mater.,* 85 157-164.

Hussain, Z., Maqsood, R., Din, M. I., Khan, S. M., Shahnaz, A., Rashid, M., and Ameen, S. (2017). "Enhanced mechanical properties of wood ash and fly ash as supplementary cementitious materials." *Adv.Appl.Ceram.,* 116(7), 355-361.

Ibrahim, W. M. W., Hussin, K., Bakri Abdullah, M.,Mustafa Al, and Kadir, A. A. (2017). "Geopolymer Lightweight Bricks Manufactured From Fly Ash and Foaming Agent." *AIP Conference Proceedings,* 1835(1), 1-5.

ISO (2015). "Plastics - Determination of thermal conductivity and thermal diffusivity - Part 2: Transient plane heat source (hot disc) method (ISO 22007-2:2015)." .

Jhatial, A. A., Inn, G. W., Mohamad, N., Johnson Alengaram, U., Hung Mo, K., and Abdullah, R. (2017). "Influence of polypropylene fibres on the tensile strength and thermal properties of

various densities of foamed concrete." *IOP Conference Series: Materials Science and Engineering,* .

Jiang, J., Lu, Z., Niu, Y., Li, J., and Zhang, Y. (2016). "Investigation of the properties of high-porosity cement foams based on ternary Portland cement-metakaolin-silica fume blends." *Constr.Build.Mater.,* 107 181-190.

Karam, G. N., and Tonyan, T. D. (1993). "Fractal morphology of cement foams." *Mater Lett,* 16(5), 278-280.

Kearsley, E. P., and Wainwright, P. J. (2001). "The effect of high fly ash content on the compressive strength of foamed concrete." *Cem.Concr.Res.,* 31(1), 105-112.

Kim, H. K., and Lee, H. K. (2010). "Acoustic absorption modeling of porous concrete considering the gradation and shape of aggregates and void ratio." *Journal of Sound and Vibration,* 329(7), 866-879.

Kim, H., Hong, J., and Pyo, S. (2018). "Acoustic characteristics of sound absorbable high performance concrete." *Appl.Acoust.,* 138 171-178.

Krmer, C., Schauerte, M., Mller, T., Gebhard, S., and Trettin, R. (2017). "Application of reinforced three-phase-foams in UHPC foam concrete." *Constr.Build.Mater.,* 131 746-757.

Laukaitis, A., and Fiks, B. (2006). "Acoustical properties of aerated autoclaved concrete." *Applied Acoustics,* 67(3), 284-296.

Legland, D., Arganda-Carreras, I., and Andrey, P. (2016), "MorphoLibJ: integrated library and plugins for mathematical morphology with ImageJ", *Bioinformatics (Oxford Univ Press,)* 32(22), 3532-3534

Leventhall, H. (2004). "Low frequency noise and annoyance." *Noise Health,* (23), 59-72.

Lia, Q., Wanga, H., Zhanga, Z., and Reidb, A. (2013). "Numerical simulation of porosity on thermal properties and fire resistance of foamed concrete." *J.Sustain.Cem.Based Mater.,* 2(1), 13-19.

Liu, Z., Fan-long Kong, Ning-ning Shao, Ju-jia Zhang, Zhen-zhen Chen, and Dong-min Wang. (2016). "Strength and Microstructure of alkali-activated fly ash-slag foam geopolymer." *Journal of Solid Waste Technology & Management,* 42(1), 16-26.

Log, T., and Gustafsson, S. E. (1995). "Transient plane source (TPS) technique for measuring thermal transport properties of building materials." *Fire Mater.,* 19(1), 43-49.

Lu, T. J., Chen, F., and He, D. (2000). "Sound absorption of cellular metals with semiopen cells." *J.Acoust.Soc.Am.,* 108(4), 1697-1709.

Luo, X. (1,2), Li, W (1), Zeng, L (1), and Jin, X (3). (2011). "Effects of porosity and pore size on sound absorption characteristic of ceramsite porous material." *Kuei Suan Jen Hsueh Pao/Journal of the Chinese Ceramic Society,* 39(1), 158-163.

Ma, Y., Yu, B., Zhang, D., and Zou, M. (2003). "A self-similarity model for effective thermal conductivity of porous media." *J.Phys.D,* 36(17), 2157-2164.

Madrid, M., Orbe, A., Rojí, E., and Cuadrado, J. (2017). "The effects of by-products incorporated in low-strength concrete for concrete masonry units." *Constr.Build.Mater.,* 153 117-128.

Mamun, M., and Bindiganavile, V. (2017). "Fractal Nature of Cementitious Systems Exposed to Sustained Elevated Temperatures." *Procedia Engineering,* 557-564.

Mamun, M., and Bindiganavile, V. (2010). "Drop-weight impact response of fibre reinforced cement based foams." *International Journal of Protective Structures,* 1(3), 409-424.

Mamun, M., Batool, F., and Bindiganavile, V. (2014). "Thermo-mechanical properties of fibre reinforced cement-based foam exposed to sulphate." *Constr.Build.Mater.,* 61 312-319.

Mamun, M., and University of Alberta. (2010). *Loading rate effects and sulphate resistance of fibre reinforced cement-based foams.*

Matoušek Tomáš. "Foams pore size estimation and their acoustic properties".

Matousek, T (1), Ponizil, P. (1,2), Kremen, F (1), Buresova, I (3), and Dvorakova, P (4). (2011). "Pore size estimation." *Recent Researches in Geography, Geology, Energy, Environment and Biomedicine - Proc.of the 4th WSEAS Int.Conf.on EMESEG'11, 2nd Int.Conf.on WORLD-GEO'11, 5th Int.Conf.on EDEB'11,* (-), 372-377.

Mobasher, B. (2012). *Mechanics of fiber and textile reinforced cement composites. [electronic resource].* Boca Raton : CRC Press, 2012, .

Modolo, R. C. E., Senff, L., Ferreira, V. M., Tarelho, L. A. C., and Moraes, C. A. M. (2017). "Fly ash from biomass combustion as replacement raw material and its influence on the mortars durability." *J.Mater.Cycles Waste Manage.,* 1-10.

Nambiar, E. K. K., and Ramamurthy, K. (2007). "Air-void characterisation of foam concrete." *Cem.Concr.Res.,* 37(2), 221-230.

Neithalath, N., Sumanasooriya, M. S., and Deo, O. (2010). "Characterizing pore volume, sizes, and connectivity in pervious concretes for permeability prediction." *Mater Charact,* 61 802-813.

Nicholls, D., and Zerbe, J. (2012). "Cofiring biomass and coal for fossil fuel reduction and other benefits-status of North American facilities in 2010." *USDA for.Serv.Gen.Tech.Rep.PNW GTR,* (867), 1-22.

Novais, R. M., Ascensão, G., J.A. Labrincha, L.H. Buruberri, and M.P. Seabra. (2016). "Porous biomass fly ash-based geopolymers with tailored thermal conductivity." *J.Clean.Prod.,* 119 99-107.

NRMCA (National Ready Mixed Concrete Association Concrete). (2012). "CO2 Fact Sheet." *NRMCA Publication Number 2PCO2,* .

Othuman Mydin, M. A., Mohamed Shajahan, M. F., Ganesan, S., and Sani, N. M. (2014). "Laboratory investigation on compressive strength and micro-structural features of foamed concrete with addition of wood ash and silica fume as a cement replacement." *MATEC Web of Conferences,* .

Park, J. H., Yang, S. H., Lee, H. R., Yu, C. B., Pak, S. Y., Oh, C. S., Kang, Y. J., and Youn, J. R. (2017). "Optimization of low frequency sound absorption by cell size control and multiscale poroacoustics modeling." *J.Sound Vib.,* 397 17-30.

Peyrega, C., and Jeulin, D. (2013). "Estimation of tortuosity and reconstruction of geodesic paths in 3D." *Image Analysis and Stereology,* 32(1), 27-43.

Provis, J. L., and Van Deventer, Jan Stephanus Jakob. (2014). *Alkali activated materials : state-of-the-art report, RILEM TC 224-AAM.* Springer, Dordrecht.

Rattanasak, U., and Chindaprasirt, P. (2009). "Influence of NaOH solution on the synthesis of fly ash geopolymer." *Minerals Engineering,* 22(12), 1073-1078.

Sagoe-Crentsil, K. (2009). "Role of oxide ratios on engineering performance of Fly-ash geopolymer binder systems." *Ceramic Engineering and Science Proceedings,* 175-184.

Samson, G., Phelipot-Mardelé, A., and Lanos, C. (2017a). "Thermal and mechanical properties of gypsum-cement foam concrete: effects of surfactant." *Eur.J.Environ.Civ.Eng.,* 21(12), 1502-1521.

Samson, G., Phelipot-Mardelé, A., and Lanos, C. (2017b). "A review of thermomechanical properties of lightweight concrete." *Mag Concr Res,* 69(4), 201-216.

Schindelin, J., Arganda-Carreras, I., Frise, E., Kaynig, V., Longair, M., Pietzsch, T., Preibisch, S., Rueden, C., Saalfeld, S., Schmid, B., Tinevez, J.Y., White, D. J., Hartenstein, V., Eliceiri, K., Tomancak, P., and Cardona, A. (2012). "Fiji: an open-source platform for biological-image analysis", *Nature Methods,* 9(7**)**, 676-682

Seddeq, H. S. (2010). "Sound absorption improvement for cementitious materials." *Can Acoust,* 38(4), 31-35.

Seep, B., Glosemeyer, R., Hulce, E., Linn, M., and Aytar, P. (2000). "Classroom Acoustics ." .

Setayeshgar, P., Boluk, Y., and Bindiganavile, V. (2017). "Efficacy of forest based ash as a supplementary cementing material for concrete." *Can.J.Civ.Eng.,* 44(8), 652-660.

She, W., Zhao, G., Cai, D., Jiang, J., and Cao, X. (2018). "Numerical study on the effect of pore shapes on the thermal behaviors of cellular concrete." *Constr.Build.Mater.,* 163 113-121.

Shishkin, R. A., Erkhova, N. A., Beketov, A. R., and Elagin, A. A. (2014). "Water-glass-based thermal paste for high-temperature applications." *J.Ceram.Sci.Technol.,* 5(3), 199-202.

Singh, B., Ishwarya, G., Gupta, M., and Bhattacharyya, S. K. (2015). "Geopolymer concrete: A review of some recent developments." *Construction and Building Materials,* 85 78-90.

Skujans, J., Iljins, U., Ziemelis, I., Gross, U., Ositis, N., Brencis, R., Veinbergs, A., and Kukuts, O. (2010). "Experimental research of foam gypsum acoustic absorption and heat flow." *Chem. Eng. Trans.,* 19.

Skvara, F., Jilek, T., and Kopecky, L. (2005). "Geopolymer materials based on fly ash." *Journal Ceramic-Silikaty,* 49(3), 195-204.

Skvara, F., Sulc, R., Zdenek, T., Petr, S., Vit, S., and Zlamalova, C. Z. (2014). "Preparation and Properties of Fly Ash-Based Geopolymer Foams." *Ceramics-Silikty, Vol 58, Iss 3, Pp 188-197 (2014),* (3), 188.

Tian, W. L., Yang, J. B., and Zhao, X. Y. (2011). "Study on properties of foam concrete based on fractal theory." *Adv. Mater. Res.,* 194-196.

Tiong-Huan Wee, D.,Saradhi Babu. (2006). "Air-Void System of Foamed Concrete and its Effect on Mechanical Properties." *Materials Journal,* 103(1),.

Tiuc, A. E., Vasile, O., Usca, A. -., Gabor, T., and Vermesan, H. (2014). "The analysis of factors that influence the sound absorption coefficient of porous materials." *Rom.J.Acoustics Vib.,* 11(2), 105-108.

Tiwari, V., Shukla, A., and Bose, A. (2004). "Acoustic properties of cenosphere reinforced cement and asphalt concrete." *Appl.Acoust.,* 65 263-275.

Vorländer, M. (2008). *Auralization.* Springer, Berlin.

Wang, P., and Zhao, C. (2015). "Study on reducing railway noise by porous concrete sound-absorbing panel." *Mater.Res.Innov.,* 19 S51160.

Wang, X., and Lu, T. J. (1999). "Optimized acoustic properties of cellular solids." *J.Acoust.Soc.Am.,* 106(2), 756-765.

Wee, T. -., Babu, D. S., Tamilselvan, T., and Lim, H. -. (2006). "Air-void system of foamed concrete and its effect on mechanical properties." *ACI Mater.J.,* 103(1), 45-52.

Wei, S., Yonggan, Y., Deqing, X., and Yunsheng, Z. (2014). "Finite volume numerical analysis of the thermal property of cellular concrete based on two and three dimensional X-ray computerized tomography images." *Proceedings of the 4th International Conference on the Durability of Concrete Structures, ICDCS 2014,* 304-311.

Yu, P., Duan, Y. H., Chen, E., Tang, S. W., and Wang, X. R. (2018). "Microstructure-based fractal models for heat and mass transport properties of cement paste." *Int.J.Heat Mass Transf.,* 126 432-447.

Zarr, R., Chavez, J., Lee, A., Dalton, G., and Young, S (2016). *NIST Heat Transmission Properties of Insulating and Building Materials, NIST Standard Reference Database Number 81.* National Institute of Standards and Technology, Gaithersburg MD, 20899, .

Zhang, C., Hu, Z., Zhu, F., Huang, Y., and Li, J. (2012). "Correlation between the acoustic and porous cell morphology of polyurethane foam: Effect of interconnected porosity." *Mater Des,* 41 319-325.

Zhang, Z., Provis, J. L., Reid, A., and Wang, H. (2015). "Mechanical, thermal insulation, thermal resistance and acoustic absorption properties of geopolymer foam concrete." *Cement & Concrete Composites,* 62 97-105.

Zhang, Z., and Wang, H. (2016). "The pore characteristics of geopolymer foam concrete and their impact on the compressive strength and modulus." *Frontiers in Materials, Vol 3 (2016),* .

Zhang, Z., Zhang, Z., Wang, H., Provis, J. L., and Reid, A. (2014). "Geopolymer foam concrete: An emerging material for sustainable construction." *Constr.Build.Mater.,* 56 113-127.